Dissertation

submitted to the
Combined Faculties for the Natural Sciences and for Mathematics
of the Ruperto-Carola University of Heidelberg, Germany
for the degree of
Doctor of Natural Sciences

presented by
Mamatha Sauermann, M.Sc. in Biotechnology
Born in Srikakulam, India

Date of oral-examination: 27th September, 2006

Development and application of a high throughput cell based assay to identify apoptosis inducing proteins, and functional characterization of the candidate Vacuole Membrane Protein 1 (Vmp1)

Referees: PD. Dr. Stefan Wiemann

PD. Dr. Frank Breitling

To my husband and parents

Summary

The aim of the project was to identify and functionally characterize novel human proteins that dominantly induce apoptosis upon overexpression. To achieve this, a cell-based high throughput assay was developed. The assay is based on the detection of activated caspase-3 in cells overexpressing proteins tagged C- and N-terminally with YFP. Apoptotic cells were detected by staining with a specific antibody directed against the activated form of caspase-3. The assay was automated and data acquisition was done using a flow cytometer with an integrated 96-well plate reader. A total of 200 proteins have been screened in the assay, out of which five were identified to be significant activators of apoptosis.

One of the candidates, Vacuole Membrane Protein 1 (Vmp1), which forms vacuoles in cells and subsequently induces apoptosis when overexpressed, has been functionally characterized in detail. It has been reported that *VMP1* mRNA is differentially expressed in cancer, acute pancreatitis and kidney ischemia and that the overexpressed protein is localized to the Endoplasmic reticulum. But the function of this protein and its role in cancer and other diseases was previously unknown. In this study I show that the vacuoles are formed by the Endoplasmic reticulum due to accumulation of overexpressed Vmp1, and that Vmp1 is actually a plasma membrane protein involved in the formation of initial cell-cell contacts. Its function as a cell-cell adhesion protein was confirmed by identifying that Vmp1 interacts with the tight junction protein ZO-1, and that down regulation of Vmp1 induces cell detachment. Further, down regulation of Vmp1 resulted in a massive increase in the invasion potential of kidney cancer cells, which is consistent with the findings that *VMP1* mRNA level is significantly lower in kidney metastases compared to primary tumours. Thus, these results are the first to show that Vmp1 is a cell adhesion protein, and that its expression level is a critical determinant of cancer cell invasiveness, metastasis formation and induction of apoptosis.

In summary, I have established and applied a high throughput cell-based assay to screen for inducers of apoptosis. Functional characterization of one of the candidates from this screen revealed it to be a disease relevant regulator of cell-cell adhesion. This demonstrates the strength of this high throughput approach in the identification of proteins involved in diseases.

Zusammenfassung

Das Ziel dieses Projektes war die Identifizierung und funktionelle Charakterisierung unbekannter Proteine, die nach Überexpression Apoptose induzieren. Dazu wurde ein zellbasierter Hochdurch-Assay entwickelt, welcher auf der Detektion aktivierter Caspase-3 basiert, nachdem die Zellen Fusionsproteine mit YFP am C- und N-Terminus überexprimierten. Apoptotische Zellen wurden mittels eines spezifischen Antikörpers gegen die aktivierte Form der Caspase-3 detektiert. Der Assay wurde automatisiert und die Datenaufnahme wurde mit einem Durchflußzytometer mit integriertem 96-Well-Platten Lesegerät durchgeführt. Insgesamt wurden 200 Proteine in diesem Assay untersucht, fünf wurden als signifikante Apoptose-Aktivatoren identifiziert.

Eines der Kandidaten-Proteine, das Vacuole Membrane Protein 1 (Vmp1), welches nach Überexpression die Bildung von Vakuolen und Apoptose induziert, wurde in Detail untersucht. In vorherigen Untersuchungen war gezeigt worden, dass die *VMP1* mRNA in Krebserkrankungen, akuter Pankreatitis und Nieren-Ischämie differentiell exprimiert wird. Das überexprimierte Vmp1-Protein ist im Endoplasmatischen Retikulum lokalisiert, die Funktion des Proteins und seine Rolle bei der Entstehung von Krankheiten wurde bis jetzt jedoch nicht untersucht. In der vorliegenden Studie zeigte ich, dass die Bildung der Vakuolen durch die Akkumulation des überexprimierten Vmp1 verursacht wird. Das Protein ist in der Plasmamembran lokalisiert, wo es in die Bildung von initialen Zell-Zell Kontakten involviert ist. Seine Funktion als Zell-Zell-Adhäsions Protein habe ich durch den Nachweis einer direkten Interaktion mit dem Tight Junction-Protein ZO-1 bestätigt. Wird die Expression von Vmp1 mittels spezifischer siRNAs reduziert, verlieren die Zellen ihre Adhäsion und in Nierenkarzinomzellen resultiert die Reduktion in einem deutlichen Ansteigen der Invasivität. Diese Ergebnisse sind im Einklang mit Ergebnissen der mRNA-Messungen für *VMP1*, die eine signifikant niedrigere Expression in Nierenkrebs-Metastasen als in primären Nierenkarzinomen zeigen. Diese Resultate zeigen zum ersten Mal, das Vmp1 ein Zelladhäsions-Protein ist, und dass das Maß der Expression ein kritischer Indikator für die Invasivität von Krebszellen, die Bildung von Metastasen und die Auslösung von Apoptose ist.

Zusammengefaßt habe ich 200 Proteine auf die Induktion von Apoptose in einem zellbasierten Hochdurchsatz-Assay untersucht. Durch die funktionelle Charakterisierung eines der Kandidaten-Proteine habe ich die Verwendbarkeit des Assays zur Identifizierung krankheitsrelevanter Gene nachgewiesen.

1 Introduction

Sequencing of the human genome has revealed the presence of 20,000 to 25,000 protein coding genes [1]. Since the classical concept of ´one gene-one protein` does not always hold true, the number of proteins resulting from these genes would be enormous. The function and biological role of many of these proteins and their variants is yet unknown. So the challenge ahead is to identify the function of these proteins, which will allow us to gain a molecular understanding of the causes and cures of diseases. Therefore, it is necessary to develop and apply parallel high throughput approaches for an efficient functional characterization of the human proteome.

In order to systematically characterize proteins with unknown functions, we have adopted the idea of functional profiling, in which the same set of proteins would be screened in different functional assays [2] [3]. A single high throughput assay by itself does not always provide clear information regarding the function of a protein. However, integration of data from a set of well defined assays that probe various biological processes would help in drawing valid conclusions. To this end, a range of assays that investigate the activity of proteins in cancer related processes have been established in our department (Figure 1.1).

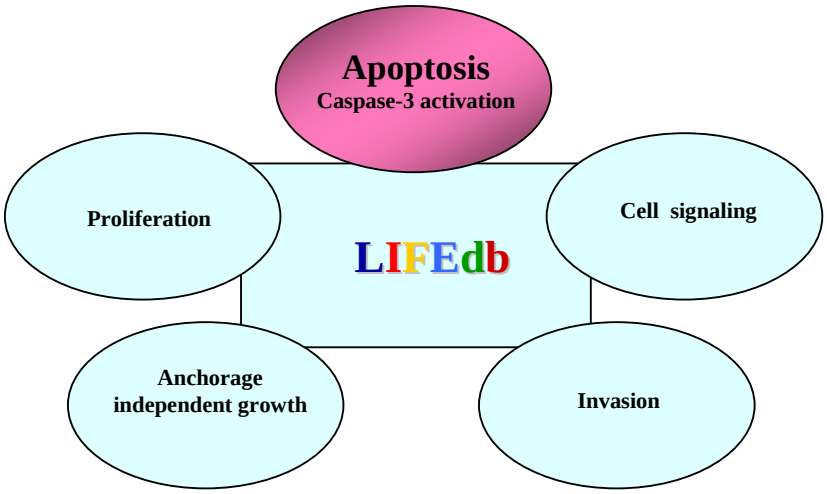

Figure 1.1. Assays to screen for novel cancer relevant proteins.
Several assays have been established to screen for novel proteins involved in disease relevant processes. The data generated from these assays and the subcellular localization of the proteins would be integrated into a database (LIFEdb).

The assays are based on the effect of protein overexpression in well characterized mammalian cell systems. The proliferation assay measures effect of the overexpressed proteins on BrdU incorporation during DNA synthesis (S) phase [3], while the MAP kinase assay detects changes in phosphorylation of p42/p44 (ERK1/2) in the first growth phase (G1). Apart from this, other assays which probe the function of the proteins in processes like invasion and anchorage independent growth of cells were also established in the department. In this line, I have established a high throughput apoptosis assay to identify proteins whose overexpression leads to the activation of caspase-3. The data generated from all the assays as well as the subcellular localization of the proteins [4] would be integrated into a database, LIFEdb [5]. Such a comprehensive approach would allow us to identify proteins involved in diseases like cancer.

Dysregulation of normal programmed cell death mechanisms play an important role in the pathogenesis of cancer and several other diseases. Though apoptosis research is progressing at a rapid pace, only the death receptor and the mitochondrial apoptotic pathways seem to be the most widely studied and understood. However, recent evidences showed that other organelles of the cell also initiate apoptotic pathways [6] [7] [8], and the key players regulating such pathways largely remain unidentified. The availability of cDNA resources provides an opportunity to identify proteins that have previously not been associated with any apoptotic pathway. This would ultimately lead to a better understanding of the cell death program.

1.1 Types of cell death

Cell death is a part of normal development of an organism and is essential in the maintenance of tissue homeostasis. Several mechanisms of cell death have been identified and can be broadly classified into ´non-apoptotic` and ´apoptotic` cell death. The non-apoptotic cell death mechanisms include Autophagy [9] [10], Necrosis [11] and Senescence [12], while the apoptotic mechanism includes a form of Programmed cell death, termed ´apoptosis` [13]. Many diseases are associated with the deregulation of one or more of these cell death mechanisms, out of which apoptosis and necrosis are two major processes by which the cells die.

1.1.1 Necrosis

Necrosis, also called ´accidental cell death`, is an unregulated and passive form of cell death caused by forced destruction of vital cellular machinery, and does not encompass activation of any specific cellular pathway. Necrosis is characterized by rapid swelling of the cell that is caused by the accumulation of water and electrolytes. The plasma membrane of the cell finally ruptures, releasing the cell contents into the surroundings, and thus causing damage and inflammation to the tissue concerned. Necrosis only occurs as a consequence of pathophysiological conditions such as infection, inflammation or ischemia. The molecular mechanisms that regulate necrosis are less clearly understood than that of apoptosis, though increasing evidence shows that these two forms are much closer to each other than previously thought [14].

1.1.2 Apoptosis

Apoptosis, also called ´programmed cell death`, is a genetically programmed process of selectively eliminating unwanted or abnormal cells in the body. The term ´apoptosis` was first introduced by John Kerr in 1972, referring to the morphological features of apoptotic cells forming ´membrane blebs` [13]. The main criterion that distinguishes apoptosis from other forms of cell death is that it is an active and physiological mode of cell death, in which the cell itself activates and executes the genetic program of its own death. Apoptosis is associated with a distinct set of physical and biochemical changes of the cytoplasm, nucleus and the plasma membrane. Unlike necrosis, cells undergoing apoptosis exhibit a reduction in size and become granular (Figure 1.2). Changes to the plasma membrane and cytoskeleton lead to the formation of apoptotic bodies that enclose fragments of nucleus and cytoplasm. The apoptotic bodies displaying phagocytic signals on the outer membrane are engulfed and digested by phagocytes and neighbouring endothelial cells, thus clearing the cell corpses from the tissue. No inflammatory response is triggered during this process, which is considered as the most characteristic feature of apoptosis [15].

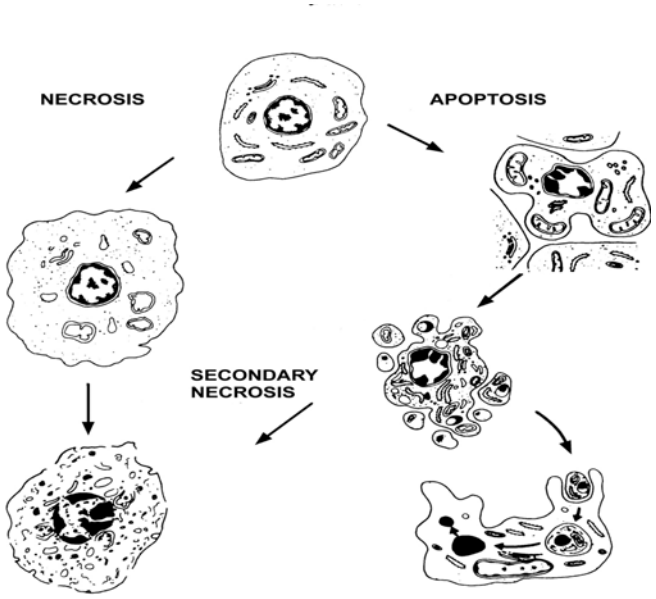

Figure.1.2. Morphological differences between necrosis and apoptosis.
Necrotic cells swell and finally the plasma membrane ruptures, releasing the cell contents into surrounding tissue. Apoptotic cells shrink and the plasma membrane invaginates forming apoptotic bodies, which are engulfed by the phagocytes. The late stage apoptotic cells undergo secondary necrosis, where the membrane of the apoptotic bodies rupture.

Apoptosis serves many important functions in the normal development of an organism, such as cell deletion during embryonic development, balancing cell numbers in continuously renewing tissues, immune system development, selective immune cell deletion and many other physiological processes. Dysregulation of apoptosis have implications in the development of several diseases like Alzheimers, cancer, autoimmune disorders, AIDS etc. Apoptosis is regulated by a complex set of pathways, originating from different cellular organelles, the understanding of which is necessary for therapeutic manipulation.

1.2 Organelle specific initiation of apoptosis pathways

Previous studies have demonstrated that there are two major pathways for inducing apoptosis, one that is mediated by the death receptors on the plasma membrane (Extrinsic pathway) and another that involves mitochondria (Intrinsic pathway). However, it is now well established that most organelles of the cells can act as sensors for stress and other perturbations and initiate organelle specific cell death pathways. Whereas mild perturbation of different organelles triggers apoptosis, a sudden and massive destruction leads to unregulated necrotic cell death.

1.2.1 Death Receptor pathway from the plasma membrane (Extrinsic pathway)

The receptors triggering this pathway are present in the plasma membrane of the cell and are activated by extracellular ligands (Figure 1.3).

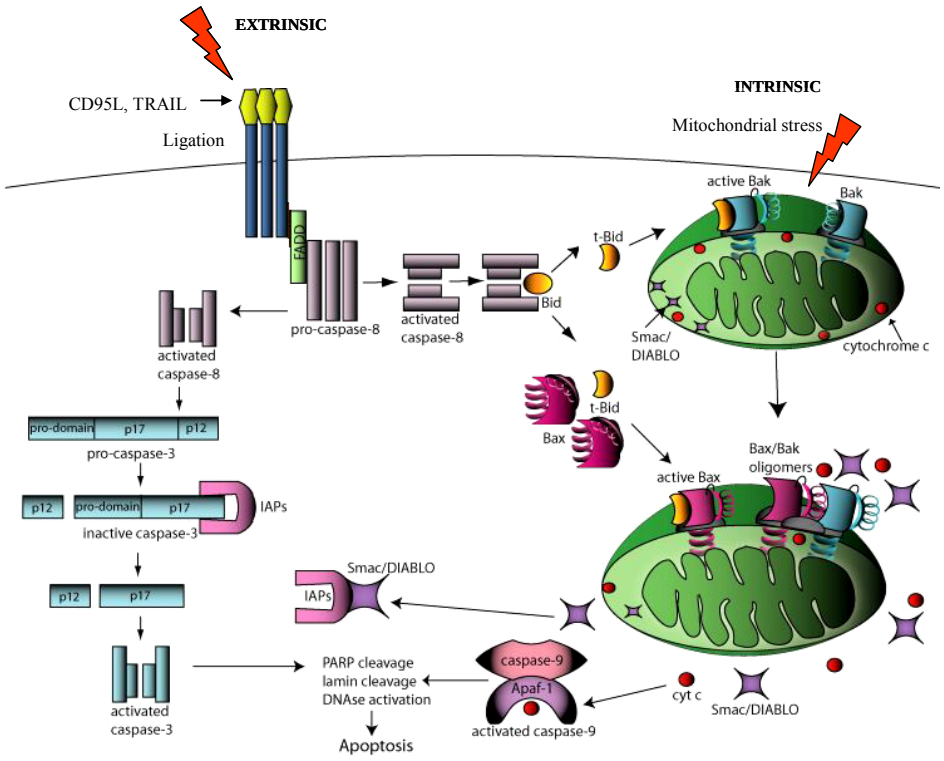

Figure.1.3. The extrinsic (death receptor) and intrinsic (mitochondrial) pathways of apoptotsis.
The death receptor pathway is initiated by the binding of death ligands to their receptors, leading to the activation of the caspase cascade. Mitochondrial stress leads to the activation of pro-apoptotic Bcl-2 family proteins which causes the release of cytochrome c and Smac/DIABLO into the cytoplasm and subsequent activation of caspases.

Death receptors of the tumour necrosis factor receptor (TNFR) superfamily, including TNF receptor 1 (TNFR1), Fas (also known as APO-1 or CD95), Death receptor 4 (DR4, also known as TRAIL receptor 1) or Death receptor 5 (DR5, also known as TRAIL receptor 2) interact with their respective ligands Tumour necrosis factor (TNF), Fas ligand (also known as CD95L or APO1L), Tumour necrosis factor apoptosis inducing ligand (TRAIL, also known as APO2L) and TNF ligand superfamily member 10 (TNFSF10) respectively [16] [17] [18] [19]. Upon interaction with the respective ligands, the intracellular death domains of the receptors trimerize [20] and bind to the adaptor proteins via their death domains (DD) [21] [22]. FADD is the adaptor protein for all the death receptors except for TNF-R1, while TRADD (TNFR1-associated death domain protein) is the adaptor protein for TNF-R1 [23]. The death effector domain (DED) of the adaptor protein then binds to the DED of procaspase-

8, leading to the formation of DISC (Death inducing signalling complex) [24]. The complex of ligand, receptor, adaptor and procaspase-8 is called DISC. The procaspase-8 molecules are brought into close proximity in the DISC, which facilitates the transactivation of one another [25] [26]. The active caspase-8 then directly cleaves procaspase-3 and other executioner caspases. Caspase-8 also cleaves Bid which then moves to the mitochondria and activates the mitochondrial pathway of apoptosis.

1.2.2 Mitochondrial pathway of apoptosis (Intrinsic pathway)

The first report indicating that mitochondria are essential for apoptosis was shown in a cell free model using apoptotic Xenopus egg extracts [27]. The generation of reactive oxygen species (ROS), a by-product of the mitochondrial respiratory chain, was initially considered as a common mediator of apoptosis [28]. However, the observation that several cell lines undergoing apoptosis showed a reduction in the mitochondrial membrane potential indicated that alterations of mitochondrial function is an important feature in apoptosis [29] [30]. This reduction in the mitochondrial membrane potential was later shown to be due to opening of the Permeability Transition (PT) pore complex [31] [32], which led to further investigations regarding the involvement of mitochondria in apoptosis.

Bax and Bak are the crucial pore forming proteins that induce mitochondrial membrane permeabilization and release the death inducing molecules from the mitochondrial intermembrane space (Figure 1.3). The proapoptotic protein Bax exists in normal conditions as monomer in the cytoplasm [33] [34]. Upon receiving the apoptosis stimulus, Bax undergoes conformational change due to interaction with Bid [35] [36], resulting in the translocation and insertion of Bax into the outer mitochondrial membrane as large oligomers [37] [38]. In contrast to Bax, its homologue Bak constantly resides on the outer mitochondrial membrane [39] and following stimulation by Bid, undergoes conformational change and oligomerization, thus releasing cytochrome c [40] [41] and Smac/DIABLO [42] from the mitochondria. The anti apoptotic Bcl-2 family members (Bcl-2 and Bcl-xl) inhibit cytochrome c release by blocking the activation of Bax and Bak [39]. Once released from the mitochondria, Cytochrome c binds to Apoptotic Protease Activating Factor-1 (Apaf-1) triggering the formation of *apoptosome,* an oligomeric complex that catalyzes activation of caspase-9 [43] (Figure 1.3). The activated caspase-9 in turn activates the effector caspases like caspase-3. The effector caspases then cleave essential cellular substrates, leading to cell death.

In normal conditions, members of the protein family of Inhibitor of apoptosis (IAP), bind to and inhibit caspases and block apoptosis signalling [44]. SMAC (Second

mitochondria-derived activator of caspase, also known as DIABLO), once released from the mitochondria following the apoptosis signal, binds to IAPs and antagonizes their anti-apoptotic activity [45].

1.2.3 The nuclear death pathway

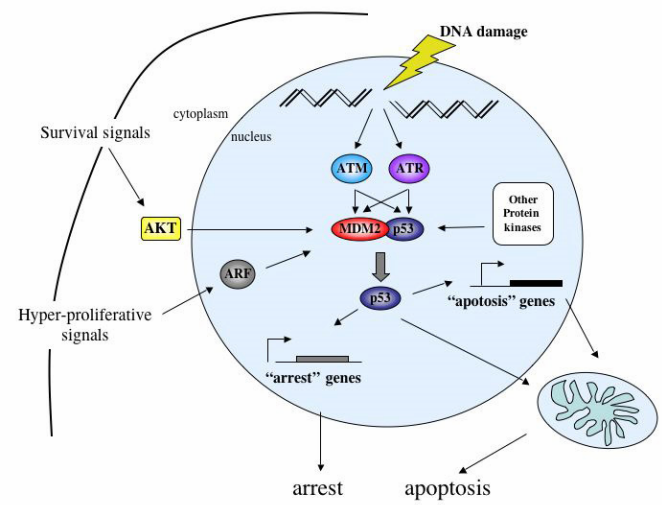

Figure.1.4. The p53 pathway of apoptosis.
DNA damage is detected by the enzymes ATM and ATR, which activate p53 by inhibiting its interaction with MDM2. The activated p53 acts as transcription factor for genes regulating apoptosis and growth arrest.

Activation of p53 is the best defined nuclear death pathway leading to apoptosis [6]. DNA damage caused by exposure to various agents like ultraviolet or ionizing radiations, chemicals etc., is detected by ATM (ataxia teleangiectasia mutated) and ATR (ataxia teleangiectasia Rad3 related) [46] [47], enzymes of the PtdIns-3-OH kinase family (Figure 1.4). These enzymes together with other protein kinases phosphorylate p53 [48] [49], a modification resulting in inhibiting the interaction of p53 with MDM2 (Mouse double minute-2), a ubiquitin E3 ligase. Under normal conditions, MDM2 protein binds to the p53 transactivation domain causing ubiquitylation and degradation of p53 [50] [51] [52]. Inhibition of the interaction with MDM2 prevents destruction of the p53 protein, which accumulates rapidly [53] and acts as a transcription factor for genes favouring growth arrest and apoptosis [54].

p53 inhibits the expression of anti-apoptotic protein Bcl-2 and induces the expression of pro-apoptotic proteins like Fas, Bax, Noxa, PUMA, p53AIP1, Apaf-1 [55] [56] [57] [58] [59]. In addition, p53 may also serve as a direct link to the activation of caspase-2. p53

induced death domain protein (PIDD), RIP-associated ICE-like death domain protein (RAIDD) and caspase-2 form an apoptosome-like complex, which activates caspase-2 [60]. The activated caspase-2 acts as an initiator caspase and triggers the membrane permeability of mitochondria, which further amplifies the caspase cascade [61].

1.2.4 Endoplasmic reticulum (ER) mediated apoptosis

Role of ER in the initiation of apoptosis is recently gaining attention. ER is an important sensor of cellular stress, and it may initiate apoptosis, by at least two mechanisms- the unfolded protein response (UPR) and release of Ca^{2+}.

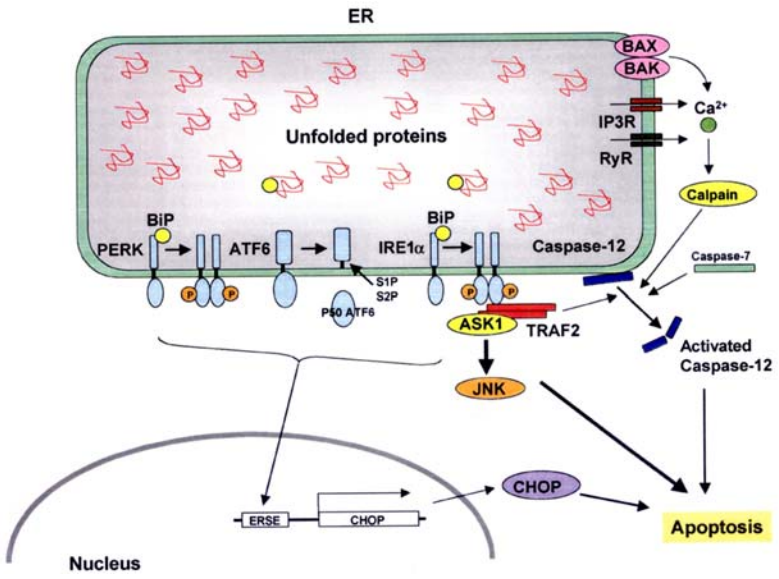

Figure. 1.5. Mechanism of Endoplasmic reticulum mediated apoptosis.
Accumulation of unfolded proteins in the ER triggers apoptosis by the activation of caspase-12, the JNK pathway and induction of the transcription factor CHOP which regulates the expression of pro-apoptotic proteins. Release of calcium from the ER activates calpains which in turn activate the caspases. (Figure taken from Kadowaki,H et al. [62])

1.2.4.1 Unfolded protein response and apoptosis

When the capacity of ER to fold proteins properly is compromised, unfolded proteins accumulate in the ER leading to the onset of UPR. The UPR stops further protein synthesis and upregulates ER resident chaperones and other regulatory components of the secretory pathway [63] that aid in protein folding. However, if the damage is too strong, the UPR ultimately initiates apoptosis [7]. The ER stress response is initiated by three ER membrane receptors, Activating transcription factor 6 (ATF6), Inositol-requiring gene 1 (Ire1), and PKR-like endoplasmic reticulum kinase (PERK) [64] [65] (Figure 1.5). In normal conditions, Ire1 and PERK are kept inactive by the binding of chaperone BiP (Binding protein) to their

lumenal domains. Under conditions of ER stress, BiP dissociates from them to bind to the unfolded proteins, causing the activation of Ire1 and PERK. Activated Ire1 stimulates the transcription of ER chaperone and CHOP encoding genes [66], while PERK, via phosphorylation of eIF2α, stops further protein translation to prevent accumulation of proteins in the ER [67]. Activation of ATF6 also results in the upregulation of ER chaperone genes [68] [69]. When the survival signals mediated by these proteins are not sufficient, the cells undergo apoptosis.

Ire1 signalling plays an important role in coupling UPR with the apoptosis cascade. Activated Ire1 interacts with TNF receptor associated factor 2 (TRAF2), which further interacts with procaspase-12, activating it [70]. Murine caspase-12 localizes at the cytosolic face of the ER, but once activated due to ER stress, it translocates to the cytoplasm [71], and activates other executioner caspases. The human orthologue of caspase-12 is non-functional due to inactivating mutations [72] and its involvement in ER mediated apoptosis is not yet known. Interaction of TRAF2 with Ire1 also activates the c-Jun amino-terminal kinase pathway (JNK pathway) [73] via association with Apoptosis signal-regulating kinase 1 (ASK1) [74]. The ASK1-JNK pathway activates the pro-apoptotic Bcl-2 family members like Bim [75], while it inactivates anti-apoptotic Bcl-2 [76]. Expression of CHOP during ER stress conditions regulates the expression of many apoptosis inducing genes, including that of Bcl-2 family [77]. Overexpression of CHOP in cells was also reported to induce cell cycle arrest and apoptosis [78] [79].

1.2.4.2 Role of Ca^{2+} in ER stress-induced apoptosis

Endoplasmic reticulum serves as the principle storage site for calcium in the cell. Calcium in the ER is regulated by the uptake through Sarcoplasmic/ER Ca^{2+} ATPase (SERCA) and release via inositol 1,4,5-triphosphate receptor (IP3R) or ryanodine (RyR)-mediated Ca^{2+} channels [80] [81]. Conditions resulting in the depletion of Ca^{2+} from the ER or increase in the cytoplasmic Ca^{2+} levels result in cytotoxicity and apoptosis. Increase of cytoplasmic Ca^{2+} leads to the activation of cytoplasmic cysteine proteases called calpains [82](Figure 1.5). Activated calpains in turn activate procaspase-12 and also cleave Bcl-XL, converting it into a proapoptotic protein [83]. The proapoptotic Bcl-2 family members Bax and Bak have also been reported to localize to the ER in some cell types [84], where they might regulate Ca^{2+} dependent cross link between ER and mitochondria. Another proapoptotic protein Bim translocates to the ER during ER stress [85] where it probably acts as a trigger for caspase-12 activation. Caspase-7 was shown to activate caspase-12 [86],

which in turn activates caspase-9 [87] and caspase-3 [88]. This shows that the ER stress response is directly connected to the caspase activation cascade. Although many studies implicate a regulatory role for ER in apoptosis, the exact mechanism how it is regulated remains largely unclear.

1.2.5 Golgi apparatus and apoptosis

Golgi apparatus is enriched with several apoptosis signalling proteins like Caspase-2 [89], and other death receptors of the plasma membrane such as Fas, TNF-R1, TRAIL-R1, TRAIL-R2 etc. Reports showing that p53 mediated apoptosis induced transient translocation of golgi-located Fas to the cell surface [90], indicate that Golgi might act as a temporary storage organelle for the cell surface death receptors. At present it is not known whether the Golgi apparatus functions as a stress sensor in the regulation of apoptosis. However, inhibition of protein glycosylation by an alkaloid, swainsonine, resulted in the induction of apoptosis [91], which suggests that Golgi apparatus might also initiate apoptosis signalling, by an yet unknown mechanism.

1.2.6 Lysosome-mediated apoptosis

The lysosomal cysteine proteases, also called Cathepsins, are the largest group of proteolytic enzymes in the lysosomes. The type of cell death mediated by lysosomes depends on the extent of lysosomal membrane permeabilization, and consequently the amount of proteolytic enzymes released into the cytoplasm. A complete release of the lysosomal enzymes into the cytosol causes necrosis, while a partial permeabilization triggers apoptosis [92] [93]. The precise mechanism by which lysosomes are involved in apoptosis and the possible functional relationships or cross-talks with other known apoptotic pathways is still unknown. Possible mechanisms by which the lysosomal proteases trigger apoptosis would be either by direct cleavage and activation of caspases or by inducing mitochondrial dysfunction. Cathepsin B has been shown to activate procaspase- 1 and -11 *in vitro* [94] [95], though both these caspases have very limited role in apoptosis. Cathepsin L has also been proposed to trigger activation of caspase-3 indirectly [96]. The proapoptotic Bcl-2 family protein Bid is shown to be cleaved and translocated to the mitochondria following disruption of the lysosomes [97]. Cathepsin D triggers activation of Bax and translocation to the mitochondria, resulting in mitochondrial membrane permeabilization and the release of Apoptosis inducing factor (AIF) [98].

1.2.7 Role of cytoskeleton and cell adhesion in apoptosis

The cytoskeleton controls the induction of apoptosis by binding to the Bcl-2 family proteins like Bim and Bmf, thus keeping them inactive [99]. These two proteins act as sensors for changes in the actin cytoskeleton. Cytoskeletal changes caused due to loss of cell adhesion or by chemicals damaging the cytoskeleton causes the release of these proteins, which then translocate to the mitochondria and activate the mitochondrial apoptotic pathway.

An intact cytoskeleton is required for the cell-matrix and cell-cell adherence based signalling pathways. Cells interact with the components of the extracellular matrix through integrins [100], while the interactions with the neighbouring cells are mediated by proteins of the cell junctions (Cadherins, Catenins, Zonula Occludens etc) [101].

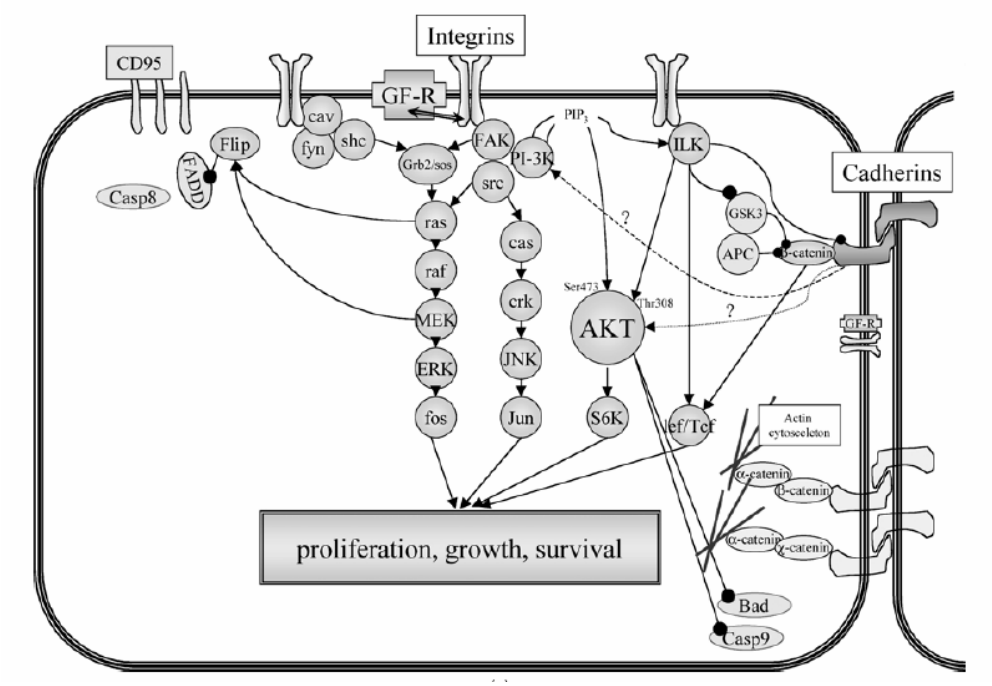

Figure 1.6. Cell adhesion mediated signalling.
Proteins involved in cell-cell and cell-matrix adhesion (cadherins and integrins respectively) mediate several pathways leading to cell proliferation, growth and survival. Loss of cell adhesion abrogates these pathways and triggers apoptosis. (Figure taken from Grossmann,J et al.[8])

Integrins and the Cadherins mediate several pathways including Erk/MAPK, JNK, and AKT pathways which result in proliferation, growth and cell survival (Figure 1.6). Activated AKT inhibits the proapoptotic proteins like caspase-9 and Bad [8]. Activation of the Erk/MAPK leads to the inhibition of Bim [102] and the Fas associated death pathway [8]. However, loss of cell adhesion leads to abrogation of these survival pathways, resulting in apoptosis (Reviewed by Grossmann et al, 2002) [8]. Upon cessation of these pathways, Bad

and Bim translocate to the mitochondria and induce the mitochondrial membrane permeability, release of cytochrome c and finally activate the caspase cascade. Loss of cell adhesion also leads to activation of p53 and an increase in expression levels of Fas and Fas ligand. Loss of cell anchorage seem to trigger apoptosis not via a single specific pathway, but through multiple molecular pathways, which often integrate with the traditional mediators of apoptosis, like caspases and Bcl-2 family proteins.

1.2.8 Integration of different apoptosis pathways

All the cellular compartments are equipped with sensors that can detect different stress signals and relay them to the rest of the cell. Though the apoptotic pathways originate in an organelle-specific manner, they converge on the central executioner, which is the activation of the caspase cascade. Caspases are cysteine proteases that cleave their substrate proteins behind an aspartate residue. There are 14 caspases indentified to date [15]. Functionally caspases can be divided into 3 subclasses: (i) the initiator caspases (Caspase-2,-8,-9 and-10) start the caspase cascade in the specific pathway and activate the effector caspases (ii) the effector or executioner caspases (Caspase-3,-6 and -7) execute the actual cleavage of the cellular substrates and lead to the apoptotic morphology (iii) the remaining caspases whose main role is cytokine maturation rather than apoptosis [103]. Under normal conditions, caspases are present as inactive proenzymes. Upon receiving the apoptosis signal, they get activated either by dimerization (initiator caspases) [104] [105] or by cleavage at specific internal aspartate residues (executioner caspases) [106].

Caspase-3 is a major effector caspase that cleaves many important cellular substrates. Activation of caspase-3 is the point of no return and results in the activation of many down stream effector functions including ICAD (inhibitor of caspase activated DNase), ROCK1 (Rho-associated coiled-coil forming kinase 1), PARP (poly(ADP-ribose)polymerase) a DNA repair enzyme etc. Active caspase-3 causes membrane blebbing (via ROCK 1 cleavage) [107] and DNA fragmentation (via ICAD cleavage) [108] which eventually lead to cell death.

1.3 Apoptosis dysregulation and its clinical implications

Regulation of homeostatic balance between cell proliferation and cell death is essential for development and maintenance of multicellular organisms. Dysregulation of apoptosis is associated with many pathological conditions. Too little apoptosis result in cancer,

autoimmune or other chronic inflammatory diseases, and too much apoptosis result in AIDS and neurodegenerative/neurodevelopmental diseases.

1.3.1 Apoptosis and cancer

Cancer is a condition which is characterized by abnormal and uncontrolled cell division. Normal cells become cancerous as a consequence of several genetic alterations that allow the cell to disable apoptotic signalling. Human tumours harbour several inactivating mutations in pro-apoptotic genes and show increase in expression or activity of anti-apoptotic proteins. Mutations in pro-apoptotic p53 tumour suppressor gene or the regulators of its activity are the most common genetic abnormalities in cancer [6]. Other alterations that confer resistance to apoptosis are increased expression of anti-apoptotic Bcl-2 family proteins, survivin or other inhibitor of apoptosis (IAP) family members, anti-apoptotic heat shock proteins, cathepsin inhibitors; activating mutations of protein kinase B (PKB, also called Akt) and inactivation or loss of pro-apoptotic protein Apaf-1 [109] [110] [111] [112] [99] [113] [114] [115].

1.3.2 Apoptosis and autoimmunity

Autoimmune diseases are characterized by production of antibodies against cellular constituents which are not recognized as antigens in healthy people. Defects in apoptosis pathways were identified in the autoimmune diseases like Rheumatoid arthritis, Type I diabetes, Autoimmune lymphoproliferative syndrome (ALPS) etc. Among several mechanisms responsible for causing these diseases, one possibility is the failure of the immune system to remove by apoptosis those lymphocytes which develop reactivity against self antigens. An alternative mechanism of how dysregulation of apoptosis may contribute to autoimmunity is that if rates of apoptosis are abnormally high in certain tissues, this may result in the presentation of increased levels of autoantigens to the immune system [116]. Mutations of Fas receptor and/or its ligand (FasL) resulting in decreased apoptosis of lymphocytes [117] [118] [119], and defects in the NF-κB related pathways resulting in increased apoptosis [120] have been observed in many autoimmune diseases.

1.3.3 Apoptosis and AIDS

This disease is caused by the infection of $CD4^+$ T lymphocytes with Human immunodeficiency virus (HIV), resulting in the death of infected as well as the uninfected bystander T lymphocytes. The major mechanism by which the T cells die is by apoptosis, primarily Fas mediated apoptosis [121]. HIV infected patients show increased levels of Fas receptor, Fas ligand, caspase-8, pro-apoptotic Bax and Bim. The NF-κB survival pathway was found to be suppressed leading to reduced expression of anti-apoptotic Bcl-2 family proteins like Bcl-2 and Bcl-XL [122].

1.3.4 Apoptosis and Neurodegeneration

Many neurodegenerative diseases like Alzheimers, Parkinsons, amyotrophic lateral sclerosis, retinitis pigmentosa, Friedreich´s ataxia etc. are associated with increased apoptosis of the neurons. Mitochondrial dysfunction, disruption of Ca^{2+} homeostasis, expression of mutant proteins and other cellular stresses causing accumulation of misfolded proteins have been implicated in the development of these diseases [123]. Diseases like Alzheimers and Parkinsons are characterized by accumulation of abnormal protein aggregates in the nucleus or cytoplasm of the neurons. Mutations in Presenilins and Parkin have been implicated in the pathogenesis of Alzheimers and Parkinsons diseases respectively. Mutations in these proteins result in protein misfolding and formation of aggregates, leading to the onset of Unfolded protein response (UPR) and finally apoptosis of the neurons through the endoplasmic reticulum stress pathway [124] [125].

Apart from the above described diseases, hereditary deficiencies in lysosomal enzymes cause Farbers disease, Niemann-pick disease, Batten´s disease, infantile neuronal ceroid lipofuscinosis (NCL) etc, which are characterized by an increase in apoptosis [126]. It has been classically considered that tissue damage leading to ischemia occurs due to necrosis. However, in myocardial infarction, ischaemic renal damage or cerebrovascular accidents, the cells surrounding the ischaemic zone die through apoptosis [127] [128].

1.4 Detection of apoptosis

Because (dys)regulation of apoptosis is associated with such a wide range of diseases, it has become increasingly necessary to precisely identify and quantify cells which died by apoptosis. Apoptotic cells exhibit certain morphological and biochemical features which serve

as markers to differentiate apoptosis from other forms of cell death. Numerous methods have been developed which recognize apoptotic cells based on their characteristic features.

1.4.1 Analysis of cell morphology

One of the early events of apoptosis is cell dehydration that is caused due to inhibition of $Na^+/K^+/Cl^-$ cotransporter system [129]. This leads to condensation of the cytoplasm followed by an increase in cytoplasmic granularity and reduction in cell size. The cells round up and detach from the neighbours. Convolutions of the plasma membrane occur progressively, leading to the formation of ´membrane blebs` and ´apoptotic bodies`, which subsequently detach from the surface of the dying cell.

1. The typical morphology of apoptotic cells i.e. the membrane blebbing and the apoptotic bodies can be detected by light microscopy.
2. The reduction in size and increase in the granularity of apoptotic cells can be detected by flow cytometry based on the light scatter property of the cells. Light scattered by cells in the forward direction (forward scatter) is dependent on cell size; while light scattered at wide angles (Side scatter) is dependent on the granularity of cells [130]. Apoptotic cells exhibit an increased side scatter and decreased forward scatter compared to the normal cells. In contrast to apoptosis, necrosis is associated with transient increase in forward scatter, reflecting cell swelling.

1.4.2 Plasma membrane changes

The key feature distinguishing dead from live cells is the loss of integrity and transport function of the plasma membrane. Early apoptotic cells maintain the plasma membrane integrity, while late apoptotic and necrotic cells lose their membrane integrity. The most characteristic change in the plasma membrane is the loss of asymmetry of the phospholipids. Phosphatidylserine (PS), a phospholipid which in viable cells is present on the cytoplasmic side of the plasma membrane, externalizes upon induction of apoptosis [131]. PS translocation occurs early in apoptosis when the cell membrane integrity appears to be still intact.

1. Charged cationic dyes such as trypan blue, propidium iodide (PI) or 7- amino actinomycin-D (7-AAD) are excluded from live cells with intact plasma membranes. When unfixed and unpermeabilized cells are incubated for a short time with such

dyes, only the late apoptotic or necrotic cells are stained positive, while early apoptotic and healthy cells exclude the dye [132]. This is a suitable assay for flow cytometry.

2. The externalization of PS can be detected using Annexin V, which binds preferentially to negatively charged phospholipids such as PS. By conjugating a fluorophore of interest to Annexin V, early apoptotic cells can be identified either by microscopy or flow cytometry [133].

1.4.3 Mitochondrial changes

Apoptotic cells exhibit loss of mitochondrial membrane potential, which can be used as a marker for detecting apoptosis.

1. A drop in the mitochondrial membrane potential can be monitored by the uptake of fluorescent probes such as JC-1 by the mitochondria [134]. Uptake of JC-1 by mitochondria of healthy cells results in a change of fluorescence emission from green to orange due to formation of dye aggregates upon mitochondrial membrane polarization. Apoptotic cells that exhibit loss of membrane potential fluoresce green. These changes can be detected by flow cytometry.

1.4.4 DNA and nuclear changes

Apoptotic cells undergo a massive DNA fragmentation due to the activation of endonucleases. The DNA is initially cleaved into fragments of 300-50 kbp, followed by cleavage of the DNA between nucleosomes thus producing fragments of 180 bp and its multiples [135]. Many methods have been developed to detect the DNA fragmentation and are described by Allen et al [136].

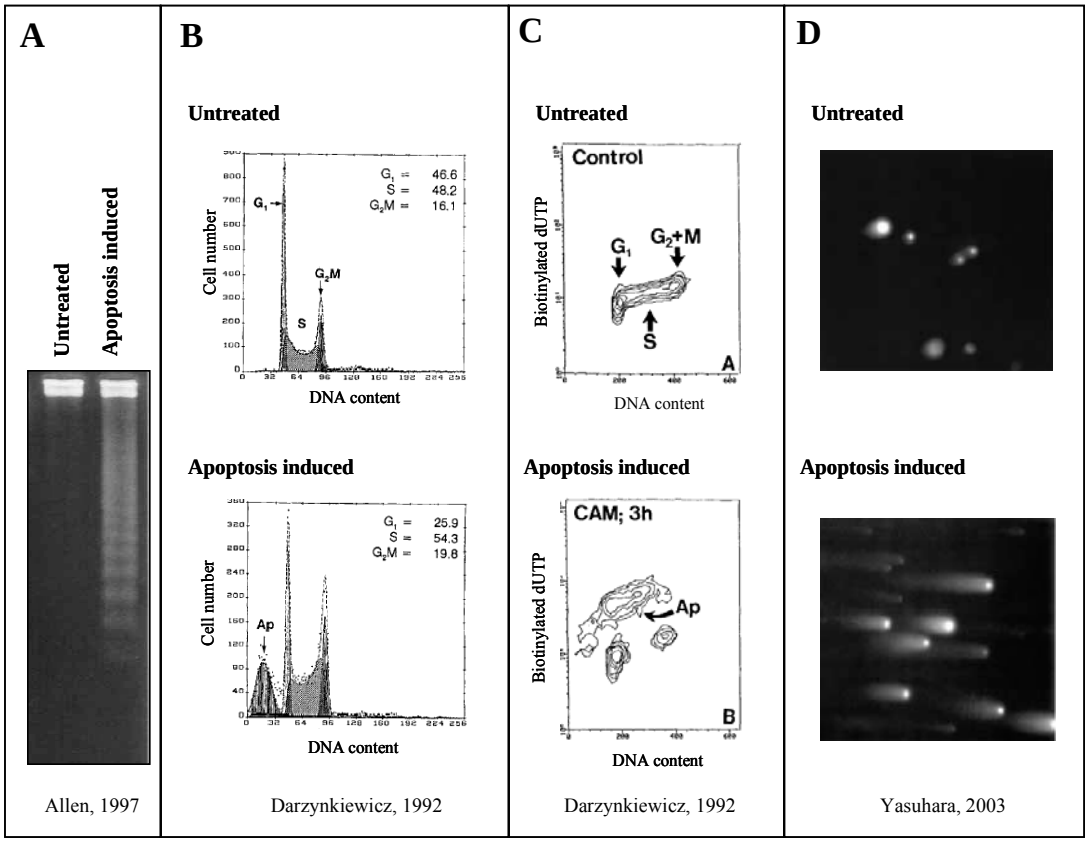

Figure 1.7 Detection of DNA changes associated with apoptosis.
(A) Fragmented DNA can be seen as a ´ladder` by agarose gel electrophoresis. **(B)** Apoptotic cells containing less intact DNA can be visualized as a sub-G1 peak after staining with DNA staining dyes. **(C)** In the TUNEL assay, cells with DNA strand breaks incorporate labelled nucleotides and can be distinguished by flow cytometry. **(D)** In a comet assay, the fragmented DNA of apoptotic cells is pulled out by electric field into the agarose layer. The apoptotic cells appear as comets containing characteristic ´heads` and ´tails`.

1. The DNA of the cells can be extracted by standard procedures and assayed on agarose gels. Fragmented DNA form a characteristic ´ladder` pattern [136] (Figure 1.7.A).
2. After selective extraction of low molecular weight DNA (fragmented DNA) from cells, the cells containing the remaining DNA can be stained with DNA staining dyes like PI, and cell cycle can be analyzed by flow cytometry. The apoptotic cells form a sub-G1 peak [137] (Figure 1.7.B).
3. The 3´OH ends at DNA strand breaks can be detected by attaching them with biotin or digoxygenin conjugated nucleotides in a reaction catalyzed by exogenous TdT (TUNEL assay) [137] (Figure 1.7.C). A new development of this method is the incorporation of BrdUTP into the DNA strand breaks, which can then be detected by using antibodies directed against BrdU. This method can be used to identify apoptotic cells by microscopy or by flow cytometry.

4. When individual cells embedded in a thin layer of agarose gel are subjected to electrophoresis, the fragmented DNA is pulled out from the cells by electric field (Comet assay). After staining the gel with DNA staining dyes, the apoptotic cells appear as ´comets`, with characteristic ´heads` representing cells with high molecular weight DNA, and ´tails` representing degraded DNA [138, 139] (Figure 1.7.D).
5. DNA fragmentation can be detected immunochemically using antibodies against DNA and histones which react with nucleosomes. This is an ELISA based method.

Nuclear changes of apoptotic cells include condensation of the chromatin, disintegration of the nuclear envelope and subsequent break down or segmentation of the nucleus. Fragmentation of the nucleus can be detected by staining cells with DNA staining dyes such as DAPI. This method is suitable for microscopy.

1.4.5 Biochemical changes

Activation of caspases is now well known as a key event in apoptosis. In particular, caspase-3 activity is a common effector of most of the apoptotic pathways. Several assays have been developed which use caspase-3 or its activity as an indicator for apoptosis.

1. Incorporation of caspase-3 substrate into living cells and detection of the cleavage product using Fluorescence Resonance Energy Transfer (FRET) is one of the recently developed methods [140]. Changes in the FRET signal can be detected by fluorescence microscopy, flow cytometry or a fluorescence plate reader.
2. Caspase-3 activity can also be measured *in vitro* in a colorimetric or a fluorometric assay. This assay involves the cleavage of a chromogenic/fluorogenic caspase-3 substrate by activated caspase-3 present in cell lysates of apoptotic cells. The resulting change in colour/fluorescence can be detected using a plate reader.
3. Apoptotic cells can be detected by staining activated caspase-3 with a specific antibody [141]. This method is suitable for flow cytometry or fluorescence microscopy.

1.5 cDNA resources for identification of novel apoptosis activators

The cDNA resources required for the apoptosis screen were provided by the German cDNA consortium. The German cDNA consortium is a large scale cDNA project which was established in 1997 as part of the German genome project. The aim of the consortium is to systematically identify and clone novel human genes by means of cDNA library production, EST Sequencing, and subsequent full-length sequencing of candidate cDNAs [142]. To date, more than 13,000 novel ORFs have been identified and full-length sequenced, out of which more than 1000 full length ORFs have been cloned into expression vectors. Cloning was done using the Gateway™ cloning system (Invitrogen), which allows the cloning of PCR-amplified ORFs by site-specific recombination [4]. To circumvent the possibility of protein localization to a wrong cellular compartment as a result of masking of signal peptide by the tag, two expression clones were generated for each ORF, allowing the expression of ORF as C- and N-terminal fusions with yellow fluorescent protein (YFP). These clones serve as starting material for the subsequent screening of proteins in cell based functional assays.

1.5.1 Selection of novel full-length cDNAs for screening

Our department has identified genes differentially expressed in tumours of the brain, breast, kidney and gastrointestinal stroma using a 31,500-element whole transcriptome cDNA array [143] [144]. Genes with differential expression between normal and tumour samples or between different tumour types were selected by a two-sample *t* test. From these differentially expressed genes, we have initially selected 100 proteins for screening in the apoptosis assay based on the availability of full–length cDNAs. Such a pilot screen with these 100 proteins enabled us to test the functionality and reliability of the assay. Later, 100 previously uncharacterized proteins were randomly selected from the cDNA collection and screened in the apoptosis assay. Thus, a total of 200 proteins were selected for screening in the functional assays. Extending our approach to large sets of proteins in the future will contribute to better understanding of the regulation of apoptosis.

1.6 Aim of the project

The objective of the present study was to establish a high throughput apoptosis assay and to identify and functionally characterize novel human proteins that induce apoptosis upon overexpression. Thus, the aims of this project were to:

1. Establish a suitable apoptosis assay and adapt it for high throughput applications
2. Select, clone and test positive controls for the assay
3. Automate the assay
4. Screen novel proteins to identify apoptosis inducers
5. Validate the candidates with a conventional apoptosis assay
6. Functionally characterize one of the cancer relevant candidates from the assay

2 Materials and Methods

2.1 Materials

2.1.1 Equipment

Autoradiography cassettes	IEC 60406, Rego
Centrifuge	RC5B PLUS, Sorvall
Cytospin 3	Shandon
DNA Gel electophoresis chamber	Renner GmbH
Electronic expandable pipettor	Impact^2, Matrix
Electroporator	Gene Pulser II, Bio-Rad
Film developer	Hyper processor, Amersham pharmacia
Flow Cytometer	FACSCalibur, Becton-Dickenson
Fluorescence Microscope	Axiovert 25, Zeiss
Freezer (-20°C)	Liebherr Premium
Freezer (-80°C)	Sanyo, München
Fridge (4°C)	Liebherr Premium
Fusion^{TM} α	PerkinElmer
Haemocytometer	Neubauer, Brand
Incubator (cell culture)	Binder GmbH
Laser scanning microscope	Axiovert 200M, Zeiss
Light microscope	Hund Wetzler
Magnetic Stirrers	Neolab
Multi-channel pipettes	Brand
PCR Machine	GeneAmp, Applied Biosystems
pH-meter	Hanna Instruments
Pipetteboy	Integra Biosciences
Pipetteman	Gilson
Pipetting Robot	MultiProbe II^{EX}, PerkinElmer
Precision weigher	Neolab
Protein Gel Apparatus	MiniProtean II, Biorad

Real time PCR machine (Taqman)	ABI Prism 7900HT sequence detection system, Applied Biosystems
Rocker Platform	PolyMax 1040, NeoLab
Semi-dry protein transfer apparatus	Trans-blot SD, Bio-Rad
Spectrophotometer	SmartSpec3000, BioRad
Spectrophotometer	SpectraMax190,Molecular Devices
Stepper	Neolab
Sterile Workbench	HeraSafe, Heraeus
Table top centrifuge	Biofuge Fresco, Heraeus
Thermomixer	Eppendorf
UV transilluminator	Herolab
Vortex Mixer	NeoLab
Waterbath	Julabo, Seelbach

2.1.2 Chemicals

0.01% Poly L-Lysine	Sigma
0.4% Trypan blue solution	Sigma
Agarose	Gibco BRL
Albumin Standard	Pierce
Ampicillin	Sigma
APS	Roth
Bacto-Agar	Difco
Bacto-Tryptone	BD Bioscience
Blocker ^{TM} BSA (10X)	Pierce
Bromophenolblue	Sigma
DAPI	Sigma
DMEM, high glucose	Gibco BRL
DMSO	Sigma
DNA Ladder	Invitrogen
EDC	Sigma
EDTA	Roth
Effectene transfection reagent	Qiagen
Ethanol absolute	Sigma

Ethidium bromide	Merck
FBS	Gibco BRL
Gateway BP-Clonase Enzyme Mix	Invitrogen
Gateway LR-Clonase Enzyme Mix	Invitrogen
Geneticin (G 418)	Roche
Gentamycin	Sigma
Glycerol	Roth
Glycin	AppliChem
Isopropanol	Sigma-Aldrich
Kanamycin	Sigma
L-Glutamine	Sigma
Lipofectamine™ 2000	Invitrogen
Magnesium Chloride ($MgCl_2$)	New England BioLabs
Methanol	Riedel-de Haen
Milk-Powder	Roth
n-Butanol	Sigma
Non essential amino acids (100 x)	Invitrogen
PBS	Gibco
Pellet Paint	Novagen
Penicillin / Streptomycin	Invitrogen
PFA	Applichem
Ponceau-S Solution	Serva
Potassium Chloride (KCl)	Sigma
Potassium hydrogen phosphate (KH_2PO_4)	Merck
ProLong Gold anti fade reagent	Molecular Probes
Protease inhibitor cocktail, EDTA-free	Pierce
Rainbow protein molecular weight marker	Amersham Pharmacia
Restore™ Western blot stripping buffer	Pierce
Roti-Load 1 (4X)	Roth
Rotiphorese Gel 30	Roth
RPMI 1640 Medium	Gibco BRL
SDS	Gerbu
SOC Medium	Invitrogen
Sodium acetate (NaAc)	Novagen, Wisconsin

Sodium Chloride (NaCl)	J.T.Baker, Griesheim
Sodium Hydroxide (NaOH)	Gerbu
Staurosporine	Roche
TEMED	Roth
Topoisomerase	Invitrogen
Tris-Base	Sigma
Tris-Sodiumcitrate	Fluka,
Triton X-100	Sigma
Trypsin-EDTA solution 0.25%	Sigma
Tween 20	Gerbu
X-ray film	Amersham Bioscience

2.1.3 Kits

BioCoat^{TM} Tumor Invasion system	BD Biosciences
Cell death detection ELISA^{PLUS} kit	Roche
ECL Western Blotting detection kit	Amersham
Expand high fidelity PCR system	Roche
Gateway BP-Clonase Enzyme Mix	Invitrogen
Gateway LR-Clonase Enzyme Mix	Invitrogen
Invisorb Spin Cell RNA mini kit	Invitek
Micro BCA Protein Assay Reagent Kit	Pierce
ProFound^{TM} Mammalian co-immunoprecipitation kit	Pierce
QIAprep Plasmid Maxi Kit	Qiagen
QIAprep Spin Miniprep Kit	Qiagen
QIAquick Gel extraction kit	Qiagen
QIAquick PCR purification kit	Qiagen
Rapid DNA ligation kit	Roche
RevertAid^{TM} minus first strand cDNA synthesis Kit	Fermentas

2.1.4 Plastic and glassware

5ml Polystyrene round-bottom tubes	BD Falcon
96-well U-bottom storage plate	BD Falcon
Adhesive plate seals	ABgene

Blotting Paper	Sartorius
Cell culture flasks	Greiner Labortechnik
Chamber slides	Labtek
Cover slips	Roth
Filter tubes, Ultra Free-MC with 0.45µm Filter Unit	Millipore
Filtertips	Star lab
Microcentrifuge tubes	Eppendorf
Multiwell plates (96, 24 and 6-well plates)	Nunc
Petri dishes	Greiner Labortechnik
Pipettes	Greiner Labortechnik
Polypropylene tubes (15ml and 50ml)	Greiner Labortechnik
PVDF-membrane	Millipore
Serological pipettes (2ml, 5ml, 10ml, 25ml)	BD Falcon
Slides	Roth
Sterile filters	Millipore

2.1.5 Oligonucleotides

For construction of FRET vector

mbYFPE1B1_fw	5`-AT CTG AAT TCT GTG AGC AAG GGC GAG GAG CTG-3´
mbYFPE1B1_rv	5´-G ATC GGA TTC TTA CTT GTA CAG CTC GTC CAT GCC-3´
mbFRETspacer_up	5´-CC GGA CTC AGA TCT GGA GGC GAC GAG GTG GAC GGC GGA TCG-3´
mbFRETspacer_down	5´-AAT TCG ATC CGC CGT CCA CCT CGT CGC CTC CAG ATC TGA GT-3´
mbCFPDEVDYFP_seqfw	5´-CGA CAA CCA CTA CCT GAG C-3´
mbCFPDEVDYFP_seqrv	5´-CAA GTT AAC AAC AAC AAT-3´

For cloning of controls

mbCIDEC_fw	5´-GCT GGC ACC ATG GAA TAC GCC ATG AAG TCC-3´
mbCIDEC_rw	5´-GCT GGG TCG CCC TGC AGT ATC TTC AGA CAG-3´

mbcytochr_fw	5′-GCT GGC ACC ATG GGT GAT GTT GAG AAA GGC-3′
mbcytochr_rv	5′-GCT GGG TCG CCC TCA TTA GTA GCT TTT TTG AG-3′
mbAIF_fw	5′-GCT GGC ACC ATG GGG TCC CAG GTC TCG GTG G-3′
mbAIF_rv	5′-GCT GGG TCG CCA GGT GGA GAC TGC CTC ATG G-3′
stattB1_PAGE_R	5′-GGG GAC AAG TTT GTA CAA AAA AGC TGG CAC CAT G-3′
stattB2_PAGE_S	5′- GGG GAC CAC TTT GTA CAA GAA AGC TGG GTC GCC-3′

The primers were obtained from MWG Biotech.

2.1.6 siRNAs

The siRNAs were designed by Dharmacon using the SMARTselection technology. siRNAs with the following sense and antisense sequences were used:

VMP1

duplex 1: 5′- GAACAGGGCUGCACACCUUUU-3′ (sense),
5′- PAAGGUGUGCAGCCCUGUUCUU-3′ (antisense);

duplex-2: 5′- CCACAUAUAGCCUCAGUUAUU-3′(sense),
5′- PUAACUGAGGCUAUAUGUGGUU-3′(antisense);

duplex-3: 5′- GGAAUGGACCUCAAAAUUAUU-3′(sense),
5′- PUAAUUUUGAGGUCCAUUCCUU-3′(antisense);

duplex-4: 5′- CGUAUUAUGUUGAAGGAGUUU-3′(sense),
5′- PACUCCUUCAACAUAAUACGUU-3′(antisense);

GFP

5′- PGGCUACGUCCAGGAGCGCACC-3′(sense),

5′- PUGCGCUCCUGGACGUAGCCUU-3′(antisense).

The complementary sense and antisense siRNA strands were annealed according to the manufacturer′s instructions. The four duplex siRNAs targeting *VMP1* were mixed in equimolar ratios and the aliquots were stored at –20°C.

2.1.7 Peptides

The following peptides of Vmp1 were designed using PeptideSelect™ tool (Invitrogen) and selected for generation of rabbit polyclonal antibodies (Inno-Train Diagnostik).

Peptide 1: SSVNEKKRREREERQN

Peptide 2: ARLSGAEPDDEEYQEFE

Peptide 3: EAQRQKLHHKSEMGTP

Antibody against peptide 2 was used for further experiments with endogenous Vmp1.

2.1.8 Antibiotics

Antibiotic	Source	Stock solution	End concentration	Plasmid used
Ampicillin	Sigma	50mg/ml in 50% ethanol	50µg/ml	pdEYFP-amp
Gentamycin	Sigma	10mg/ml in ddH_2O	10µg/ml	pdEYFP-gen
Kanamycin	Sigma	50mg/ml in ddH_2O	50µg/ml	pDONR 221 pCaspase-3 Sensor pECFP-C1
Geneticin	Roche	25mg/ml in ddH_2O	1.1mg/ml	pECFP-C1

2.1.9 Restriction enzymes and buffers

Restriction enzyme	Buffer
*Bsr*G I	NEB 2
*Bam*H I	NEB U
*Bsp*E I	NEB 3
*Eco*R I	NEB U

All enzymes were obtained from New England BioLabs (NEB)

2.1.10 Bacterial Strains

DH10B

DH10B™ (Invitrogen) cells are a strain of *Escherichia coli*. They have a high transformation efficiency, which makes them ideal for generating cDNA or genomic libraries. The *mcr*A, *mcr*BC, *mrr*, and *hsd*RMS restriction systems were eliminated to allow construction of more representative genomic libraries

DB3.1

DB3.1™ (Invitrogen) is a genetically modified bacterial strain and contains plasmid-derived DNA sequences. This strain contains the *gyr*A462 allele which renders cells resistant to the toxic effects of the *ccd*B gene [145]. So these cells were used to propagate the vectors of the Gateway™ System (Invitrogen) that are toxic to other bacterial strains, because of the presence of the *ccd*B gene in the death cassette of these vectors.

2.1.11 Cell Lines

Cell line	Description	Source	Growth Medium
HEK293T	Human embryonic Renal Cells, Virus-transformed	ATCC (CRL-11268)	DMEM low Glucose +10% FBS
Caki-1	Human kidney cancer	ATCC (HTB-46)	RPMI 1640 + 10%FBS
Caki-2	Human kidney cancer	ATCC (HTB-47)	RPMI 1640 +10%FBS
NIH3T3	Mouse fibroblast cells	ATCC (CRL-1658)	DMEM high glucose+10% FBS

2.1.12 Antibodies

Primary Antibodies

Antibody	Company	Origin	Dilution
Calnexin	BD Biosciences	Mouse Monoclonal	1:1000 for WB
Caspase-3	Cell Signaling Technology	Rabbit Polyclonal	1:1000 for WB
Cleaved Caspase-3	Cell Signaling Technology	Rabbit Polyclonal	1:50 for FC
Cleaved Caspase-3	BD Biosciences	Rabbit Monoclonal	2µg/ml lysatefor IP 1:1000 for WB
Connexin-43	BD Biosciences	Mouse Monoclonal	1:50 for IF
Desmoglein-2	Santa Cruz	Mouse Monoclonal	1:50 for IF
GFP	Roche	Mouse Monoclonal	1:1000 for WB
Golgin-97	Molecular Probes	Mouse Monoclonal	1µg/ml for IF
N-cadherin	Santa Cruz	Mouse Monoclonal	1:50 for IF
VMP1	Inno-Train Diagnostik	Rabbit Polyclonal	1:25 for IF 1:500 for WB
Zonula occludens-1	Zymed	Mouse Monoclonal	20µg/ml for IF 1:350 for WB

Secondary Antibodies

Antibody	Company	Dilution
anti rabbit IgG HRP conjugated	Sigma	1:10,000 for WB
anti mouse IgG HRP conjugated	Sigma	1:10,000 for WB
Goat anti-rabbit IgG, APC crosslinked	Molecular Probes	1:350 for FC
Goat anti-rabbit IgG, Alexa Fluor 488 conjugated	Molecular Probes	1:500 for IF
Goat anti-mouse IgG, Alexa Fluor 488 conjugated	Molecular Probes	1:500 for IF
Donkey anti-rabbit IgG, Alexa Fluor 647 conjugated	Molecular Probes	1:500 for IF
Donkey anti-mouse IgG, Alexa Fluor 647 conjugated	Molecular Probes	1:500 for IF

WB: Western blotting ; IP: Immuno precipitation ; IF: Immunofluorescence ;
FC: Flow cytometry

2.1.13 Plasmids

Gateway™ vectors:

Entry vector:

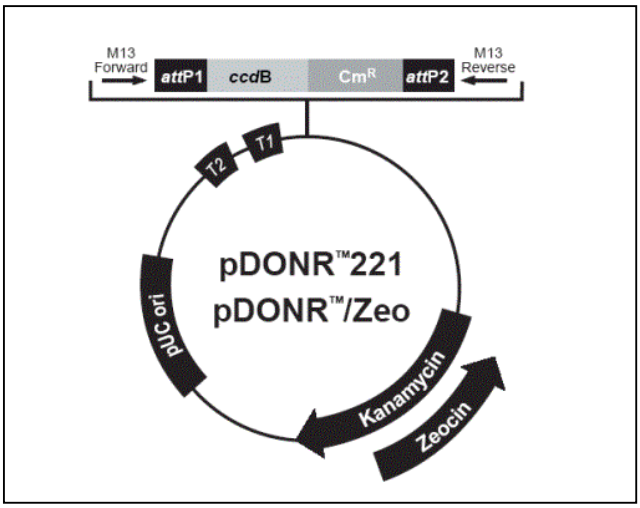

Figure 2.1. pDONR™ 221
This vector was used to generate the entry clones required to shuffle the cDNA into destination vectors.

This is a Gateway™ system compatible donor vector, obtained from Invitrogen. This plasmid was used to generate entry vectors, which were further used to shuffle the cDNA into destination vectors. The ORF is cloned by BP reaction between the two recombination sites *att*P1 and *att*P2. The *ccd*B gene present in the death cassette inhibits the growth of this plasmid in many bacterial strains. The plasmid encodes resistance for kanamycin, which is used for the selection of positive clones, while the chloramphenicol resistance gene is replaced by the ORF during BP reaction.

Destination vectors:

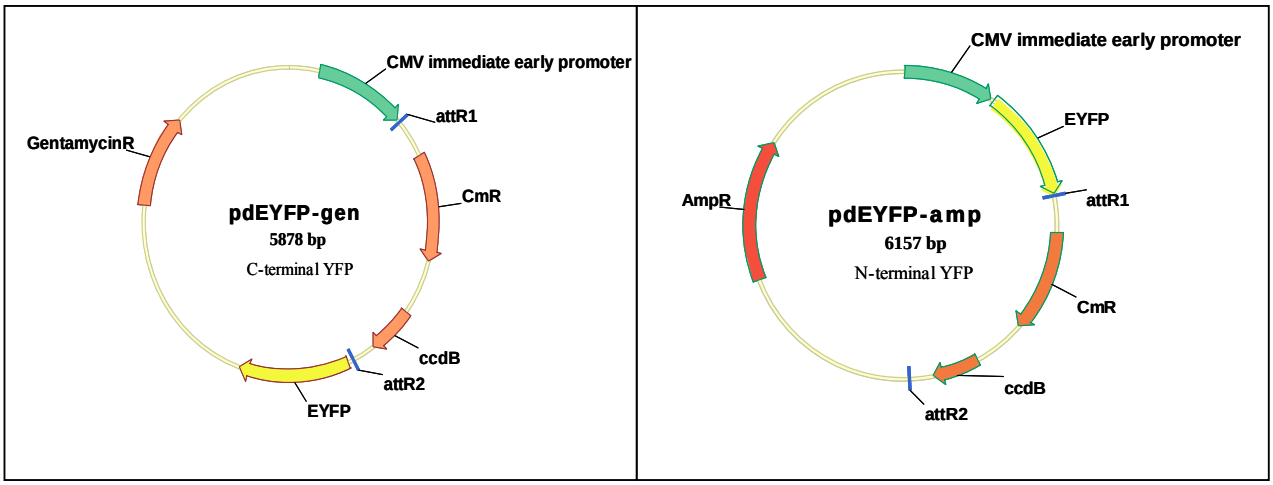

Figure 2.2. pdEYFP-gen and pdEYFP-amp
These destination vectors were used to express YFP tagged proteins in mammalian cells.

Expression vector encoding YFP was obtained from BD Clontech and modified by Wiemann et al to generate pdEYFP-gen and pdEYFP-amp. The pdEYFP-gen (encoding gentamycin resistance) generates a fusion protein with YFP at the C-teminal of the protein, while the pdEYFP-amp (encoding ampicillin resistance) generates a N-terminally tagged protein. The ORF is cloned by LR reaction between the two recombination sites *att*R1 and *att*R2. Both vectors contain the death cassette with *ccd*B gene, which facilitates the selection of positive clones. The transcription is driven by CMV promoter.

Plasmids used for the construction of FRET vector:

pCaspase-3 Sensor

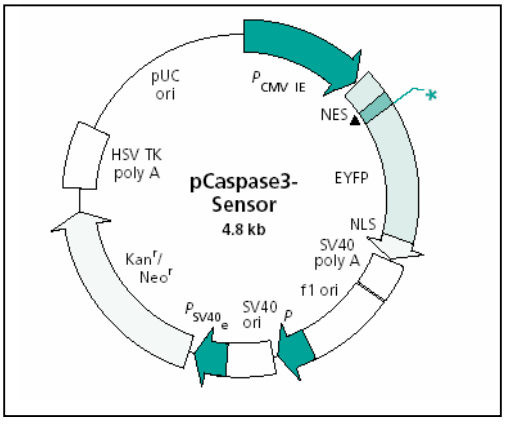

Figure 2.3. pCaspase-3 Sensor
This vector was used to amplify YFP for the construction of FRET vector

This plasmid obtained from BD Clontech was used to amplify YFP for the construction of FRET vector. It encodes a unique Caspase-3 sensor protein containing a nuclear export signal (NES), caspase-3 cleavage site (DEVD) fused C-terminally to EYFP, and a nuclear localization signal (NLS). The transcription is driven by CMV promoter.

pECFP-C1:

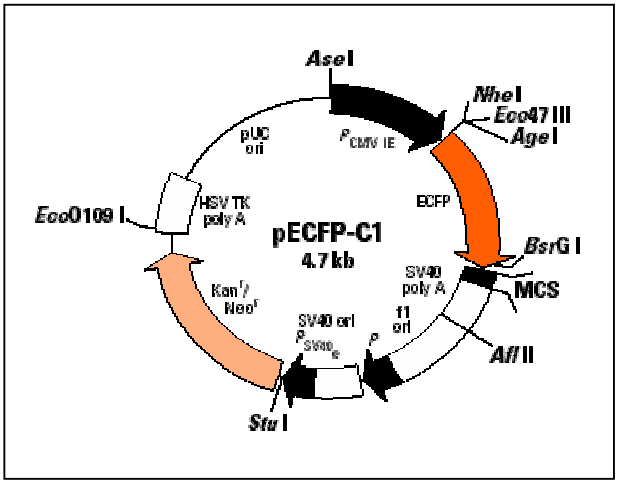

Figure 2.4. pECFP-C1
YFP was cloned in the multiple cloning site of this plasmid to generate the FRET vector

This plasmid was used for the construction of FRET vector. The multiple cloning site (MCS) present at the C-terminus of ECFP allows for the construction of a N-terminally tagged fusion protein. The CMV promoter drives transcription of the fusion protein. This vector confers kanamycin resistance for selection in bacteria, and Neomycin resistance for selection in mammalian cells which facilitates the establishment of stable cell lines.

2.2 Methods

2.2.1 Molecular Biology methods

2.2.1.1 Polymerase Chain Reaction (PCR)

Polymerase Chain Reaction is a technique used to amplify the DNA of interest in order to produce adequate amount required for down stream applications. This method makes use of the ability of thermostable DNA polymerases to synthesize new DNA strand from a template at high temperatures.

PCR was used for 2 different purposes.

1. For the construction of FRET vector – To amplify EYFP from the vector pCaspase-3 sensor
2. For the construction of Gateway Vectors – To amplify the cDNA of interest from the vector pCMV-SPORT6 and clone it into Gateway™ compatible vectors.

For the construction of FRET vector:

The following components were mixed together on ice to set up the PCR reaction:

Template (pCaspase-3 Sensor)	100ng	1µl
10x Buffer (with 15mM $MgCl_2$)		5µl
dNTPs	10mM	1µl
Primer 1 (mbFRETspacer_up)	10pM	1µl
Primer 2 (mbFRETspacer_down)	10pM	1µl
Taq Polymerase		1µl
ddH_2O		40µl
		50µl

The cycling parameters were as follows:

Initial denaturation	95°C	5 minutes	
Denaturation	95°C	30 seconds	30 cycles
Annealing	60°C	1 minute	
Extension	72 °C	3 minutes	
Final extension	72°C	10 minutes	
Hold	4°C	α	

For the construction of Gateway Vectors:

Expand High Fidelity PCR System (Roche) was used to amplify DNA for the Gateway system. This kit uses a mixture of two polymerases, Taq polymerase for high yield and Pwo DNA polymerase for high fidelity.

The PCR was done in 2 separate steps. The primers were designed in such a way that the melting temperature was approximately 75°C. The melting temperature (Tm) of the primers was calculated according to the following formula:

$$2 \times (A+T) + 4 \times (G+C) = Tm\ °C$$

Primers for the 1st PCR contain an ORF specific sequence as well as a short overhang compatible with the recombination sequence of the Gateway cassette. Primers for the 2nd PCR further extend the Gateway cassette overhang of the 1st PCR product.

Design of primers for the two steps of the PCR is shown in Figure 2.5.

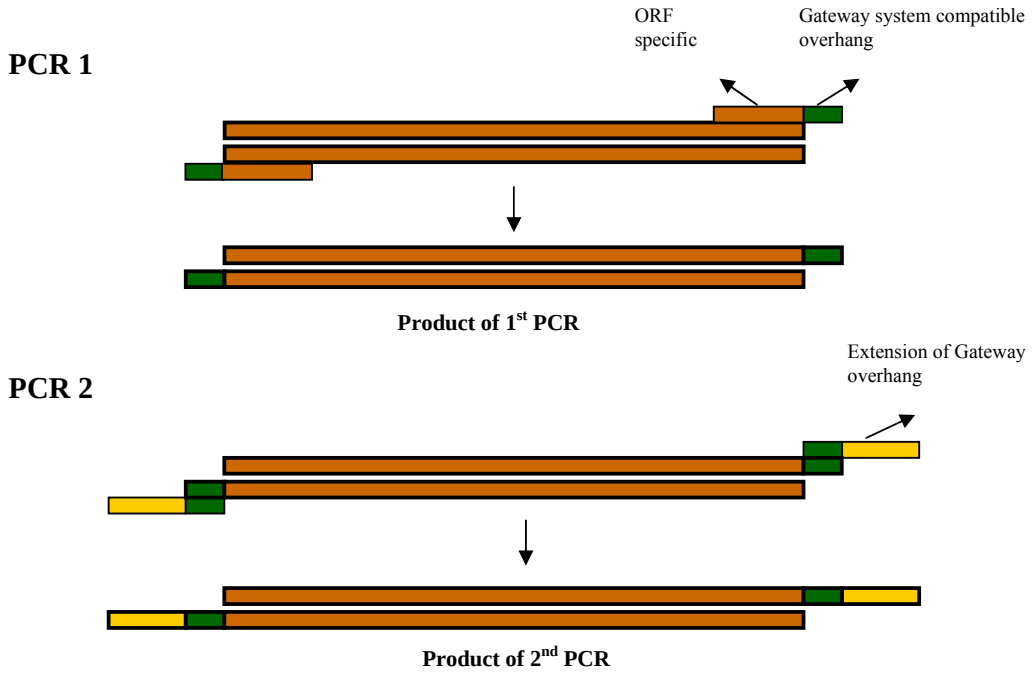

Figure 2.5. Principle of the 2 step PCR
In the first step of PCR, the ORF is amplified using primers that create overhangs compatible with a part of the gateway cassette specific primers. In the second PCR, the overhangs of the ORF are further extended using Gateway cassette specific primers. The product of PCR 2 is then used in the BP reaction to create an Entry vector.

PCR 1:

The following components were mixed together on ice to set up the PCR reaction:

Template (Vector containing the ORF)	50ng	1µl
10x Buffer (with 15mM $MgCl_2$)		5µl
dNTPs	10mM	1µl
forward primer (gene specific)	10pM	1µl
reverse primer (gene specific)	10pM	1µl
Polymerase mix		1µl
ddH_2O		40µl
		50µl

The cycling parameters were as follows:

Initial denaturation	95°C	2 minutes	
Denaturation	95°C	15 seconds	13 cycles
Annealing	58°C	15 seconds	
Extension	68°C	1 minute	
Final extension	68°C	10 minutes	
Hold	4°C	α	

PCR 2:

The following components were mixed together on ice to set up the PCR reaction:

Template (product of the 1st PCR)		1µl
10x Buffer (with 15mM $MgCl_2$)		5µl
dNTPs	10mM	1µl
forward primer (stattB1_PAGE_R)	10pM	1µl
reverse primer (stattB2_PAGE_S)	10pM	1µl
Polymerase mix		1µl
ddH_2O		40µl
		50µl

The cycling conditions were the same as for PCR 1. Both the PCR products, i.e 10µl from PCR 1 and 5µl from PCR 2 were loaded on an agarose gel to check if the expected product

had been amplified. The product from PCR 2 was slightly bigger than that of PCR 1 due to the addition of the Gateway cassette compatible sites. The product from PCR 2 was directly used in the BP reaction (section 2.2.1.4a) to create the entry vector.
For applications that require purified DNA, the PCR product was either purified using QIAquick PCRpurification kit or extracted from a preparative agarose gel.

2.2.1.2 Purification of PCR products

The PCR products were purified to remove the unincorporated primers, primer dimers and other reaction components which might interfere with post-PCR applications. QIAquick PCR purification kit was used when there were no unspecific amplification products. The required amplification product was purified from a preparative agarose gel when more than one product was amplified during the PCR.

PCR purification kit

The purification was done with QIAquick PCR purification kit, according to the manufacturer's protocol. Five volumes of buffer PB (high-salt buffer) was added to 1 volume of PCR reaction and the sample was applied to a column containing a silica gel membrane. After a brief centrifugation, the flow-through was discarded, and the column was washed with 750µl buffer PE. The DNA was eluted by adding 50µl water to the column and centrifuging for 1 minute at 13,000 rpm.

Extraction of DNA from agarose gel

Preparative gel was run at 100V until the desired band was well isolated from the others. The desired band was cut out from the gel under UV light and the gel slice transferred into a microcentrifuge tube. DNA from the gel was extracted using QIAquick gel extraction kit. Briefly, the gel slice was dissolved by adding 3 volumes of buffer QX1 to one volume of the gel and heating at 50°C for 10 minutes. The tube was vortexed every 2-3 minutes. After the gel has dissolved completely, 1 gel volume of isopropanol was added and the sample was applied to the column provided by the manufacturer. The column was then centrifuged for 1 minute and the flow-through discarded. The column was washed once with buffer PE and the DNA was eluted with water.

2.2.1.3 Ligation

Ligation is the process of covalently joining two DNA fragments. T4 DNA ligase encoded by the bacteriaophage T4 was used for the ligation reactions. This enzyme catalyzes the formation of a phosphodiester bond between a terminal 5´-phosphate group and the 3´-hydroxyl group of adjacent nucleotides. The ratio between the vector and insert varies depending on the type of ends (staggered or blunt) generated during the restriction digest.

Two types of ligation were done for the construction of the FRET vector- insertion of YFP (~700 base pairs), and ligation of oligonucleotides of 41 base pairs. The two ligation procedures differ slightly in the molar ratio of the vector and the insert and the pre-ligation treatments.

a. Insertion of YFP

Since cohesive (staggered) ends were generated by the restriction digest of the vector, a molar ratio of 1/1-5 of vector/insert was used for ligation. The following reagents are combined in a final volume of 10µl.

Vector:	50ng
Insert:	100ng
10x ligation buffer:	1µl
T4 DNA Ligase:	1µl

The reaction mixture was incubated at 12-15°C overnight and later used to transform the bacteria.

b. Ligation of oligonucleotides

Before inserting the two nearly complimentary oligonucleotides (mbFRETspacer_up and mbFRETspacer_down) into the vector, they were annealed together to form a short double stranded insert. A molar ratio of 1/100 of vector/insert was used for this purpose. The following components were mixed together:

Vector:	50ng
Oligo1 (mbFRETspacer_up):	18.98ng
Oligo1 (mbFRETspacer_up):	18.98ng

Make up to 8 µl with water.

This reaction mixure was incubated at 65°C (in waterbath) for 15 minutes, and then slowly allowed to cool down to room temperature. This process of slow cooling anneals the two single stranded oligonucleotides, thus forming the insert required for the ligation. To this mixture, 1µl

of 10x Ligation buffer and 1µl of T4 DNA ligase were added, incubated overnight at 12-15°C for the ligation to proceed and was later used to transform the bacteria. The construct was then checked by restriction digest and was later sequenced using the primers mbCFPDEVDYFP_seqfw and mbCFPDEVDYFP_seqrv.

2.2.1.4 Gateway Reactions

The reactions of the Gateway cloning technology (BP and the LR reaction) are based on the site-specific recombination property of the bacteriophage lambda (Landy A et al., 1989). Generation of an expression clone (termed destination clone) through the Gateway system is a two step process [4]. The first step is the cloning of the gene of interest into an *entry vector* through the *BP reaction*. The cDNA present in the entry clone can then easily be shuffled into different Gateway compatible expression vectors by recombination. The second step is subcloning the gene of interest from the Entry Clone into a *Destination Vector* through the *LR Reaction* producing the expression Clone.

a. BP reaction

The BP reaction was used to generate an Entry vector from the gene specific PCR product. This reaction is driven by BP Clonase™ enzyme mix (Invitrogen), a formulation containing the bacteriophage lambda recombination protein Integrase (Int) and the E.coli-encoded protein Integration Host Factor (IHF). The following reagents were mixed together and incubated overnight at 25°C.

5x BP clonase reaction buffer	2µl
PCR product (obtained from amplification of cDNA)	6µl
Entry vector (pDONR 221) (150ng/µl)	1µl
BP Clonase enzyme mix	1µl
Make upto 10µl with water	

The following day, 1µl of Proteinase K (2µg/µl) was added to the reaction mix and incubated at 37°C for 10 minutes to stop the reaction. The DNA was then precipitated using Pellet paint (Novagen). For this, 2µl Pellet paint, 1µl of 3M Sodium acetate, 20µl absolute ethanol and 10µl Isopropanol were added to the BP reaction, mixed well and centrifuged at 13,000 rpm for 15 minutes at room temperature. The supernatant was carefully removed without disturbing the pink coloured DNA pellet at the bottom of the tube. The pellet was dried at 37°C, resuspended in 5µl ddH_2O and 1µl was used to transform the bacteria (DH10B). The mini-prep

DNA obtained from the clones was tested by restriction digest and DNA from the positive clone was used for the LR reaction.

b. LR reaction

LR reaction was used to generate the expression clone, called the Destination vector, from the Entry vector. LR Clonase™ enzyme mix (Invitrogen) was used for this purpose. This is a mixture of bacteriophage lambda Integrase (Int) and Excisionase (Xis), and the E.coli-encoded protein Integration Host Factor (IHF). Since circular destination vector (and not a linear one) was used, Topoisomerase I was included in the reaction to relax the super coiled destination vector. The LR reaction was set up by mixing together the following reagents and incubating overnight at 25°C.

5x LR clonase reaction buffer	4µl
Entry clone (110-150ng/µl)	1µl
Destination vector (150ng/µl)	3µl
Topoisomerase I	0.5µl
LR Clonase enzyme mix	1µl
Make upto 20µl with water	

The reaction was stopped the next day by adding Proteinase K and the DNA was precipitated as described for the BP reaction. 1µl of the DNA was used to transform bacteria (DH10B).

2.2.1.5 Transformation of bacteria

Transformation is a process by which the genetic material of an organism is modified by incorporation of exogenous DNA into its genome.

Preparation of electro-competent cells

The bacteria were first made competent – that is, capable of taking up exogenous DNA molecules. For this, a 1:100 dilution of an overnight culture of DH10B bacterial cells was made in LB medium (without antibiotics) and incubated at 37°C in a shaking incubator until OD_{600} of 0.4 to 0.55 has reached. The cells were spun down by centrifuging at 4000 rpm for 15 minutes at 4°C and the supernatant was discarded. The bacterial pellet was resuspended in 300ml ice cold water and the centrifugation step repeated. The cells were again resuspended in 300ml ice cold water, centrifuged and the pellet was resuspended in 10ml ice cold 10% glycerine. After another centrifugation, the bacterial pellet was resuspended in 1–1.5ml ice cold 10% glycerine and the cells were aliquoted into portions of 25–30µl. The

microcentrifuge tubes containing the competent cells were snap frozen in liquid nitrogen and stored at -80°C until further use.

Electroporation

This method of transformation is based on the observation that biomembranes can be made transiently permeable by the application of short electric pulses [146]. The permeabilized membranes of the bacteria are thus able to take up the exogenously applied DNA.

The electrocompetent cells were allowed to thaw on ice. One µl of the precipitated DNA was added to the thawed cells just prior to electroporation and mixed well. The cell-DNA mixture was pipetted into a chilled electroporation cuvette, taking care not to introduce any air bubbles. The cuvette was then inserted in the electroporator and the cells were pulsed at 1.7kV for approximately 2-3 seconds. The cells were immediately resuspended in 500µl SOC medium (without antibiotic), transferred to a microcentrifuge tube and incubated in a shaking incubator for 1 hour at 37°C. Different aliquots of the bacterial suspension were spread on agar plates and the plates incubated overnight at 37°C. Individual colonies were picked and cultured to analyze for the presence of the required insert.

LB Medium (*Luria Bertani*-medium)

Bacto-Tryptone	10g
Yeast extract	5g
NaCl	10g

Make up to 1 liter with water
Autoclave

LB-Agar plates

Agar	15g

Dissolve in 1 liter LB Medium
Autoclave

2.2.1.6 Small – scale preparation of plasmid DNA (mini prep)

A single isolated bacterial colony from an agar plate (with the appropriate selection marker, refer section 2.1.8) was inoculated into 5ml of LB medium containing the same selection marker. The culture was incubated overnight at 37°C in a shaking incubator (300 rpm). The Qiaprep spin miniprep kit was used to extract and purify the plasmid DNA. Two ml of the culture was taken into a microcentrifuge tube and centrifuged at 6000 rpm for 2 minutes at room temperature. The medium was removed by aspiration, taking care not to suck off the bacterial pellet. 250µl of buffer P1 was added to resuspend the pellet. Then 250µl of

buffer P2 was added and the tubes were inverted to mix. After 5 minutes, 350µl of buffer N3 was added and mixed immediately by inverting the tubes 4-6 times followed by centrifugation at 13,000 rpm for 10 minutes at room temperature. The supernatant was transferred into the column provided by the manufacturer and centrifuged at 13,000 rpm for 1 minute at RT. The flowthrough was discarded, the column washed with 750µl of buffer PE and centrifuged at 13,000 rpm for 1 minute. The flowthrough was discarded and the column centrifuged again at 13,000 rpm for 1 minute. Finally the DNA was eluted by adding 50µl of water and centrifuging at 13,000 rpm for 1 minute at RT. The eluted DNA was then analyzed by a restriction digest with the appropriate enzyme.

2.2.1.7 Large – scale preparation of plasmid DNA (maxi prep)

This was done by using the Qiaspin maxi prep kit (Qiagen). After inoculation with a bacterial culture, 100ml of LB medium (with the appropriate antibiotic as indicated in section 2.1.8), was incubated overnight at 37°C in a shaking incubator (300 rpm). The next day, stocks were made by combining 900µl of bacterial culture with 100µl of 10 x HMFM, followed by freezing at -80°C. The bacteria were harvested by centrifugation at 6000x g for 15 minutes at 4°C. After discarding the supernatant, the bacterial pellet was resuspended in 10ml of buffer P1. To lyse the cells, 10ml of buffer P2 was added to the samples, mixed by inverting the tube 4-6 times, and incubated at room temperature for 5 minutes. To stop the lysis, 10ml of chilled buffer P3 was added, mixed well, incubated on ice for 20 minutes, and then centrifuged at 13.000x g. In the mean time, the QIAGEN-tip 500 columns were equilibrated by applying 10ml of buffer QBT, and the column was allowed to drain by gravity. The supernatant containing the plasmid was filtered through a filter paper into the column and allowed to enter the filter by gravity. The column was washed 2 times with 30ml of buffer QC. To elute the plasmid DNA, 15ml of buffer QF was applied to the column and the eluate was collected into a fresh tube. The DNA was precipitated by adding 0.7 volumes (10.5ml) of isopropanol, followed by centrifugation at 4°C for 30 minutes. The DNA pellet was washed with 5 ml of 70% ethanol and centrifuged again at 4°C for 15 minutes. After pouring off the ethanol, the pellet was dried at room temperature and then resuspended in required amount of sterile water.

10x Hogness Modified Freezing Medium (HMFM)

Solution 1

$MgSO_4.7H_2O$	5mM
Tri-Sodium citrate 2 H_2O	20mM
$(NH_4)_2SO_4$	85mM
Glycerol	45%

Solution 2

KH_2PO_4	0.66M
K_2HPO_4	1.3M

Autoclave both the solutions separately.
Before use, mix Solution 1 and Solution 2 in a ratio of 1:4

2.2.1.8 Measurement of DNA concentration

The concentration of DNA was determined by measuring the absorbance at 260nm using a spectrophotometer (SmartSpec3000, BioRad). The purity of plasmid DNA can be determined by calculating the ratio of A_{260} to $A_{280.}$ A ratio of 2:1 indicates high purity. For measuring the absorbance, the spectrophotometer was first calibrated with 100µl of water. Five µl of DNA was mixed with 95µl of water, transferred to a quartz cuvette, and the absorbance was recorded at 260 and 280 nm. The concentration of double stranded DNA was calculated by using the following formula:

Absorbance at 260nm (A_{260}) x dilution factor x 50µg/ml = Xµg/ml

2.2.1.9 Restriction digest

This method makes use of the property of restriction endonucleases to recognize a specific and short sequence of the DNA and cut it at that point. The required amount of DNA (150ng in case of maxi-prep and 3µl in case of mini prep), one-tenth the final volume of the appropriate 10× restriction buffer (refer section 2.1.9), and the enzyme were mixed together. The reaction thus prepared was incubated at the temperature specified for the enzyme for a minimum of 1 hour to overnight. Loading dye was added to the digested DNA to a final concentration of 1x, and the DNA was then analyzed by agarose gel electrophoresis.

2.2.1.10 Gel electrophoresis

Many biological molecules are charged species that can move in an electric field. Electrophoresis techniques are based on this property. Under neutral or alkaline pH conditions, the phosphate groups of DNA chains become ionized into *polyanions*. As a consequence, DNA fragments placed within a porous matrix and subjected to an electric field travel towards the anode. Under these conditions, smaller DNA molecules migrate faster through the pores of the gel relative to their larger counterparts. By using this technique known as *gel electrophoresis*, it becomes possible to separate molecules of different size.

Agarose gel electrophoresis

Here, agarose gel is used to separate DNA fragments of different sizes. Agarose is a neutral polysaccharide polymer generally extracted from the cellular walls of Rhodophyceae algae, a sea weed. A 1% agarose gel was used for the separation of DNA fragments. For this, 0.3gm agarose was dissolved in 30gm 1x TAE buffer by heating the mixture in a microwave. Heating was continued until a clear, transparent solution was obtained. The solution was then poured into the electrophoresis chamber and allowed to solidify. Before loading samples onto the gel, the gel was covered with the electrophoresis buffer (1x TAE). Electric field was applied across the gel at 100-150V. The DNA moves towards the anode due to the negatively charged phosphate groups. The gel was then stained in Ethidium bromide solution for 5 to 10 minutes. Ethidium bromide is a fluorescent dye that can reversibly intercalate between the bases of DNA molecules and emits an orange fluorescence upon excitation by UV light. The DNA was then visualized using a UV illuminator. The size of the DNA fragments was checked by comparing their size with that of the DNA ladder (Invitrogen).

50× TAE buffer

Tris Base	2M
EDTA	0.1M

Adjust the pH to 8.0 with glacial acetic acid.

6x Loading dye

Bromophenol blue	0.25%
Xylene cyanol FF	0.25%
Ficoll (Type 400)	15%

2.2.1.11 Extraction of total RNA from cells

Total RNA was extracted from mammalian cells using Invisorb spin cell RNA mini kit (Invitek) according to the manufacturer's instructions. Briefly, the adherent cells were

detached by trypsinization, and pelletted by centrifugation at 1500 rpm for 5 minutes. The cell pellet was resuspended in lysis solution R, and the lysate (including the precipitate) was pipetted into the DNA-binding spin filter to bind the DNA. To precipitate the RNA, 1 volume of 70% ethanol was added to the RNA-containing lysate, and then pipetted onto the RNA binding spin filter. After washing the filter 2 times with wash buffers, the RNA was eluted with 50µl of elution buffer R into a fresh RNAse free elution tube. The RNA was quantified and used immediately or stored at -80°C until further use.

2.2.1.12 Quantification of the RNA using Ribogreen

The total amount of RNA present in the elution was quantified by staining with a fluorescent dye called Ribogreen. Ribogreen reagent is non-fluorescent when free in solution. However, the fluorescence increases more than 1000 fold upon binding to the RNA. For quantification, the RNA standard (RNA ladder from Ambion diluted to 2ng/µl) was serially diluted in a final volume of 100µl RNAse free TE buffer in a black 96-well plate to get final concentrations of 0, 2, 5, 10 and 25ng of RNA. In a similar way, the RNA samples from the cells were diluted in TE buffer. To each well, 100µl of Ribogreen (diluted 1:1000 in TE buffer) was added, incubated in dark at room temperature for 5 minutes and then the fluorescence was measured with the fluorescence plate reader (Fusion ^{TM} α). The filter sets used were Excitation: 480/20 and Emission: 515/30. The amount of RNA present in the samples was then calculated based on the standard curve obtained from the standards.

2.2.1.13 Reverse transcription

Generation of first strand cDNA from the mRNA was done using RevertAid H minus first strand cDNA synthesis kit (Fermentas) according to the manufacturer's instructions. For this, equal amount of RNA from each sample (in a final volume of 3µl) was denatured at 72°C for 2 minutes. The denatured RNA was immediately placed on ice and the reverse transcription reaction was set up by mixing the following reagents:

Denatured RNA:	3µl
5x reaction buffer:	1.2µl
Oligo$(dT)_{18}$ (100pmol/µl)	0.25µl
10mM dNTPs	0.6µl
Prime RNAse inhibitor (30u/µl)	0.2µl
RevertAid RTase (200u/µl)	0.2µl
RNAse free water	0.55µl

The reagents were mixed thoroughly and then incubated at 37°C for 5 minutes, 42°C for 1 hour and finally at 70°C for 10 minutes. The cDNA thus generated was used immediately for Taqman reaction or frozen at -20°C until further use.

2.2.1.14 Quantitative Real - time PCR (TaqMan)

This method uses fluorogeneic probes that enable the detection of PCR product as it accumulates during the PCR.

a. TaqMan analysis of cell lines

HEK293T and Caki-2 cell lines were transfected with siRNAs, and 72 hours later the total RNA of floating and adherent was extracted, quantified and reverse transcribed (as described in sections 2.2.1.11, 2.2.1.12 and 2.2.1.13). The cDNA obtained by reverse transcribing 10ng total RNA (in a volume of 5µl) was used for each reaction of the quantitative real-time PCR. The cDNA was pipetted into a 384 well plate and 5.5µl of the PCR master mix and 0.5µl of the assay (containing gene specific primers and fluorogenic probe) was added to each well. Quantitative RT PCR was performed using the ABI Prism 7900HT Sequence Detection System (Applied Biosystems). Triplicate reactions were performed for each gene of interest using the assay on demand Hs00229548_m1 (VMP1) and Hs00212817_m1 (COPB) (Applied Biosystems). For each sample, the median Ct values were taken, and the standard deviations were calculated from the triplicates. Gene expression levels were determined by relative quantification using *COPB* as internal control gene for normalization.

b. TaqMan analysis of patient samples

Fifty-six clear cell renal cell carcinoma primary tumour (n=37) and metastasis (n=19) samples were collected at the University of Göttingen between 1996 and 2002. Viable tissue samples were excised by pathologists immediately after surgery. Parts of the tumours were

snap frozen in liquid nitrogen and stored at -80°C. Tissue homogenization and RNA isolation were performed as described [144]. RNA quality was checked with an Agilent 2100 bioanalyzer (Agilent Technologies GmbH, Waldbronn, Germany). Only high-quality RNA (28S/18S rRNA and E_{260}/E_{280} ratios close to 2) was selected for the experiments. Single-stranded cDNA was transcribed from 1.5µg total RNA using 200U of Revert Aid reverse transcriptase. Quantitative real-time PCR for *VMP1* was performed with the ABI Prism 7900HT Sequence Detection System using the assay on demand Hs00229548_m1. Triplicate reactions using 0.5ng cDNA per IDC sample were performed. Standard curves were prepared through a cDNA dilution series for every gene. For each sample, the median C_T values were taken, and the standard deviations were calculated from the triplicates. Gene expression levels were determined by relative quantification using *ACTB*, *COPB*, and *HPRT* as internal control genes for normalization.

2.2.2 Cell biology methods

2.2.2.1 Subculturing of cells

The cells were regularly passaged to prevent the monolayers from getting confluent and to maintain them constantly in an exponential growth phase. Confluency of the monolayer was especially critical in case of NIH3T3 cells, which exhibit the property of high contact inhibition.

The cells were cultured in the recommended growth medium in 75cm^2 flasks until they achieve a confluency of 70-80%. Before passaging the cells, the medium, 1x PBS and 0.25% Trypsin-EDTA were pre-warmed to 37°C. The medium from the flask was removed and the cells were rinsed once with 7ml PBS to remove all traces of serum. Two ml of trypsin was added to the flask and the cells were incubated at 37°C until they detach from the surface. The cells were gently resuspended in 8ml of complete growth medium to stop the trypsin activity and counted (as described in section 2.2.2.3). Subsequently the cells were transferred into new culture vessels and then incubated at 37°C in an atmosphere of 5% CO_2.

Culture medium

Medium	500ml
FBS	10%
Penicillin	50U/ml
Streptomycin	50µg/ml
Non essential amino acids	1x

2.2.2.2 Freezing and thawing the cells

To make frozen stocks, actively growing cells were trypsinized, centrifuged at 1200 rpm for 5 minutes to remove the medium and then resuspended in freezing medium. Vials containing the cells were immediately placed on ice, then allowed to freeze at -20°C for 2 hours and then at -80°C overnight. The cells were then transferred to liquid nitrogen for long term storage. To get cells back into culture, the frozen cells were thawn in a water bath at 37°C (approximately 2-3 minutes) and immediately resuspended in pre-warmed medium. The cells were centrifuged at 1200 rpm for 5 minutes to remove the freezing medium containing DMSO. The cell pellet was resuspended in complete growth medium, transferred into the culture flask and incubated at 37°C and 5% CO_2 until the cells were ready to be subcultured.

Freezing medium

Medium	70%
FBS	20%
DMSO	10%

2.2.2.3 Counting of cells

The cells were counted using a *Neubauer* hemocytometer. Equal volumes of cells and 0.4% Trypan blue solution (100µl of cell suspension and 100µl Trypan blue) were mixed together in a microcentrifuge tube and left undisturbed for 3 minutes. Trypan blue is a dye which stains dead cells blue, while the live cells remain unstained. The chamber of the hemocytometer was filled with the stained cell suspension by capillary action. The total number of cells in the four marked squares (Figure 2.6) was counted using a microscope. Each chamber of the hemacytometer is divided into nine 1.0mm squares. A cover glass is supported over these squares so that the total volume over each square is 0.0001ml or 10^{-4} ml (length x width x height; i.e., 0.1cm x 0.1cm x 0.01cm). Since $1cm^3$ is equivalent to 1ml, the cell concentration per ml will be the average count per square x dilution factor x 10^4.

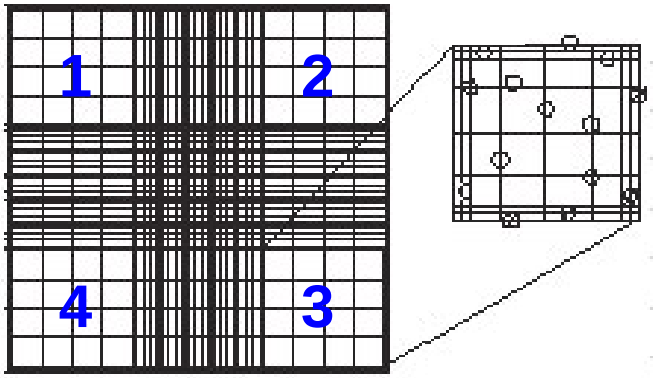

Figure 2.6. Counting cells with *Neubauer* hemocytometer
Cells stained with trypan blue were loaded onto the hemocytometer and the total number of cells in the four big squares (shown with blue numbers) was counted. The number of cells/ml of cell suspension is then calculated as described.

2.2.2.4 Transfection with plasmid DNA and siRNA

Transfection is a process of integrating new genetic material, DNA or RNA into a eukaryotic cell. Two different transfection reagents, Lipofectamine™ 2000 and Effectene™, were used depending on the nucleic acid to be transfected. Effectene™ was used for transfections with plasmid DNA, while Lipofectamine™ 2000 was used for transfections with siRNA. Lipofectamine™ 2000 is a cationic liposomal formulation which interacts with the negatively charged nucleic acid to form lipoplexes that are subsequently endocytosed by the cell (Felgner et al., 1987). A new improvement to the liposomal transfection is the use of non-liposomal lipids. Effectene™ is a non-liposomal transfection reagent, whose positively charged micellar surfaces bind to the DNA for introduction into the cell.

a. Transfection with plasmid DNA

One day before transfection, the cells were seeded into the required culture vessel (petri dish, 6-, 24-, or 96- well plate) so that they attain a confluency of not more than 60% at the time of transfection. The transfection was done according to the following protocol.

Transfection using Effectene™

The required amount of DNA was first diluted in EC-buffer. The DNA-condensing reagent, Enhancer, was then added to the diluted DNA and mixed well by vortexing. The DNA-Enhancer mixture was incubated for 5 minutes at room temperature. Effectene was added to this mixture, mixed well by vortexing and incubated for 10 minutes at room temperature. The complexes were then directly added to the cells in complete growth medium (containing serum

and antibiotics). The cells were incubated with the complexes at 37°C until the required time. The quantity of the reagents used for transfection in one well is shown in the table 2.1.

Table 2.1

	Chamber slides	**96-well plate**	**24-well plate**	**6-well plate**	**Petri-dish ∅ 100 mm**
DNA (ng)	100	100	200	400	2000
Enhancer (µl)	0.8	0.8	1.6	3.2	16
EC-buffer (µl)	50	30	60	100	300
Effectene (µl)	1	0.5	5	10	60
Final volume of medium on cells (ml)	0.2	0.1	0.75	2.0	10

b. Transfection with siRNA

One day before transfection, the cells were seeded in either 24-well or 6-well plates in medium containing 10% FBS (but *without antibiotics*) so that they were 50-60% confluent at the time of transfection. Lipofectamine^{TM} 2000 was used for transfecting with siRNA.

Transfection using Lipofectamine 2000^{TM}

All reactions during the transfection were done in *serum free medium*. The required amount of siRNA and Lipofectamine were diluted separately in serum free medium. After incubation for 5 minutes at room temperature, they were mixed and incubated again for 20 minutes. In the mean time, the cells were washed once with 1x PBS, and fresh medium *(with 10% FBS, without antibiotics)* was added to the wells. The complexes were then given to the cells and mixed well by gently rocking the plate. The cells were incubated at the normal culture conditions for 24-72 hours to allow for the protein knockdown. The quantity of the reagents used for transfection in one well is shown in the table 2.2.

Table 2.2

	24-well plate	**6-well plate**
Lipofectamine (µl)	1	5
Total volume of complexes added to cells (µl)	100	500
Final volume of medium on cells (ml)	0.75	2

2.2.2.5 Generation of Stable cell line

Stable cell lines constitutively expressing the FRET vectors CFP-YFP and CFP-DEVD-YFP were generated using the NIH3T3 cells. The vectors encode Neomycin (G418) resistance which allows for selection of stable transfectants in mammalian cells. An antibiotic, Geneticin disulphate (G418), was used for the selection of stable clones. Geneticin is lethal to normal cells, but the cells expressing the Neomycin resistance gene are resistant to the toxic effects. Generation of the stable cell lines was done in the following steps:

Determination of optimum cell density

Since NIH3T3 cells are very sensitive to cell-cell contact, it was important to determine the minimum cell density at which the cells survive. For this purpose, the cells were seeded into 6-well plates at different densities ranging from 5000 to $3x10^5$ cells/well and incubated overnight at 37°C and 5% CO_2. The cell density of $1.5x10^5$ cells/well was found to be optimum for survival.

Determination of optimum Geneticin concentration

The minimum concentration of Geneticin required to kill the cells not expressing the G418 resistance was determined. This was done by titrating the Geneticin concentration over a period of 8 days. $1.5x10^5$ cells/well were split into 6-well plates and incubated overnight. The following day, Geneticin was added to each well at different concentrations ranging from 150µg/ml to 1.1mg/ml of medium. After 4 days, the medium was replaced with fresh medium, again containing Geneticin, and the cells incubated for 4 more days. After 8 days the viability of cells at different concentrations of Geneticin was checked by microscopy. It was found that approximately 30% of the cells survived at 1mg/ml, while all the cells died at a concentration of 1.1mg/ml. So, a concentration of 1.1mg/ml Genetic was chosen for the generation of stable cell line.

Transfection and selection with Geneticin

$1.5x10^5$ cells/well were split into 6-well plates (in medium with out Geneticin) and the cells were transfected with the required vectors using Lipofectamine 2000™. Two days after transfection the medium in the wells was replaced with Geneticin containing medium (1.1mg/ml) and the cells were allowed to grow for 8 days. Fresh medium was given to the cells every 3 days. Appropriate control wells with out antibiotic treatment were included in the experiment.

Seeding of cells for isolation of stable clones

After 8 days, the cells were trypsinized, resuspended in 3ml medium and seeded into different plates. Different strategies of seeding the cells were followed to isolate the clones stably expressing the FRET probes.

1. 3µl of cell suspension was diluted in 3ml medium (without Geneticin) and seeded into each well of a 6-well plate.
2. The cells were seeded into a 96-well plate in such a way that each well receives one cell. This was done by diluting the cells to a final concentration of 1 cell/100µl medium and seeding 100µl/well. 96-well plates with flat as well as round bottom were used. Since NIH3T3 cells die at high dilutions, the round bottom plates would facilitate better cell-cell contact.
3. A serial 1:1 dilution was done in a 96-well round bottom plate. For this, the plate was first prepared by adding 100µl medium/well. 10µl of cell suspension was added to the first well (A1) and mixed thoroughly. The dilution scheme is shown in Figure 2.7.

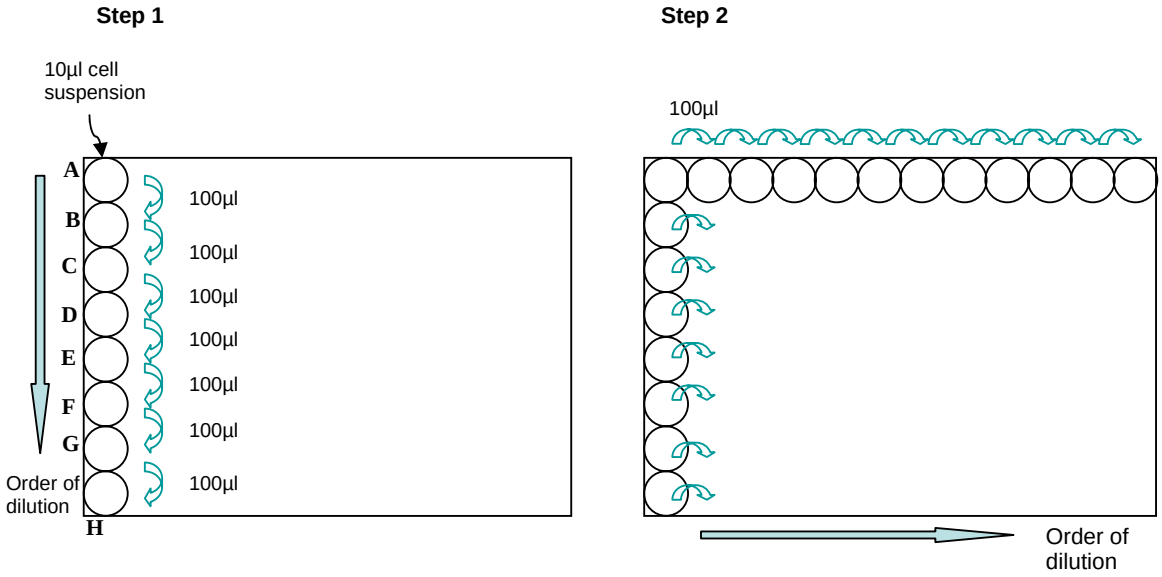

Figure 2.7. Dilution scheme followed for isolation of stable clones
The 96-well plate was initially pre-prepared by adding 100µl of medium to each well. 10µl of cell suspension was then added to well A1, mixed well and 100µl of this was transferred to the next well in the same column. In this way, the cells were serially diluted till well H1. In the second step, 100µl of the cell suspension from each well was serially diluted in the same row.

Picking of clones

Viable clones were found only in the 96-well plates where serial dilution of cells was done. To isolate the clones, the cells were trypsinized by adding 50µl trypsin/well and incubating for 2 minutes at 37°C. The viable clones from the 96-well plate were transferred into a 24-well plates and cultured until the cells were confluent. The cells were trypsinized, cultured in 6-well

plates and then transferred into T25 flasks. When the cells were confluent, an aliquot of cells from each clone was taken aside and the constitutive expression of the protein was checked by western blotting. The rest of the cells were frozen down to be used at a later time.

2.2.2.6 Immunocytochemistry

This method makes use of the specificity of the antigen-antibody interactions for the detection of specific cellular components. Cells were split into 6 well-plates and allowed to grow on cover slips for 12-24 hours prior to the required treatment. Cover slips that had been pre-coated with 0.1% (w/v) Poly-L-Lysine solution were used in case of cell lines that do not attach well to the substrate. The cover slips were treated with Poly-L-Lysine for 5 minutes, air dried and used immediately. Poly-L-Lysine has polycationic nature which strongly attracts the negatively charged molecules on the cell suface, thus retaining the cells on the cover slip.

After incubating cells for the required time, the medium from the wells was removed and the cells were fixed with 1ml 4% PFA for 15 minutes at room temperature. The cells were washed thrice with 1x PBS and then permeabilized with 0.2% Triton X-100/PBS for 5 minutes. After washing three times with 1x PBS, 1ml of blocking solution (3% BSA/1x PBS) was added to each well and incubated for 30 minutes at room temperature. This is done to block any unspecific reactive sites in the cells which might cause high background signal. Subsequently, the slides are incubated in a recommended dilution of the primary antibody (refer section 2.1.12) for 30 minutes at room temperture. The cells were washed three times, 5 minutes each wash, with 1x PBS. The slides were then incubated in the secondary antibody coupled to a fluorophore, diluted 1:400 to 1:600 in 1x PBS for 30 minutes in dark. After washing thrice in 1x PBS, slides were incubated for 5 minutes in DAPI staining solution (1μg/ml DAPI in 1x PBS), to stain the nucleus. DAPI is a fluorescent dye which binds specifically to the minor groove of DNA. The cells were washed to remove the excess staining solution and cover slips were mounted on slides using ProLong gold anti fade mounting solution. After letting them dry over night in dark, the slides were analyzed on the confocal fluorescence microscope. Images were taken using a 63x oil immersion objective.

Blocking solution

BSA	3%
PBS	1×

1x PBS

NaCl	140mM
KCl	2.7mM
KH_2PO_4	1.5mM
$Na_2 HPO_4$	8.1mM

Adjust pH to 7.4 with NaOH

2.2.2.7 Cell death detection ELISA

This is a photometric enzyme-immunoassay for the detection of histone associated DNA fragments. During apoptosis, the activated endonucleases cleave the double stranded DNA at internucleosomal regions generating mono- and oligonucleosomes. The DNA fragments thus formed are multiples of 180bp and are enriched in the cytoplasm of apoptotic cells. The Cell death detection ELISA^{PLUS} kit (Roche) detects these fragments of DNA in a sandwich ELISA based method. The principle of the assay is shown in Figure 2.8.

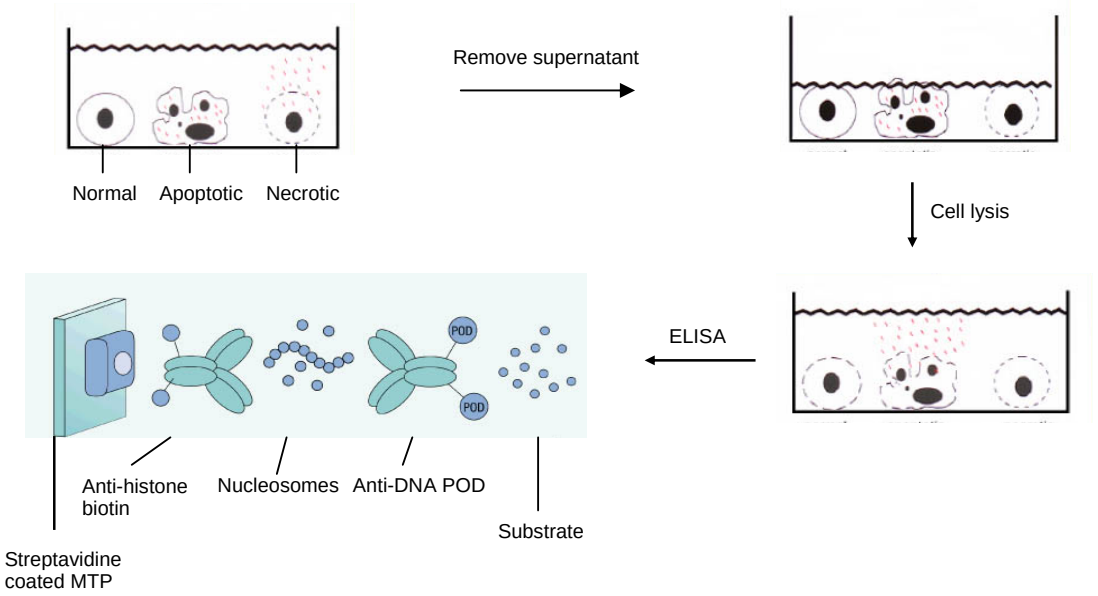

Figure 2.8. Principle of the Cell death detectection ELISA
The supernatant containing contents of the necrotic cells was initially removed and the remaining cells were lysed. Cell lysate containing the cytoplasmic nuclear fragments of the apoptotic cells was transferred into a streptavidin coated micro titre plate. The anti-histone and the anti DNA antibodies capture the DNA fragments, which can be detected in a colourimetric reaction.

After inducing apoptosis for the required time, floating and the adherent cells were collected and centrifuged at 1200 rpm for 5 minutes. The supernatant was carefully removed, the cell pellet resuspended in 200µl of lysis buffer, and incubated for 30 minutes at room temperature. The lysate was centrifuged at 200 x g for 10 minutes and then 20µl of the lysate was transferred to the streptavidin coated micro titre plate. 80µl of the immunoreagent, containing a mixture of biotin labelled anti-histone antibody and peroxidase conjugated anti-DNA antibody, was added to each well and incubated under gentle shaking (300 rpm) for 2 hours at room temperature. During the incubation time, the anti-histone antibody binds to the histones of the nucleosomes, simultaneously capturing the immunocomplex to the streptavidin coated micro titre plate. The solution was removed by suction and the wells were rinsed 3 x

with 300µl incuation buffer. 100µl of substrate solution was added to the wells and incubated for 15 minutes. The absorbance at 405nm was measured using the spectrophotometer, SpectraMax190.

2.2.2.8 Caspase-3 assay

This method is based on the detection of the activated form of caspase-3 by flow cytometry. The cells were transfected with the cDNAs of interest and then stained with an antibody specific for activated caspase-3. The principle of the assay is shown in figure 2.9.

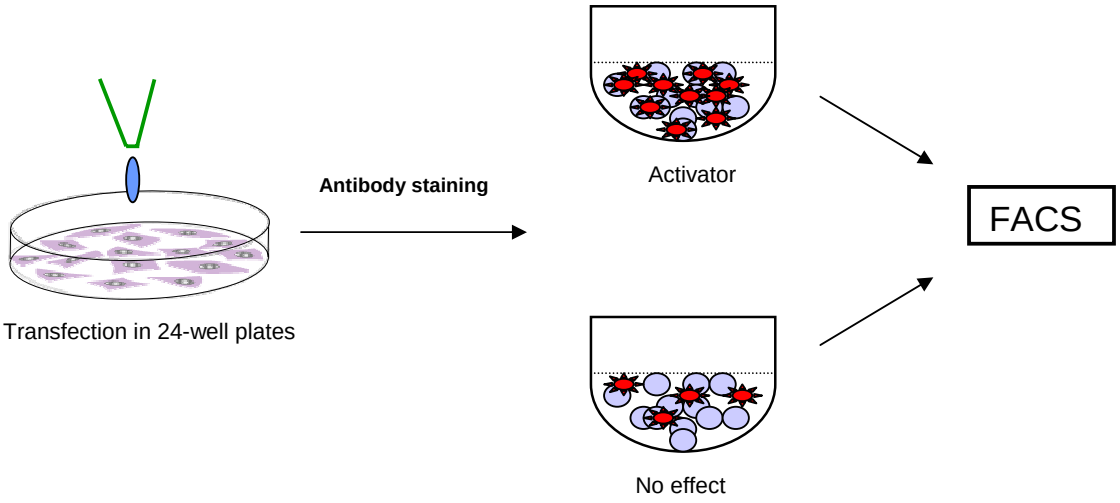

Figure 2.9. Principle of the caspase-3 assay
Cells transfected in 24-well plates with YFP tagged cDNAs were allowed to express the protein for 3 days and then transferred to 96-well plate for staining with the active caspase-3 antibody. The cells were then measured on the FACS to identify proteins that induce apoptosis upon overexpression.

The assay was done in a 24-well format and the detailed protocol is as follows:

Day 1: Seeding the cells

HEK293T cells were seeded in four 24-well plates (24 x 4= 96) at a density of 32,000 cells/well in a final volume of 600µl complete growth medium/well. The plates were rocked gently to ensure even distribution of cells in the wells.

Day 2: Transfection

The cells were transfected under the sterile hood of the robot (MultiPROBE II^{EX}) with 96 different expression clones. The transfection was carried out according to the protocol

described in section 2.2.2.4a for 24-well plates. The plates were labelled carefully according to the order of the transfection and put back in the incubator (37°C, 5% CO_2).

Day 3: Check for protein expression

The cells were checked under a fluorescence microscope for the expression of the protein and the incubation was continued.

Day 4: Incubation

Incubation continued

Day 5: Staining and measurement on FACS

Trypsinization

The medium from the 24-well plates was collected and saved in a U-bottomed polypropylene 96-deep well plate. The saved medium contains the floating apoptotic cells. The adherent cells in the 24-well plates were washed once with 1x PBS and then trypsinized by incubating with 150µl trypsin/well for 2 minutes at 37°C. After the cells have dislodged from the surface, 100µl of medium with 10% FBS was added to the wells to inhibit the Trypsin. The cells were resuspended thoroughly to dissociate the cell clumps and then transferred to the respective well of the deep well plate containing the floating cells. The cells were then stained with the specific antibody.

Staining

The plate was centrifuged at 1350 rpm for 5 minutes to pellet the cells. The medium was aspirated carefully and the cells were fixed by resuspending in 150µl 2% PFA and incubating at 37°C for 10 minutes. The cells were placed on ice for 1 minute and then centrifuged to remove the PFA. Permeabilization was done by adding 200µl ice cold 90% methanol and incubating on ice for 30 minutes. Cells can be stored at this point at –20°C, until further use. After removing the methanol, 150µl of wash buffer (0.5% BSA in PBS) was added to the cells to block any high affinity binding sites on the cells. Blocking was done by incubating in wash buffer for 10 minutes at room temperature. The wash buffer was removed and the cells were incubated in 50µl of primary antibody staining solution (Rabbit anti active caspase-3, diluted 1:50 in wash buffer) for 45 minutes at room temperature. The cells were washed twice with 150µl wash buffer and then incubated in 50µl of secondary antibody staining solution (anti-rabbit IgG-APC conjugated, diluted 1:350 in wash buffer) for 30

minutes at room temperature in dark. The unbound antibody was removed by washing twice with 150µl of wash buffer, and the cells were finally resuspended in 50µl wash buffer.

Measurement with FACS

The cells from the deep well plate were transferred into a polypropylene 96-well U-bottom plate which is compatible with the HTS (High throughput sampler) of the FACSCalibur. The settings of the instrument were adjusted to measure the signal from 20,000 cells. CellQuestPro® was the software used for the measurement. Setup and calibration of the instrument were done as described in the FACSCalibur manual.

Statistical analysis

The data obtained from the assay was analyzed using the statistical programming language R, which is openly available on the net as the software package *prada* (collaboration with Florian Hahne). Effect of a given protein on apoptosis was then quantified based on the calculation of odds-ratio. Odds-ratio is defined by

$$\frac{TP+1}{TN+1} \quad \frac{UTN+1}{UTP+1}$$

Where,

TP = Transfected, active caspase-3 Positive

TN = Transfected, active caspase-3 Negative

UTN = Untransfected, active caspase-3 Negative

UTP = Untransfected, active caspase-3 Positive

Fisher t-test was used to test for the significance against the null hypothesis of no effect. The results were then visualized as colour coded 96-well plate plots displaying various quantities of interest like odds ratio, transfection efficiency, total cell number/well etc.

2.2.2.9 Nuclear fragmentation assay

HEK293T cells were seeded in 24-well plate (32,000 cells/well) and incubated overnight at 37°C. On the following day the cells were transfected with YFP tagged ORFs and allowed to express the protein for 3 days. The floating and adherent cells were collected by trypsinization, centrifuged and fixed with 500µl of 2% PFA for 10 minutes at room temperature. After removing PFA, the cells were permeabilized by incubating with 0.2% Triton X-100/PBS for 5 minutes. The cells were then resuspended in 500µl of DAPI staining solution (diluted 1:1000 in PBS) and incubated for 5 minutes. After washing twice with PBS, the cells were fixed on slides

using Cytospin centrifuge and then mounted using Prolong Gold antifade mounting solution. Fluorescence images were obtained using a Confocal laser scanning microscope, Axiovert 200M. Images were taken using a 40x oil immersion objective.

2.2.2.10 Adhesion assay

HEK293T cells were seeded in 6-well plates ($2x10^5$ cells/well) and transfected with siRNA. After incubating for 72 hours, the culture medium from the wells was collected, centrifuged to remove the medium and the cells were fixed with 4% PFA for 15 minutes at room temperature. The pelletted cells were resuspended in PBS and the cell number was counted with FACSCalibur.

2.2.2.11 Invasion assay

BioCoat™ Tumor invasion system from BD Bioscience was used for the Invasion assay. This system consists of a 24-well insert plate with a porous membrane (8.0 micron pore size) that has been uniformly coated with BD Matrigel™ Matrix. The matrix coating mimics *in vitro,* the basement membrane of the tissue through which the matastatic cells invade. In this assay, the cells were induced to invade due to the stimulus provided by a chemoattractant (serum). The invading cells produce proteases which degrade the Matrigel coating [147]. The number of invaded cells was then measured with FACS. Figure 2.10 shows the principle of the assay.

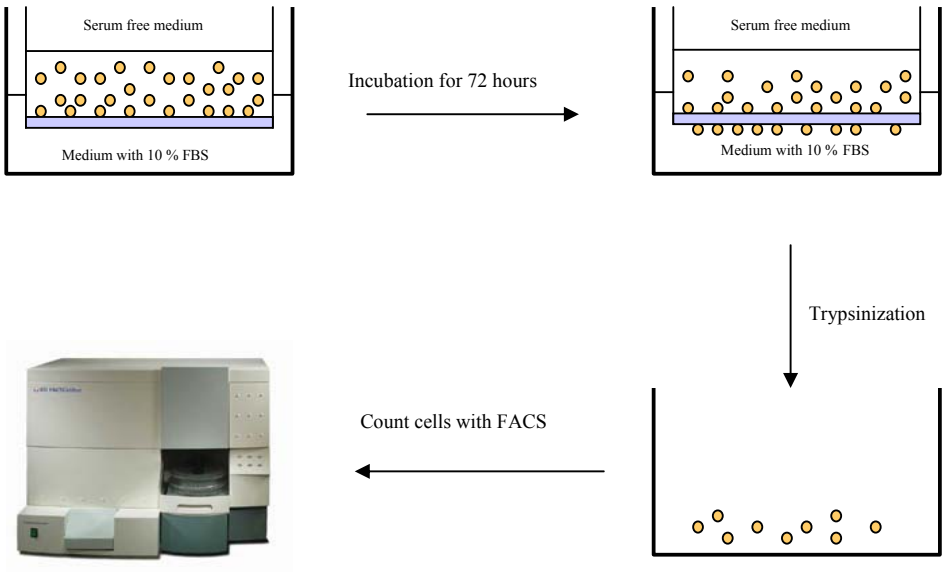

Figure 2.10. Principle of the invasion assay
Cells were transferred into the top chamber of the BioCoat™ Invasion plate containing serum free medium. The bottom chamber contains medium with 10% FBS, which acts as chemo-attractant. After incubating for 72 hours, the invaded cells were detached by trypsinization and counted on FACS.

The assay was done in the following steps:

Transfection and serum starvation

Caki-2 cells were seeded into 6-well plates ($1.2x10^5$ cells/well) and transfected with siRNA the following day. After 24 hours, the medium was removed, cells washed with 1x PBS and medium with 1% serum was given to the wells. The cells were serum starved in 1% FBS medium for 24 hours.

Rehydration of the Invasion plates

The BioCoat™ Invasion plate was allowed to warm to room temperature and 500µl of pre-warmed PBS was added to the wells of the insert. The plate was rehydrated by incubating for 2 hours at 37°C and 5% CO_2.

Seeding of cells into invasion plates

The serum starved cells from the 6-well plates were trypsinized, counted and resuspended in serum free medium. In the mean while, the PBS from the insert of the invasion plate was removed carefully without disturbing the Matrigel matrix, and 750µl of medium with 10% FBS (chemoattractant) was added to the bottom wells through the sample prots for

access to the bottom chamber. 1 x 10^5 cells, resuspended in 500µl of serum free medium, were seeded into each well of the top chamber and incubated for 72 hours at 37°C and 5% CO_2 atmosphere.

Harvesting the invaded cells

During the 72 hours of incubation the invading cells degrade the gel matrix, pass through the porous membrane towards the chemoattractant and attach themselves to the bottom of the membrane. These cells were detached from the membrane by trypsinization. For this, the 24-well insert was placed in a 24-well plate prepared with 300µl trypsin/well and incubated at 37°C for 2-4 minutes. The cells were detached from the bottom of the membrane by tapping the insert thoroughly. The trypsinization was stopped by adding 1ml of 10% FBS medium/well. The cells were centrifuged at 1000 rpm for 5 minutes to remove the medium and then resuspended in 300µl of PBS. The number of invaded cells for each condition was determined by counting the cells with FACS.

2.2.3 Protein Chemistry methods

2.2.3.1 Mammalian cell lysis

a. Extraction of Soluble and membrane proteins

48-72 hours after transfection, the medium was either removed from the culture dishes or saved to collect the floating apoptotic cells. The cells were washed once with 1x PBS. The monolayer was then scraped with 2ml of 1x PBS into a microcentrifuge tube and centrifuged at 4,000 rpm for 5 minutes at 4°C. After the supernatant was removed, the pellet was resuspended in M-Per protein extraction reagent (lysis buffer from Pierce) containing protease inhibitors, left at room temperature for 5 minutes and spun at 14,000 rpm for 5 minutes. The supernatant, which corresponds to the soluble protein fraction, was saved. The protein concentration was determined by the BCA assay.

b. Whole cell lysate

Whole cell lysates were prepared for applications where it was not necessary to determine the protein concentration. After collecting the floating cells (depending on the protein to be analyzed), the adherent cells were detached from the culture vessel by trypsinization and

were washed once with 1x PBS. The cells were resuspended in 1x SDS loading buffer (double the volume of the cell pellet) and boiled immediately at 95°C for 5 minutes. The cell lysate was either loaded directly on SDS-PAGE gel or stored at –80°C until further use.

2.2.3.2 Protein quantification

The protein extracted following the protocols described in section 2.2.3.1.a was quantified using the Micro BCA™ protein assay reagent kit (Pierce). This method is based on the detection of Cu^{+1} ions by bicinchoninic acid (BCA) [148]. The Cu^{+1} ions are formed by the reduction of Cu^{+2} by the protein in an alkaline environment. The end product is a purple-colored water soluble complex that has an absorbance^{max} at 562nm.

One volume of WR reagent (containing reagents MA:MB:MC in the ratio of 25:24:1) was mixed with equal volume of the diluted protein and incubated at 37°C for 2 hours. Reagent MA provides the alkaline environment required for the reaction, Reagents MB and MC contributes the bicinchoninic acid and Cu^{+2} ions respectively. After the purple color has developed, the microtitre plate was allowed to cool down to room temperature and the absorbance at 562nm was measured on a plate reader (SpectraMax190, Molecular Devices). The protein concentration of the unknown samples was determined from the standard curve plotted for the BSA standards.

2.2.3.3 Co-Immunoprecipitation

Co-Immunoprecipitation is the method of choice to detect Protein-protein interactions. This method uses an antibody to immunoprecipitate the antigen (bait protein) and co-immunoprecipitate any interacting partners (prey proteins). The components of the protein complex can be analyzed by SDS-PAGE (gel electrophoresis), often followed by Western blot detection to verify the identity of the antigen. Co-Immunoprecipitation was performed using the Profound mammalian Co-Immunoprecipitation kit from Pierce Biotechnology according to manufacturer's instructions. In this method, an antibody against a specific target antigen was covalently immobilized on amine-reactive gel. Co-IP methods that use Ptotein A or G result in detection of antibody along with the proteins of interest. Because the antibody heavy and light chains may co-migrate with one of the relevant bands, the important data may be masked. This problem is not encountered with this kit because the antibody is retained on the gel by covalent binding.

Antibody immobilization

The antibody coupling gel and other reagents provided by the manufacturer was equilibrated to room temperature. 100µl of antibody coupling gel was transferred into a spin column and was washed 2 times with 0.4ml of coupling buffer (0.1%Triton X-100/PBS) by inverting and gently shaking the tube 4-5 times and centrifuging the tubes briefly. 200µg of purified antibody against the bait protein diluted in coupling buffer to a final volume of 400µl was then added to the coupling gel. The beads were resuspended well by inverting the column and shaking gently. 5µl of 5M sodium cyanborohydride was added to every 100µl of diluted antibody added to the gel and the tubes were inverted 4-5 times to mix well. The coupling was performed by incubating the columns overnight at 4°C on an end to end shaker. The tubes were then centrifuged to remove the antibody solution and then washed once by adding 400µl of coupling buffer. 400µl of quenching buffer was added to the gel followed by 4µl of 5M sodium cyanoborohydride. The slurry was incubated at RT for 30 min on an end to end shaker. The tubes were centrifuged and the flow through was discarded. The gel was then washed 4 times with 400µl of washing buffer and two times with 400µl of coupling buffer. Finally the columns were stored at 4°C with the gel resuspended in 400µl of coupling buffer.

Preparation of cell lysates

HEK293T cells were seeded in 15cm dishes ($3x10^6$ cells/dish) and incubated overnight at 37°C. On the following day, cells were lysed with M-Per lysis buffer (Pierce Biotechnology) as described in section 2.2.3.1a.

Co-ImmunoPrecipitation

4mg of total protein was diluted in the coupling buffer to a final volume of 1.4ml and then added to the gel with immobilized antibody. The tubes were inverted 4-5 times and incubated for 2hrs at RT on an end to end shaker. The tubes were centrifuged and the flow through was collected for further analysis and stored at –80°C. The columns were washed 3 times with 400µl of coupling buffer by inverting the tubes 10 times followed by centrifugation. The wash fractions were collected and kept aside for further analysis. The protein complexes were eluted from the antibody coupled gel by adding 50µl of elution buffer and tapping the tubes gently to allow resuspension of the gel in the elution buffer. The columns were then centrifuged and the elution fractions were collected for further analysis. The Flow through, wash and elution fractions were resolved by SDS-PAGE and further analyzed by western blotting.

2.2.3.4 Protein gel electrophoresis (SDS-PAGE)

Sodium dodecylsulfate-polyacrylamide gel electrophoresis (SDS-PAGE) is a very common method used to separate proteins based on their molecular weight. It is based on the principle that SDS, an anionic detergent, denatures the proteins by binding to their hydrophobic regions, thus rendering them negatively charged. The negatively charged proteins are then resolved on a polyacrylamide gel. This method was used in combination with Western blotting to detect a protein of interest, or to determine the abundance or distribution of a certain protein in different sub-cellular fractions. Western blotting or immuno blotting is a method to detect a protein of interest in a sample by using a specific antibody directed against that protein.

In SDS-PAGE, a stacking gel is combined with a resolving gel. The stacking gel has a large pore size and is used to stack to proteins before they reach the resolving gel. Protein separation is achieved in the resolving portion. The separating gel (resolving gel) was cast by combining the reagents shown in table 2.3 according to the concentration of acrylamide required.

Table 2.3

Stock solutions (ml)	5%	7.5%	10%	12.5%	15%
37.5:1 Acrylamide/ bis-acrylamide	3.30	5.00	6.70	8.30	10.00
4x Running buffer	5.00	5.00	5.00	5.00	5.00
10% SDS	0.20	0.20	0.20	0.20	0.20
ddH_2O	11.40	9.70	8.00	6.40	4.70
10% APS	0.10	0.10	0.10	0.10	0.10
TEMED	0.067	0.067	0.067	0.067	0.067

The volumes shown in the above table are sufficient to make 4 mini-gels of 8 cm (W) x 7.3 cm (H). The gel was covered with water saturated n-butanol or water to get a horizontal gel surface. Polymerisation was allowed for ~60 minutes or till a clear liquid-gel interface was visible. Then the water or butanol was removed and a 4% stacking gel was cast on top of the resolving gel by combining the following:

4x Stacking gel	
37.5:1 Acrylamide / bis-acrylamide	1.33ml
4x Stacking gel buffer	2.50ml
10% SDS	0.10ml
Water	6.00ml
10% APS	0.10ml
TEMED.	5µl

The volumes shown above are sufficient for 4 gels.

When the stacking gel had polymerized for ~60 minutes, the whole assembly was immersed in a chamber containing running buffer. Typically 20-40µg of protein was loaded and the gel was run at 120V until the required resolution was obtained.

4x Stacking gel buffer	
Tris pH 6.8	0.5M

4x Running gel buffer	
Tris pH 8.8	1.5M

10x Tank buffer	
Tris	0.25M
Glycine	1.92M
Adjust pH to 8.3	

PAGE Running buffer	
Tank buffer	1 x
SDS	0.1%

2.2.3.5 Western blotting

Protein transfer

The proteins resolved by SDS-PAGE were transferred onto a PVDF membrane by semi-dry ectrophoretic transfer. This method uses a three buffer system consisting of Anode I, Anode II, and Cathode buffers. The membrane was first wet in 100% methanol for 5 seconds and then equilibrated in Anode buffer II. The blot was assembled on a semi-dry blotting apparatus in the order shown in Figure 2.11. Transfer of proteins was done for 1 hour at 40V.

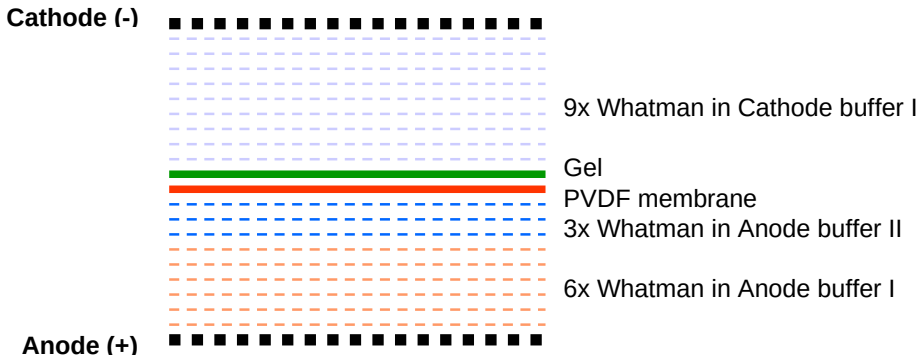

Figure 2.11. Assembly order of the blot for semi-dry blotting
From anode to cathode, the blot consists of 6 whatman papers soaked in anode buffer I, 3 in anode buffer II, PVDF membrane, gel and finally 9 whatman papers containing cathode buffer.

Cathode solution	
6-amino-n-caproic acid	40mM
Methanol	20%

Anode solution I	
Tris	300mM
Methanol	20%

Anode solution II	
Tris	25mM
Methanol	20%

Protein detection

The membrane was first stained with Ponceau S, a reversible organic stain, to check if the proteins have transferred onto the membrane. The Ponceau S staining solution was washed away with water before the membrane was blocked in the blocking solution for 1 hour at room temperature. The membrane was then incubated overnight with the primary antibody in blocking solution. Following three 10-minute washes with 0.1% Tween 20 in 1x TBS the blot was incubated for 1 hour at room temperature with the HRP-conjugated secondary antibody diluted in blocking solution. The membrane was then washed 3x 10 minutes each with 0.1% Tween 20 / 1x TBS. Equal volumes of the chemiluminescence reagents, detection solution 1 (oxidizing reagent) and detection solution 2 (enhancer reagent) from the ECL Western Blotting detection kit were mixed together and the membrane incubated in this solution for 2 minutes at room temperature. For signal detection, the blot was placed in a sheet protector, exposed to XAR film and developed at different time points using the film developing machine. The size of the proteins was determined by comparing the protein bands with that of the Rainbow protein molecular weight marker.

10x TBS	
Tris base	0.2M
NaCl	8%
Adjust pH to 7.6 with HCl	

Blocking buffer	
Non-fat dry milk	5%
Tween-20	0.1%
TBS	1 x

Wash buffer	
Tween 20	0.1%
TBS	1 x

Reprobing the immunoblot

The membrane was reprobed when it was necessary to detect another protein/proteins of interest. This was done by first stripping the membrane of the Primary antibody and the HRP conjugate. For this, the membrane was incubated at 37°C in sufficient volume of the stripping buffer with constant shaking for 20-30 minutes.

2.2.3.6 Purification of peptide antibodies

Three different antigens (peptides) per protein were designed for the production of anti-peptide antibodies (section 2.1.7). The Peptideselect™ tool from Invitrogen was used to select some regions of the full length protein which are highly antigenic, soluble and easily accessible. Polyclonal anti-Peptide antidodies were generated against three of these regions by Inno-Train Diagnostik by immunizing rabbits with synthetic peptide antigens (2 rabbits for each peptide). To avoid self-recognition of the antigen by the host animal, the rabbits to be used for immunization were selected after testing the pre-immune sera by western blotting. Three bleeds of antiserum was obtained from each rabbit, 1st bleed 1 week after initial immunization, 2nd bleed 1 month after 2nd boost, and final bleed 1 month after the 3rd boost. The antipeptide antibody was then immunopurified on an affinity column. The process of purification involves three steps:

1. Coupling of the synthetic peptide to the beads
2. Extraction / Purification of the antibody from the serum
3. Testing of the purified antibody

Coupling of peptide to beads

Affinity purification of the antibody requires the immobilization or coupling of the antigen to a matrix or a solid support. Here, the peptide was coupled to ECH Sepharose 4B (Amersham Biosciences). ECH Sepharose 4B beads are formed by covalent linkage of 6-aminohexanoic acid to Sepharose 4B. The free carboxyl groups of ECH Sepharose 4B bind to

the primary amino groups of the peptide in the presence of a carbodiimide (EDC), thus immobilizing the peptide.

The peptide (20mg) was dissolved in 1ml of distilled water adjusted to pH 4.5. Approximately 7ml of sepharose bead suspension (to get 5ml packed column of beads) was taken in a 15ml centrifuge tube and centrifuged at 1000 rpm for 5 minutes to remove the 20% ethanol in which the beads were supplied. The beads were washed with 20 column volumes of water of pH 4.5, and 500µl or 10mg of peptide was added to the beads. The ratio of matrix : ligand solution was adjusted with water (pH 4.5) to be 1:0.5 to 1:1 to produce a suspension that is suitable for coupling, and then 30mg or 250µl of EDC (in water of pH 4.5) was added to the beads. The mixture was rotated end-over-end overnight at 4°C. The pH of the mixture was checked after the first hour of incubation, which should be slightly below 7.0. When the pH had dropped down, it was adjusted by adding 0.1M sodium hydroxide. The next day, the column was washed atleast three times alternatively with high and low pH buffers to remove the excess of uncoupled peptide. The beads were washed thrice with distilled water and then stored in 0.02% sodium azide / PBS at 4°C until further use.

Acetate buffer (low pH buffer) or Elution buffer

sodium acetate	0.1M
sodium chloride	0.5M
Adjust pH to 4.0	

Tris buffer (high pH buffer)

Tris Hcl	0.1M
sodium chloride	0.5M
Adjust pH to 8.0	

Purification of antibody from the serum

The beads (coupled with the peptide) were washed twice with 1x PBS, mixed with the respective serum in a 50ml tube and incubated on an end-to-end rotator overnight at 4°C. This leads to the binding of antibody to the peptide. The beads and the serum were poured into a 5ml polypropylene column provided with a frit (Qiagen). The serum was allowed to flow through, and the beads with the peptide and the corresponding antibody were left in the column. The beads were washed with 10 column volumes (approximately 80-100ml) of 1x PBS, or until the A^{280} of the washed out PBS was nearly zero. The antibody was eluted with atleast 3-4 column volumes of elution buffer. The eluent was collected in microcentrifuge tubes on ice and the A^{280} of each fraction was measured with a spectrophotometer

(SmartSpec3000, BioRad). The fractions with high OD, which corresponds to high antibody concentation, were saved. The beads were washed with 10 column volumes of 1x PBS and stored at 4°C to be used again.

Testing of the purified antibody:

The saved antibody fractions were tested by western blotting to check if the expected protein is being recognized. The fractions with similar affinity were pooled, aliquoted and stored at –80°C.

3 Results

3.1 Establishment of high throughput apoptosis assay

The apoptotic pathways originating from different organelles converge on the activation of the caspase cascade. Caspase-3 is a major effector caspase that cleaves several important cellular substrates, and its activation is considered as the point of no return. So, activation of caspase-3 was chosen as the apoptosis marker for establishment of the apoptosis assay.

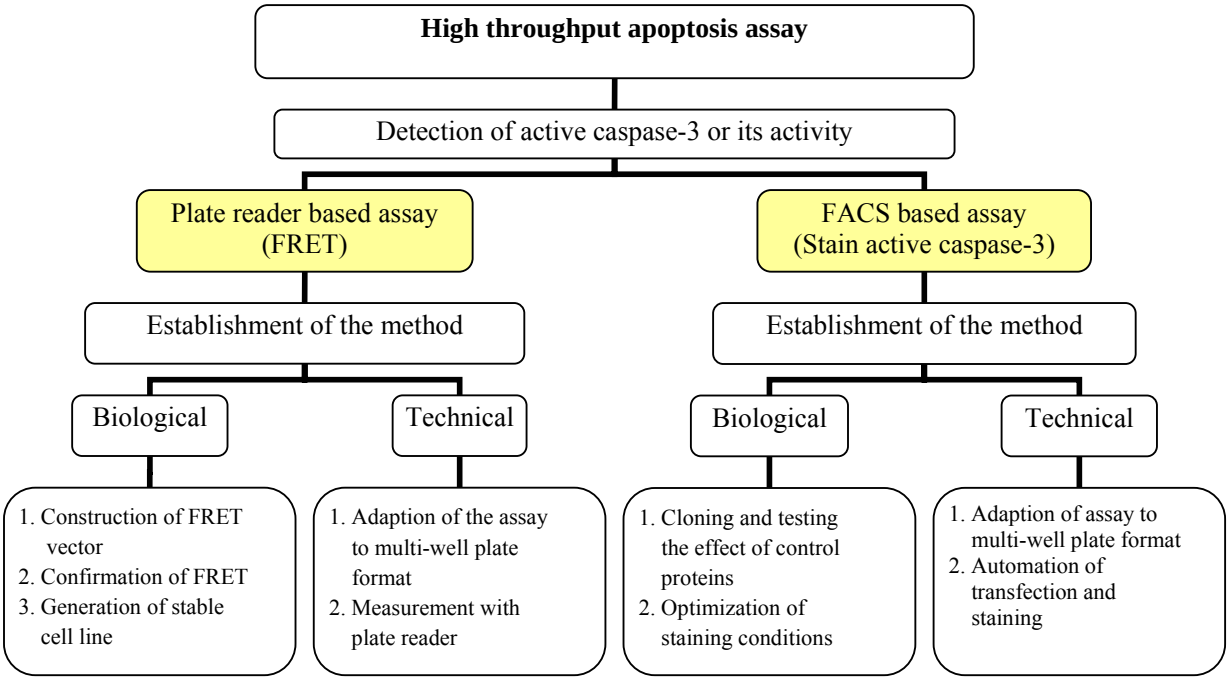

Figure 3.1. Schematic representation of various steps in the establishment of high throughput apoptosis assay
Activation of caspase-3 was selected as a marker for identification of apoptosis activators. Two assays, one FRET based plate reader assay and the other utilizing FACS to identify cells stained positive for active caspase-3 were tried. Establishment of these methods involve optimization of various biological and technical parameters, which are listed for each method.

Assaying the activity of caspase-3, and identifying the physical presence of cleaved caspase-3 are two different approaches by which activated caspase-3 can be detected. An assay to detect the activity of caspase-3 as a function of Fluorescence Resonance Energy Transfer (FRET), and another assay to detect the presence of cleaved caspase-3 by flow cytometry after staining with a specific antibody were tested for their suitability for high

throughput screening. A method suitable for high throughput screening should be sensitive enough to detect even minute changes in the parameter under question, and be amenable for automation. To meet these requirements, various biological and technical parameters of the assays need to be optimized. A schematic representation of different steps in the assay establishment is shown in Figure 3.1.

3.1.1 Induction of apoptosis with Staurosporine

NIH3T3, the mouse fibroblast cell line had been previously characterized in our department for the cell cycle regulation and activation of MAPK signalling pathway, and subsequently used for cell proliferation and signalling assays. Inorder to obtain complementary data for a set of proteins from the proliferation, MAPK and the apoptosis assays, the same cell line was chosen also for the establishment of the apoptosis assay. To determine the optimum conditions for chemically inducing apoptosis and to make sure that the apoptotic machinery necessary for programmed cell death is intact in the NIH3T3 cells, the cells were treated with staurosporine (0-3µM), and various parameters specific for apoptosis (DNA fragmentation, activation of caspase-3 and the development of morphological changes) were analyzed (Figure 3.2). Staurosporine is a broad spectrum protein kinase inhibitor which induces apoptosis through the mitochondrial pathway [149] via the activation of caspase-3 [150].

Internucleosomal DNA fragmentation was measured using the Cell death detection ELISA^{PLUS} kit (Roche) 4 hours after incubation with different concentrations of staurosporine (Figure 3.2.A). In this method, after discarding the DNA of necrotic cells, the low molecular weight DNA fragments extracted from apoptotic cells are detected using antibodies against DNA and histones in a colorimetric reaction. The absorbance measured at 405nm is indicative of DNA fragmentation (for protocol, refer section 2.2.2.7). Cells treated with 1µM staurosporine showed an absorbance of 2.6, which is >2 times higher than that of the cells treated with the vehicle alone, i.e DMSO (0µM staurosporine). However, with an increase in the concentration of staurosporine to 2 and 3µM, a corresponding decrease in the absorbance was observed. This might be due to the cytotoxic effects of higher concentration of staurosporine leading to an increase of necrosis and a decrease in the number of apoptotic cells. So, 1µM staurosporine with an incubation time of 4 hours was used for further experiments.

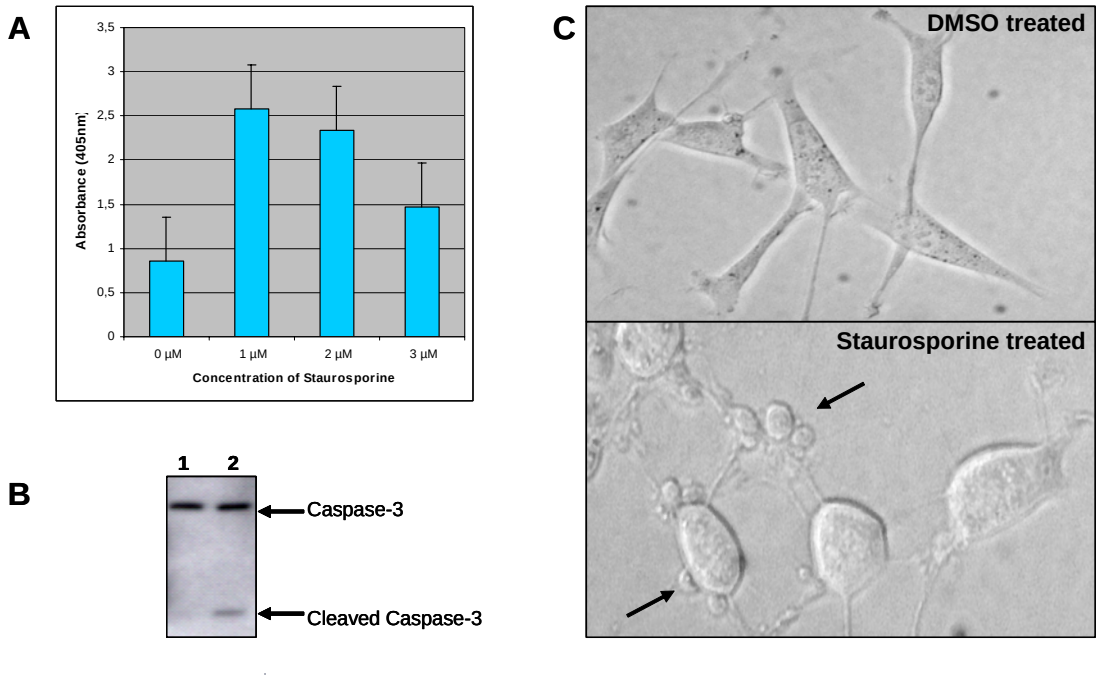

Figure 3.2. Induction of apoptosis in NIH3T3 cells
(A) The cells were treated with 0-3µM Staurosporine for 4 hours and internucleosomal DNA fragmentation was detected using the Cell death detection ELISA kit (Roche). Absorbance measured at 405nm showed that incubation with 1µM staurosporine induced maximum DNA fragmentation **(B)** Cells were treated either with DMSO (lane 1) or 1µM Staurosporine (lane 2) for 4 hours and Caspase-3 from the lysates was immunoprecipitated using an antibody detecting both uncleaved and cleaved forms of Caspase-3. The protein was then resolved by SDS-PAGE and the caspase-3 was detected using the same antibody. **(C)** Morphology of cells treated either with DMSO or 1µM Staurosporine for 4 hours. Apoptotic bodies in case of Staurosporine treated cells are shown with arrows.

Since activation of caspase-3 was selected as apoptosis marker for the assay, the cleavage of caspase-3 after treatment with staurosporine was verified by wester blotting (Figure 3.2.B). For this, NIH3T3 cells were either treated with DMSO alone or incubated with 1µM Staurosporine for 4 hours, and cell lysates made from these samples were immunoprecipitated using a caspase-3 antibody which recognizes both cleaved and uncleaved forms. The proteins were then resolved by SDS-PAGE and the membrane was probed with the same antibody. Cells treated with DMSO alone (lane 1) showed a single band at 32kDa corresponding to the size of uncleaved caspase-3. However, cells treated with staurosporine (lane 2) showed two bands, one at 32kDa and another at 17kDa corresponding to the size of uncleaved and cleaved caspase-3 respectively. This shows that treatment with 1µM staurosporine induces cleavage of caspase-3. To check if the observed effects correlate with induction of morphological changes, cells treated either with DMSO or 1µM staurosporine for 4 hours were monitored under a light microscope (Figure 3.2.C). Staurosporine induced morphological changes characteristic of apoptosis i.e. rounding off of the cells, membrane blebbing, and detachment from the surface while cells treated with DMSO alone did not show

any changes in morphology. This shows that treatment with 1µM staurosporine induces features characteristic of apoptosis, and that the components necessary for undergoing apoptosis are intact in NIH3T3 cells.

3.1.2 Establishment of FRET based assay

FRET is the radiationless transmission of energy from an excited fluorophore (donor) to another fluorophore (acceptor) when both are located within close proximity (1-10nm). Based on this principle, an assay was designed which would allow the screening for apoptosis activators in a 96-well format using a fluorescence plate reader.

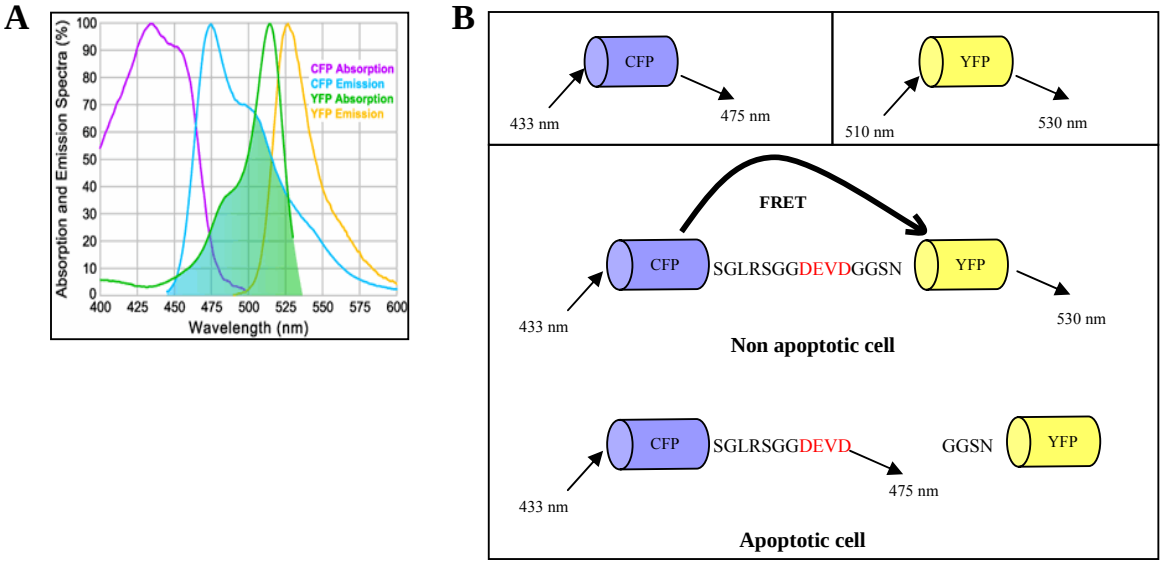

Figure 3.3. Principle of the FRET based assay
(A) Fluorescence spectra of CFP and YFP. The shaded area represents the spectral overlap between CFP and YFP which makes them an ideal FRET pair. **(B)** The top panels show the excitation and emission wavelengths of CFP and YFP. Bottom panel shows principle of FRET. In non apoptotic cells, upon excitation of the donor fluorophore (CFP) at 433nm, the emitted energy (475nm) is transferred to the acceptor (YFP) and is re-emitted at 530nm. In apoptotic cells, the linker region is cleaved by caspase-3 resulting in the elimination of FRET.

In this assay, a construct encoding CFP (donor) and YFP (acceptor) linked together with the substrate for caspase-3 (DEVD) acts as the FRET probe (Figure 3.3). CFP and YFP were chosen as the FRET pair because of overlap of the emission spectrum of CFP with the absorption spectrum of YFP which results in an efficient transfer of energy from CFP to YFP (Figure 3.3.A). In non apoptotic cells, when CFP is excited by light at 433nm, the emitted light is taken up by YFP which it in turn emits light at 530nm due to FRET (Figure 3.3.B). In apoptotic cells the linker region is cleaved by activated caspase-3, and the FRET is eliminated. So, when CFP is excited at 433nm, the detected emission would be at 475nm, and

not at 530nm. When a stable cell line constitutively expressing this FRET probe is transiently transfected with apoptosis inducers, cleavage of DEVD by activated caspase-3 would cause a decrease in FRET between CFP and YFP, which can be measured by a fluorescence plate reader. However, this method does not allow the discrimination between transfected and the untransfected cells. Therefore, cells would be transfected with ORFs tagged with 6x His, and after measuring the FRET, the same wells would be stained with anti-His antibody to determine the transfection efficiency in a colourimetric reaction.

3.1.2.1 Generation of FRET constructs

A FRET probe (designated as CFP-DEVD-YFP) was constructed with CFP and YFP fused together by a special linker containing a caspase-3 cleavage sequence (DEVD).

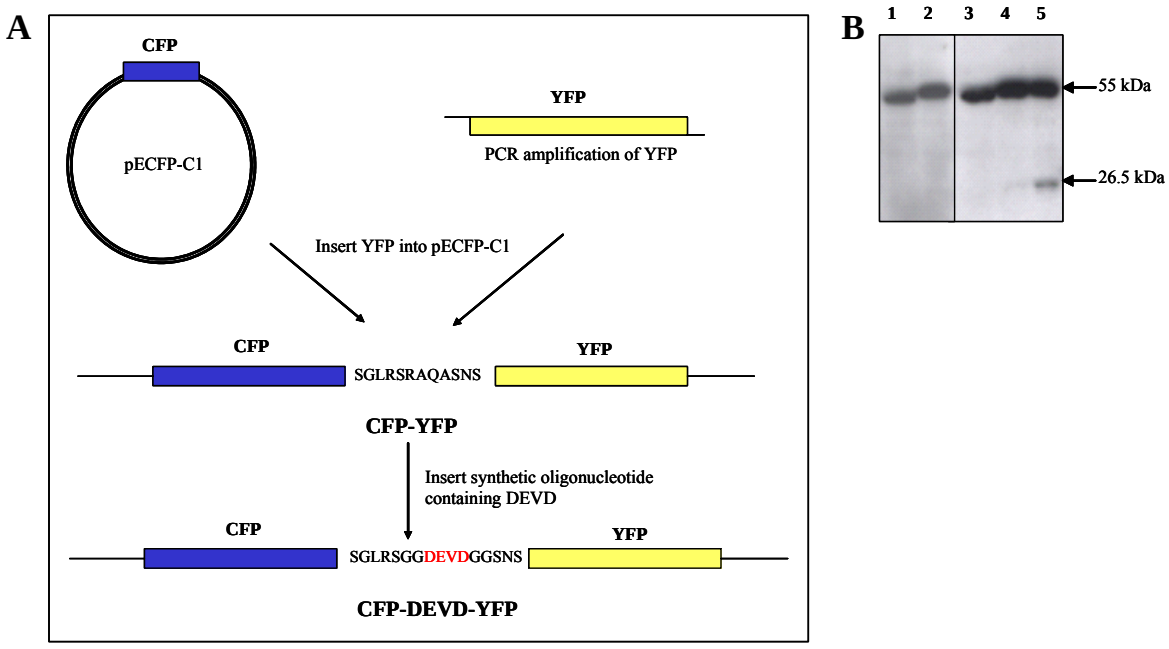

Figure 3.4. Generation of FRET vector
(A) YFP was amplified and cloned at the C-terminus of CFP in pECFP-C1 vector generating the construct CFP-YFP. Synthetic oligonucleotides encoding DEVD were inserted between CFP and YFP to generate the FRET construct CFP-DEVD-YFP. **(B)** Cells expressing CFP-YFP (lanes 1 and 3) or CFP-DEVD-YFP (lanes 2, 4 and 5) were either left untreated (lanes 1 and 2) or treated with 1µM staurosporine for 2 hours (lane 4) or 4 hours (lanes 3 and 5). Treatment with 1µM staurosporine resulted in cleavage of the linker region in CFP-DEVD-YFP, but not in CFP-YFP.

To construct the probe, YFP was amplified from pCaspase-3 sensor vector (using the primers mbYFPE1B1_fw and mbYFPE1B1_rv), and cloned at the C-terminus of CFP in the vector pECFP-C1 (Figure 3.4.A). This construct was termed as CFP-YFP, and was used as a

control probe. Two synthetic oligonucleotides (mbFRETspacer_up and mbFRETspacer_down) encoding DEVD were then inserted between the CFP and YFP to form the linker (for protocol refer to section 2.2.1.3b). This construct was called CFP-DEVD-YFP and serves as the FRET probe. The 16 amino acid linker used here was shown previously by Luo KQ et al., to produce a strong FRET effect, and also to be efficiently cleaved by caspase-3 because of the special design of the sequence flanking the DEVD substrate site [151].

To check if the DEVD substrate site present in the linker is accessible for cleavage by caspase-3, NIH3T3 cells transiently transfected with CFP-YFP or CFP-DEVD-YFP were either treated with 1μM staurosporine for 2 and 4 hours or left untreated. The cell lysates were resolved by 12% SDS-PAGE and the membrane was probed with anti-GFP antibody (Figure 3.4.B). In untreated cell lysates, both CFP-YFP (lane 1) and CFP-DEVD-YFP (lane 2) showed a single band near 55kDa which is the expected molecular weight of the FRET probe. Treatment with 1μM staurosporine for 2 hours did not yield significant amount of cleavage product (lane 4). However, in samples treated with 1μM staurosporine for 4 hours, the control probe remained unaffected (lane 3), while the FRET probe showed a second band near 27kDa (lane 5) which corresponds to the molecular weight of separated CFP and YFP due to cleavage of the linker by caspase-3. This showed that the DEVD substrate site was accessible to caspase-3.

3.1.2.2 Determination of FRET

The occurrence of FRET between CFP and YFP in the FRET probe was then determined by confocal microscopy using a technique called acceptor photobleaching [152]. When FRET occurs, there is quenching of the donor fluorescence signal since some of the donor excitation energy is transferred to the acceptor. Selective photobleaching of the acceptor abolishes FRET, and in regions where FRET occurred there will be an increase in donor emission because of dequenching.

To check if there is an energy transfer between CFP and YFP, defined areas on cells expressing CFP-DEVD-YFP were subjected to acceptor photo-bleaching. A series of time lapse images were made during the process of bleaching the acceptor (YFP). Figure 3.5.A shows the pre- bleach (a-c) and post bleach (d-f) images of a cell taken at 0 and 16 seconds respectively. The bleached region of the cell is shown with an arrow (Figure 3.5.Ae). For analysis, two regions of interest (ROI) were defined on the cell, ROI 1 being the bleached region and ROI 2 the unbleached region (Figure 3.5.Af). The fluorescence intensities of CFP

and YFP in these ROI were plotted against the time of bleaching (Figure 3.5.B). In ROI 1, loss of fluorescence intensity of YFP was observed from 5 seconds after the start of the bleaching cycle reaching a maximum at 16 seconds, after which the intensity remained constant. The decrease in the intensity of YFP was accompanied by a corresponding increase in the fluorescence of CFP, which also remained constant after 16 seconds. However, no significant differences in the spectra were noticed in case of ROI 2. These results indicate the occurrence of FRET between CFP and YFP.

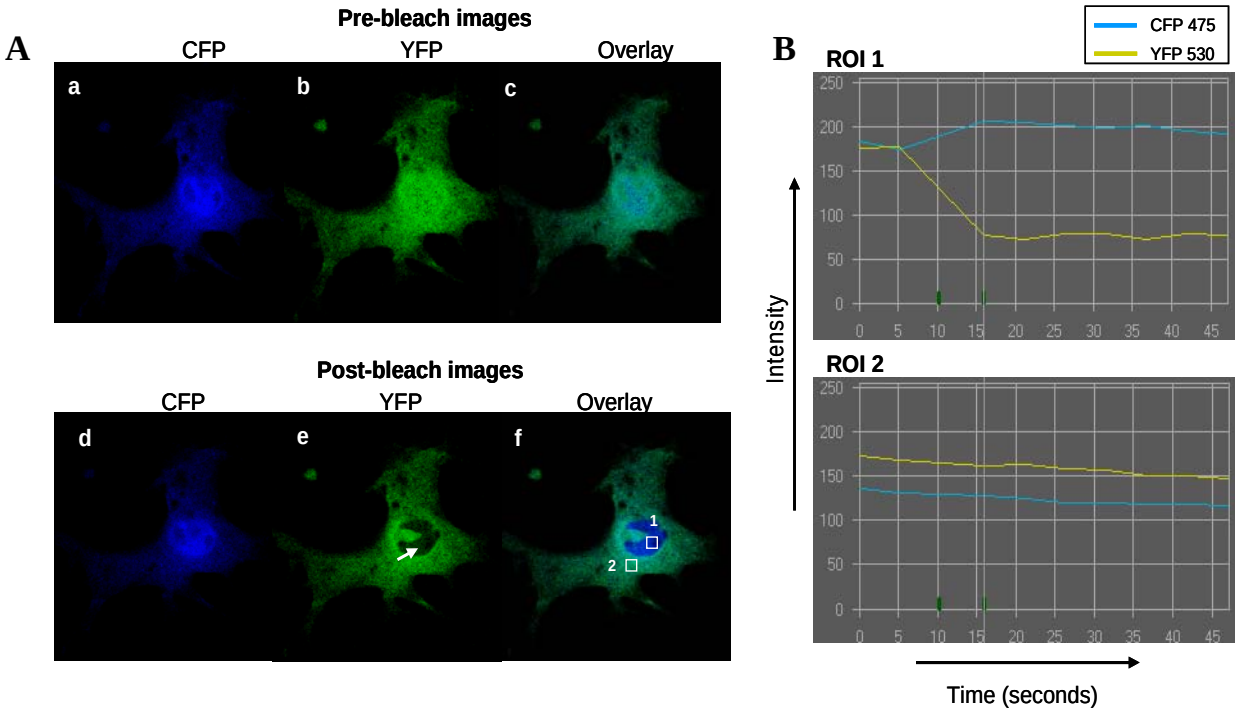

Figure 3.5. Determination of FRET by acceptor photo-bleaching
(A) NIH3T3 cells were transfected with CFP-DEVD-YFP and fixed 24 hours later. Images of the donor and the acceptor were obtained before (a-c) and after (d-e) photo-bleaching of the acceptor in the center of the cell (indicated with an arrow in e). Two Regions of Interest (ROI) were selected (indicated by 1 and 2 in f) to determine the FRET efficiency. **(B)** Inside the bleached region (ROI 1), the donor is unquenched resulting in an increase in intensity indicative of FRET, while in ROI 2 no increase in the intensity of donor was detected.

3.1.2.3 Adaption of the assay to 96-well format

Since the requirements of a FRET probe i.e., the accessibility of the cleavage site, and occurrence of FRET have been fulfilled, the next step was to adapt the assay to 96-well fluorescence plate reader. To achieve a uniform fluorescence read out from all the wells, it was necessary to generate a stable cell line expressing the control and the FRET probes.

a. Generation of stable cell line

Stable cell lines of NIH3T3 cells constitutively expressing CFP-DEVD-YFP and CFP-YFP were generated. The protein expression level of the positive clones was tested by immunoblotting using anti-GFP antibody (Figure 3.6.A). Two clones from CFP-YFP (lanes 2 and 3) and seven clones from CFP-DEVD-YFP (lanes 1,4,5,8,9,10 and 14) were found to contain the correct insert. Clone 2 from CFP-YFP and clone 4 from CFP-DEVD-YFP (due to high expression level) were selected for further experiments.

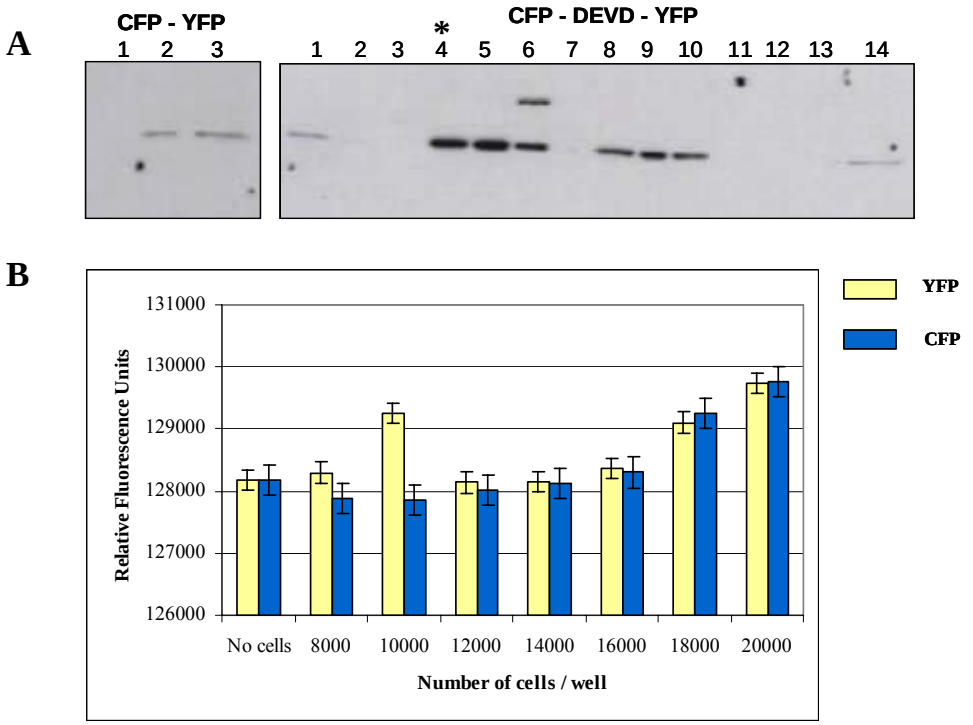

Figure 3.6. Generation of stable cell line and measurement with fluorescence plate reader
(A) Cell lysates of clones stably expressing CFP-YFP and CFP-DEVD-YFP were resolved by SDS-PAGE and the protein was detected with anti-GFP antibody. **(B)** Different cell numbers of clone 4 from CFP-DEVD-YFP were seeded in 96-well plate and the fluorescence intensities of CFP and YFP were measured with a fluorescence plate reader. Fluorescence intensity more than the back ground signal (empty wells) was observed only in wells with more than 18,000 cells/well.

b. Measurement of fluorescence intensity on a plate reader

Cells stably expressing the FRET probe (clone 4) were seeded into 96-well black culture plates (8,000 cells/well), and the fluorescence of YFP (filters: excitation 510/10nm; emission 535/10) and CFP (filters: excitation 440/35; emission 485/20) was measured on a fluorescence plate reader Fusion$^{TM}\alpha$. But the signal detected in the wells with cells was equal to that of the background signal i.e. wells with out any cells. To check if the signal intensity increases with an increase in cell number, the measurement was repeated with different cell

numbers ranging from 8,000 to 20,000 cells/well (Figure 3.6.B). The fluorescence intensity remained equal to that of the back ground signal till a cell number of 14,000 cells/well. The intensity gradually increased with increase in cell number from 16,000 to 20,000 cells/well. However, cell numbers of more than 14,000 cells/well in a 96-well plate resulted in a very confluent monolayer which is not suitable for transfection. Too many cells result in contact inhibition, making cells resistant to uptake of foreign DNA. Moreover, minute changes in the signal caused by cleavage of the FRET probe in apoptotic cells might not be detected at all when the instrument is not sensitive enough. A more sensitive way to detect changes in FRET signal would be by microscopy. But microscopy is not an ideal method for a high throughput FRET based assay because photo-bleaching of individual cells in a 96-well plate to analyze FRET is a very cumbersome and time consuming process, and difficult to automate.

So, another assay for the detection of activation of caspase-3 in apoptotic cells was developed using Fluorescence activated cell sorter (FACS).

3.1.3 Establishment of flow cytometry based assay to detect active caspase-3

Cytometry is a very sensitive method and allows rapid and accurate analysis of large populations of individual cells. Moreover, this method offers the advantage that several parameters of the same population can be measured simultaneously, and the observed effects can be correlated on a cell by cell basis. Due to these advantages, a FACS based apoptosis assay was designed to detect the presence of cleaved caspase-3 by staining cells with an active caspase-3 specific antibody. The cells would be transfected with YFP tagged ORFs so that it is possible to differentiate the transfected from untransfected cells.To speed up the process of data acquisition, the stained cells would be measured on a FACSCalibur equipped with a 96-well plate reader. When transfected cells show a higher amount of active caspase-3 compared to the untransfected cells of the same well, the protein is considered as an apoptosis inducer.

3.1.3.1 FACS measurement of active caspase-3 in staurosporine treated cells

Activation of caspase-3 requires proteolytic processing of its inactive zymogen into activated p17 and p12 fragments due to cleavage adjacent to Asp175. A rabbit polyclonal antibody (Cell signalling technology) detecting the endogenous levels of the large fragment (17kDa) of activated caspase-3 was used for establishment of the assay.

The functionality of the antibody was tested in NIH3T3 cells which were induced to undergo apoptosis by treating with 1μM staurosporine for 4 hours. Cells without any

treatment were used as control. The cells were trypsinized and stained in suspension with active caspase-3 antibody, followed by a secondary antibody labelled with allophycocyanin (APC). Data from at least 10,000 cells was acquired using FACSCalibur, and the data analysis was done with Cellquest™ Pro software (Figure 3.7).

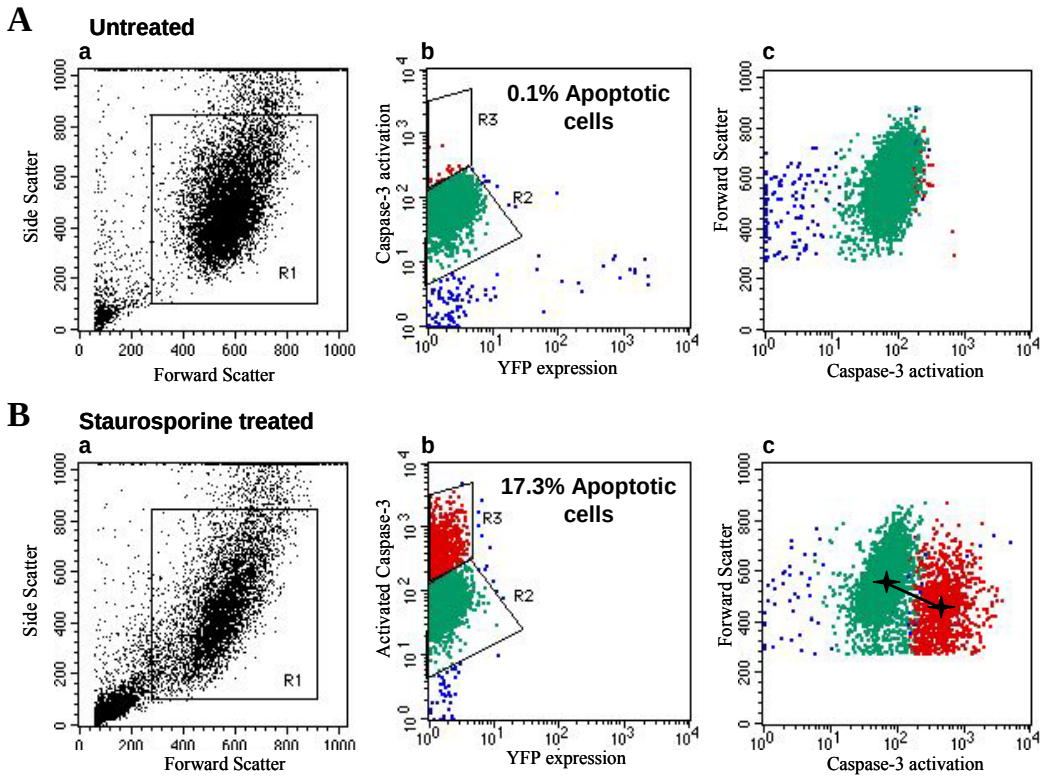

Figure 3.7. Detection of Staurosporine induced apoptosis with active Caspase-3 antibody
Cells were treated with 1µM Staurosporine for 4 hours or left untreated, stained with cleaved Caspase-3 antibody followed by allophycocyanin (APC) coupled secondary antibody and measured with FACS. **(A)** Scatter plots of untreated cells show that 0.1% of the cells are apoptotic. **(B)** Treatment with Staurosporine induced apoptosis in 17.3% of cells (indicated with red colour). These cells also displayed a reduction in size as indicated by a reduction in forward scatter (the center of each population is marked). Gates R1, R2 and R3 represent the intact, non-apoptotic and apoptotic populations respectively.

The scatter plots with forward scatter vs. side scatter show the morphology of the cells, with forward scatter representing the size, and side scatter the granularity of cells (Figure.3.7.Aa and Ba). To eliminate the interference of contaminants like cell clumps and debris in data processing, the main population of cells from the untreated sample (seen as a dense cloud in the centre of the plot) were gated as R1 (Figure.3.7.Aa). Only the cells in gate R1 were used for further analysis. The activation of caspase-3 was then analyzed from the scatter plot drawn with fluorescence intensity of YFP against APC signal which represents the activation of caspase-3 (Figure.3.7.Ab). The cells in this scatter plot are the untreated cells which are negative for activated caspase-3, and were gated as R2. Cells that show more APC signal than the cells in gate R2 were considered positive for activated caspase-3, and were

gated as R3. Therefore, gates R2 and R3 represent non apoptotic and apoptotic populations, respectively. To analyze the morphology of cells, another scatter plot was drawn with forward scatter plotted against APC signal of activated caspase-3 (Figure 3.7.Ac). The non apoptotic cells from gate R2 are shown in green and apoptotic cells from gate R3 are shown in red colour. The cells treated with staurosporine were analyzed in the same way using the same gates as that of the untreated cells (Figure 3.7.B).

As is evident from the scatter plots with forward vs. side scatter, cells treated with staurosporine showed an elongated distribution pattern compared to the normal cells (Figure 3.7.Aa and Ba). This indicates a change in the light scatter property of cells due to induction of morphological features of apoptosis. Scatter plots with intensity of YFP plotted against APC signal (activation of caspase-3) showed that 17.3% of cells from gate R1 in staurosporine treated sample were positive for activated caspase-3 compared to 0.1% in the untreated sample (Figure 3.7.Ab and Bb).

It is described that cells undergoing apoptosis show a reduction in size [130]. Since forward scatter represents the size of a cell, the reduction in size should result in a reduction in the forward scatter. So this parameter was used to verify if the cells recognized by the antibody are apoptotic. For this, scatter plots are drawn with fluorescence intensity in the APC channel plotted against forward scatter, and shift in the distribution of active caspase-3 positive cells is indicated by a line connecting the centers of both the populations (Figure 3.7.Bc). This scatter plot shows that the cells positive for active caspase-3 (shown in red) indeed show a reduction in size compared to active caspase-3 negative cells (shown in green). This indicates that the antibody can be used for flow cytometric applications and that it specifically recognizes apoptotic cells. Since the assay is based on overexpression of proteins, it was necessary to check the functionality of the assay by overexpressing some proteins which are known inducers of apoptosis.

3.1.3.2 Generation of positive controls for the assay

In order to examine the effect of protein overexpression on apoptosis, control proteins whose function is already known, were selected (table 3.1). The cDNAs were amplified and cloned into the Gateway™ destination vectors, resulting in the generation of ORFs tagged C- or N-terminally with YFP. Although it is not described for some of these proteins if overexpression induces apoptosis or not, they were shown to either directly or indirectly activate apoptosis. Along with the positive controls, proteins without any known effect on

apoptosis (neutral controls) were also selected. The list of the control proteins along with the cell line in which we overexpressed them is shown in table 3.1.

Table 3.1. Control proteins tested in the assay

Protein	Role in assay	Function	Cell line
Cathepsin B	Activator	Cysteine protease, degrades intra- and extra cellular proteins, can activate BID and caspases [97].	NIH3T3
Cathepsin D	Activator	Aspartic protease, protein degradation, involved in oxidative stress related apoptosis pathway, activates Bax by proteolytic cleavage [153].	NIH3T3
Fas receptor	Activator	Cell surface receptor of the TNFR super family, starts the death receptor pathway of apoptosis upon ligation with Fas ligand [18].	NIH3T3 and HEK293T
Death associated protein (DAP3)	Activator	It is a mitochondrial protein and acts down stream of several apoptotic stimuli like TNFα, IFNγ and Fas ligand [154].	NIH3T3
Cell death inducing DFF-A like effector (CIDE-C)	Activator	Over expression of CIDE proteins induce DNA fragmentation and apoptosis, which can be inhibited by DFF. The C-terminal domain of these proteins (CIDE-C) is sufficient for inducing apoptosis, while N-terminal (CIDE-N) is required for DFF45 to inhibit CIDE induced apoptosis [155].	NIH3T3 and HEK293T
Cytochrome-c	Activator	Following apoptotic stimulus, cytochrome c releases from the mitochondria and induces the formation of apoptosome [43].	HEK293T
Apoptosis inducing factor (AIF)	Activator	It is a mitochondrial protein, which upon receiving the apoptosis stimulus translocates to the nucleus and induces chromatin condensation and fragmentation of DNA [156].	HEK293T
Cyclin dependent kinase 2 (CDK2)	Neutral	It is a member of the protein kinase family that in association with cyclins initiates the transition of G1 to S- phase of the cell cycle and progression through the S-phase [157].	HEK293T
Yellow Fluorescent Protein (YFP)	Neutral	Spectral variant of Green fluorescent protein (GFP) [158].	NIH3T3 and HEK293T

3.1.3.3 Effect of control proteins on induction of apoptosis in NIH3T3 cells

To check if overexpression of the control proteins induces apoptosis, NIH3T3 cells were transfected with plasmid DNA maxi preparations of a subset of clones from table 3.1, stained 72 hours later with the active caspase-3 antibody and measured with FACS. The scatter plots obtained from N-terminally tagged proteins are shown in Figure 3.8. Based on the distribution of cells from mock transfected sample, quadrants were drawn on the scatter plot separating the 4 different populations (Figure 3.8a). Untransfected, non apoptotic cells are in the lower left quadrant; untransfected, apoptotic in upper left; transfected, non apoptotic

in lower right; and transfected, apoptotic cells in the upper right quadrant. The other proteins were analyzed using the same quadrants as those of the mock transfected sample. A protein was considered as an activator when the percentage of transfected apoptotic cells was significantly higher than that of the percentage of untransfected apoptotic cells. The value obtained for the neutral control (YFP) was taken as the threshold for deciding if the protein is an apoptosis activator. A summary of the effects due to overexpression of the control proteins is shown in table 3.2. The Fas protein was identified as a strong inducer of apoptosis (highlighted in table 3.2).

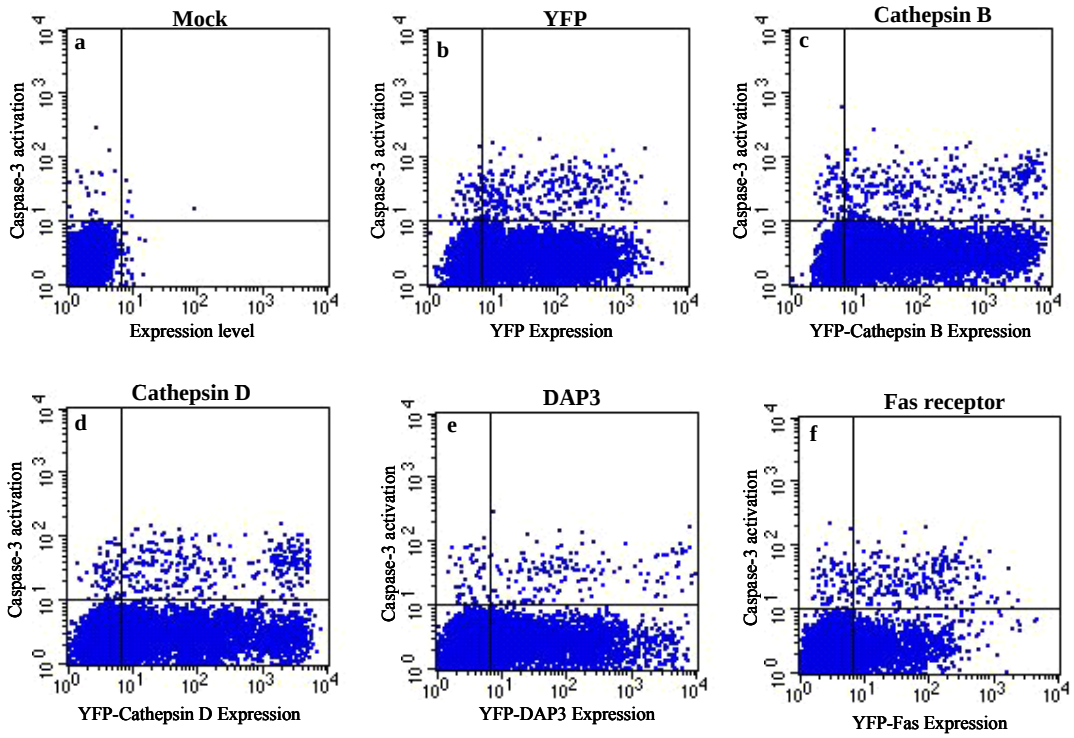

Figure 3.8. Selection of positive controls for the assay
NIH3T3 cells transfected with N-terminally tagged control proteins were stained after 72 hours with the active Caspase-3 antibody and measured with FACS. Shown are the plots with expression level of the protein plotted against the signal intensity of activated caspase-3. Quadrants are drawn to separate different populations of cells resulting from expression of the protein.

Table 3.2.

Protein	% Transfection	% Untransfected apoptotic cells (A)	% Transfected apoptotic cells (B)	Difference (B-A)
YFP	56.75	1.62	5.31	3.69
Cathepsin B	64.53	2.49	6.00	3.51
Cathepsin D	46.31	1.38	7.00	5.62
DAP 3	35.19	0.93	4.55	3.62
Fas	**16.49**	**0.98**	**14.00**	**13.02**

The transfection efficiency of different proteins ranged from 16.49 to 64.53%, with Fas receptor showing the least transfection as well as protein expression level (Figure 3.8f). The percentage of untransfected apoptotic cells did not vary much between different proteins (0.93 to 2.49%) indicating that the transfection procedure itself did not induce significant cytotoxicity. However, overexpression of YFP resulted in a slight increase in the apoptotic cells compared to the untransfected cells of the same well. The percent of apoptotic cells in Cathepsin B and DAP3 transfected wells did not differ significantly from that of YFP transfected samples. However, Cathepsin D showed a slight activating effect, with cells expressing high amount of protein undergoing apoptosis, but the total effect is not clear. Even though the transfection efficiency and protein expression level of Fas is much lower than the other proteins, overexpression of Fas induced apoptosis in 14% of the transfected cells, while only 0.98% of the untransfected cells were positive for cleaved caspase-3. These results suggest that this assay is capable of identifying proteins whose overexpression induce apoptosis. Fas would be used as a positive control and YFP as neutral control for the assay.

3.1.3.4 Automation of the assay

As the assay was ultimately intended for high throughput screening, it was necessary to minimize the number of steps which require manual intervention. So the next step in the establishment of the assay was to automate all the liquid handling steps for the process of transfection and staining (done in collaboration with Christian Schmidt). For this purpose, a pipetting robot (MultiProbe II^{EX}, Perkin Elmer) was used.

The process of transfection involves removal of medium from the cells, preparation of DNA complexes in 96-well plates and pipetting the complexes into the appropriate wells. Since NIH3T3 cells adhere well to the culture plates, the process of aspirating the medium from the wells and the washing steps done by the robot during transfection did not result in significant cell loss.

However, staining of the cells by the robot required some optimization steps to minimize loss of cells. The cells were stained in suspension in 96-well plates and the process of staining involved several washing and centrifugation steps (refer to section 2.2.2.8 for protocol). The robot removes buffers from the wells by aspiration which resulted in loss of cells in every step. To obtain sufficient cell numbers for statistical analysis, a series of test runs were performed on the robot with different conditions (as shown in table 3.3). For this, 9,000 cells/well were seeded in 96-well plates, allowed to grow overnight and the whole

staining protocol was followed (without using antibodies). The cell numbers obtained with various conditions is shown in table 3.3. Condition that gave the best result is highlighted.

Table. 3.3.

Kind of 96-well Plate	Material of plate	Method of removing buffer	Centrifugation speed (rpm)	Cell number after staining/ well
Flat bottom	Polystyrol	Aspiration at 70 µl/sec	1200	**62**
Flat bottom	Polystyrol	Tipping the plate	1200	**90**
U-bottom	Polystyrol	Aspiration at 70 µl/sec	1000	**495**
U-bottom	Polystyrol	Aspiration at 30 µl/sec	1200	**510**
U-bottom	**Polypropylene**	**Aspiration at 30 µl/sec**	**1350**	**1,270**

Lowest cell number was obtained with flat bottom plates (< 100 cells/well) and the cell number increased to 1,270 cells/well when U-bottom plates were used. Though reduction in the speed of aspiration from 70µl/second to 30µl/second and an increase in the centrifugation speed from 1,000 to 1,350 rpm had some positive effect, change in the material of the plate from polystyrol to polypropylene significantly increased the cell number. Based on these experiments, polypropylene U-bottom plates in combination with aspiration speed of 30µl/second and centrifugation at 1,350 rpm were taken as the optimum conditions for staining on the robot. Since cells cultured in polypropylene U-bottom plates can not be easily observed under a microscope (due to the material and thickness of the plate), the cells would be cultured and transfected in polystyrol flat bottom plates and transferred into a U-bottom polypropylene plate for staining on the robot.

3.1.3.5 Effect of mini-prep DNA on the assay result

Having optimized the transfection and staining on the robot, the next step was to run a test screen to verify if the automated transfection and staining conditions on the robot were optimal for identifying apoptosis activators. Since mini preparations of DNA would be used for the screening, miniprep DNA of 96 different ORFs were distributed in a 96-well plate, and the transfection of the cells with this DNA (100 ng/well) as well as the staining were done on the robot. The cells were then measured with FACS equipped with an integrated 96-well plate reader. An overview of the total cell number/well and the transfection efficiency obtained over the whole plate is shown in Figure 3.9.A.

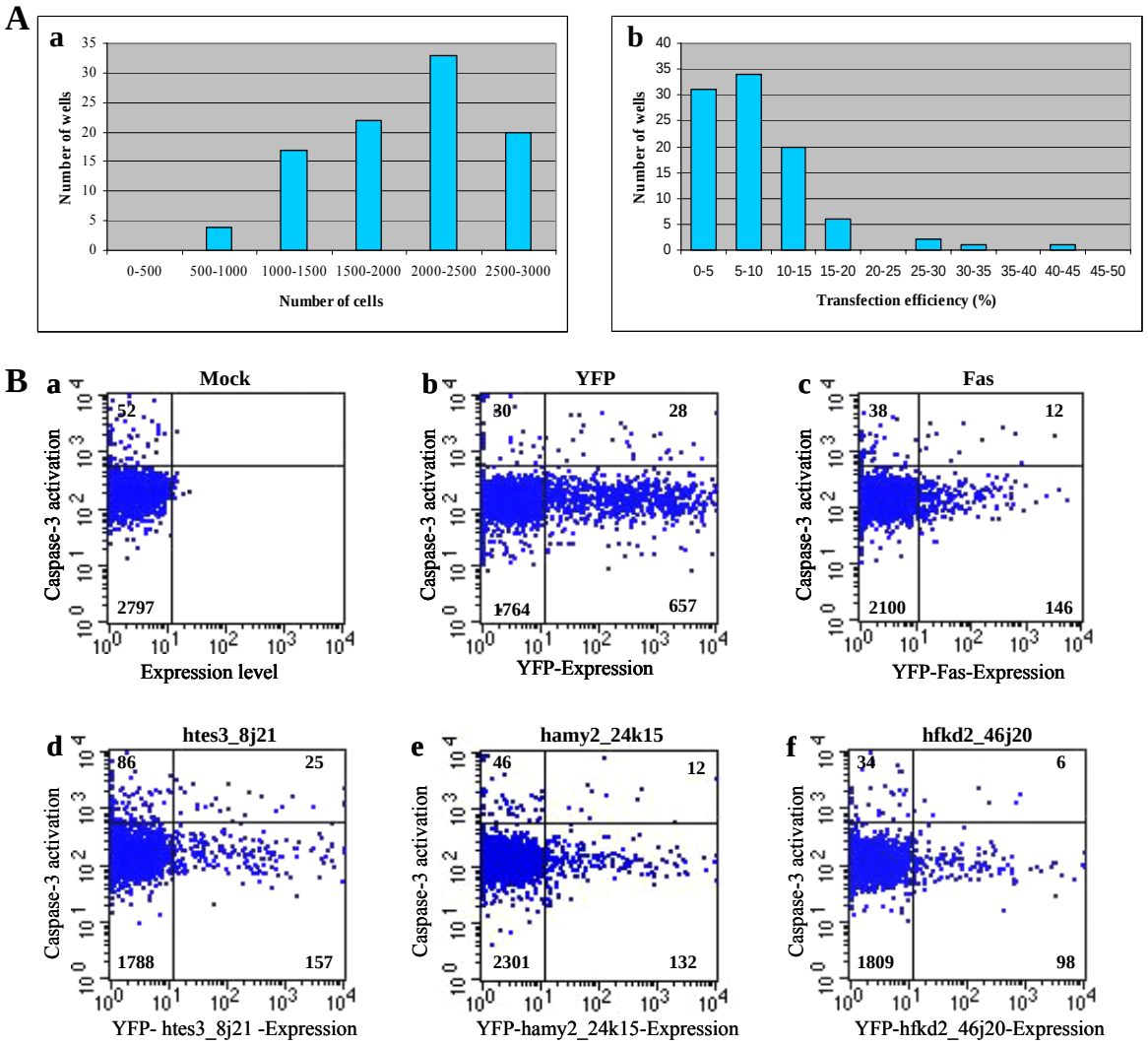

Figure 3.9. Assay effects with NIH3T3 cells in a 96-well format
NIH3T3 cells transfected in 96-well plate with miniprep DNA were stained after 72 hours with active Caspase-3 antibody and measured with FACS. Transfection and staining were done on the robot and the data was acquired using the multiwell plate reader of FACS. **(A)** Graphical overview of the cell number/well and the transfection efficiency of the 96 clones **(B)** Scatter plots of controls and 3 randomly selected proteins.

Table.3.4.

Protein	Total number of cells	Transfection (%)	Untransfected apoptotic cells (%) (A)	Transfected apoptotic cells (%) (B)	Difference (%) (B – A)	p-value of Fisher test
Mock transfected	2,849	0.00	1.82	--	- 1.82	0.672
YFP	2,479	27.6	1.67	4.08	2.41	5.07
YFP-Fas	2,296	6.88	1.77	7.59	5.82	3.24
YFP-htes3_8j21	2,056	8.85	4.59	13.7	9.11	5.34
YFP-hamy2_24k15	2,491	5.78	1.95	8.33	6.38	6.32
YFP-hfkd2_46j20	1,947	5.34	1.84	5.76	3.92	2.83

The cell number over the whole plate (after excluding the cell clumps and debris) ranged from 500 to 3,000 cells/well, with majority of the wells (92 wells) having cells

between 1,500 and 3,000 (Figure 3.9.Aa). This cell number is enough for analysis provided the transfection efficiency is more than 50%. However, the transfection efficiency of most of the wells (91 wells) ranged only between 0-20%, with majority of the wells (65 wells) lying between 0 and 10% (Figure 3.9.Ab). The maximum transfection efficiency obtained was 40-45% with only 1 well showing this.

All the wells in the plate were analyzed to verify the effect of the overexpressed proteins on the induction of apoptosis. The scatter plots obtained for wells which are either mock transfected or transfected with YFP, Fas receptor and three randomly selected ORFs are shown in Figure 3.9.B and the effects are summarized in table 3.4. Though an average cell number of more than 2,000 cells/well was obtained, the transfection efficiency of the proteins other than YFP was below 10% (Table 3.4). Since transfection with Fas and the other three unknown proteins resulted in more percentage of transfected apoptotic cells (5.76 to 13.7%) when compared to YFP (4.08%), they could be considered as activators of apoptosis. However, the transfection efficiency of these proteins is between 5.34 to 8.85%, and the effect is calculated based on only a few cells (6 to 28 cells) which are positive for activated caspase-3 (cell number shown in the upper right corner of the scatter plots in Figure 3.9.B). This is reflected by high p-values (>1) which indicates that the observed effects are statistically insignificant (table 3.4). These statistically insignificant effects are because of very low number of active caspase-3 positive cells in conjunction with very low transfection efficiency. I tried to further optimize the transfection efficiency by increasing the amount of DNA and the transfection reagent, but could not succeed in improving it to an extent that the effects in the assay were clear. So, HEK293T, a human embryonic kidney cell line that is known to have good transfection efficiency, was tested for its suitability in the assay.

3.1.3.6 Effect of control proteins in HEK293T cells

HEK293T cells were seeded in 96-well plate (15,000 cells/well, resulting in a confluency of 50-60%), transfected with maxi prep DNA of some of the control proteins shown in table 3.1, and stained manually with the active caspase-3 antibody after 72 hours. The scatter plots obtained for N- and C-terminally tagged proteins are shown in Figure 3.10, and the effects are summarized in table 3.5. Proteins which produced significant effects are highlighted.

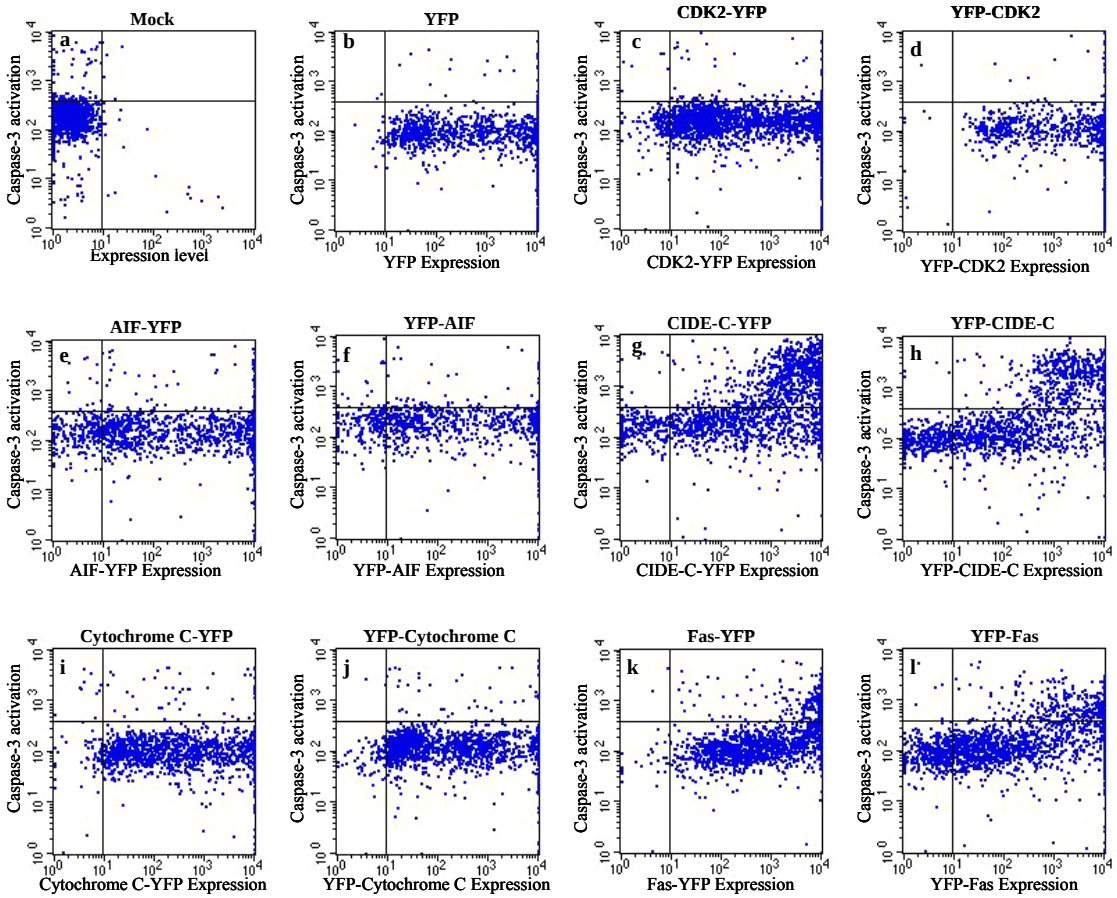

Figure 3.10. Effect of control proteins in HEK293T cells
HEK293T cells were transfected in 96-well plate with control proteins tagged C- and N-terminally with YFP and stained with active caspase-3 antibody after 72 hours. Both the tag orientations of CIDE-C and Fas showed a clear apoptosis activating effect, while the other proteins did not induce apoptosis.

Table 3.5.

Protein	Total number of cells	Transfection (%)	Transfected apoptotic cells (%)	p-value of Fisher test
YFP	1,676	99.1	1.5	0.02
CDK2-YFP	2,725	94.2	2.9	0.34
YFP-CDK2	1,334	99.3	2.3	0.19
AIF-YFP	1,605	85.7	6.2	0.88
YFP-AIF	1,080	81.7	7.9	0.47
CIDE-C-YFP	1,827	86.3	**47.3**	**2.40e-45**
YFP-CIDE-C	1,529	80.0	**39.3**	**9.12e-53**
Cytochrome C-YFP	1,296	94.7	3.9	0.0006
YFP-Cytochrome C	1,485	94.6	3.5	1.0
Fas-YFP	2,047	98.7	**36.5**	**0.001**
YFP-Fas	2,439	83.1	**40.1**	**2.59e-72**

Transfection efficiency of more than 80% was obtained for all the clones, with some clones like YFP, YFP-CDK2 and Fas-YFP showing a transfection efficiency of almost 100% (table 3.5). Though the total cell number/well ranged only between 1,080 and 2,725, the final effect of the proteins on apoptosis was very clear because of the high transfection efficiency (Figure 3.10). Over expression of the neutral controls (YFP and CDK2) induced apoptosis in less than 3% of the transfected cells, while AIF and Cytochrome C induced apoptosis in 7 and 3.7% (average effects of both tag orientations) of transfected cells respectively. However, the effect of AIF and Cytochrome C is negligible when compared to that of Fas and CIDE-C (Figure 3.10g, h, k and l). Irrespective of the tag orientation, overexpression of Fas and CIDE-C led to a strong apoptosis induction in 38.3 to 43.3% (average effects of both tag orientations) of transfected cells respectively (values high lighted in table 3.5). Moreover, the statistical significance of these effects is strengthened by p-values of less than or equal to 0.001. Based on these data, Fas and CIDE-C were selected as positive controls, while YFP and CDK2 would be used as neutral controls for the assay. The HEK293T cell system was thus validated to be suitable for a systematic screen and this cell line was determined superior to NIH3T3.

3.1.3.7 Transfection of HEK293T cells with mini prep DNA

In order to test the effect of mini prep DNA on the assay outcome, HEK293T cells were transfected with miniprep DNA of 96 clones and stained with active caspase-3 antibody after 72 hours. However, since the average cell number obtained from a 96-well plate was only 1,500 cells/well (as seen in section 3.1.3.6), to obtain higher cell numbers the transfections were done in four 24-well plates (4x24=96 wells) with 200ng DNA/well. After 72 hours the cells were transferred into a 96 well plate for staining on the robot as well as data acquisition with the FACS.

An overview of the total cell number/well and the transfection efficiency obtained over the whole plate is shown in Figure 3.11.A. Cell number ranging from 2,000 to16,000 cells/well was obtained over the whole plate, with 64 wells having cells between 6,000 and 12,000 (Figure 3.11.Aa). Moreover, the transfection efficiency of most of the wells (71 wells) is above 70%, out of which 37 wells showed transfection in 90-100% of cells (Figure 3.11.Ab). Scatter plots of the controls and 3 randomly selected proteins are shown in Figure 3.11.B and the effects are summarized in table 3.6. Proteins which showed a clear activating effect are highlighted.

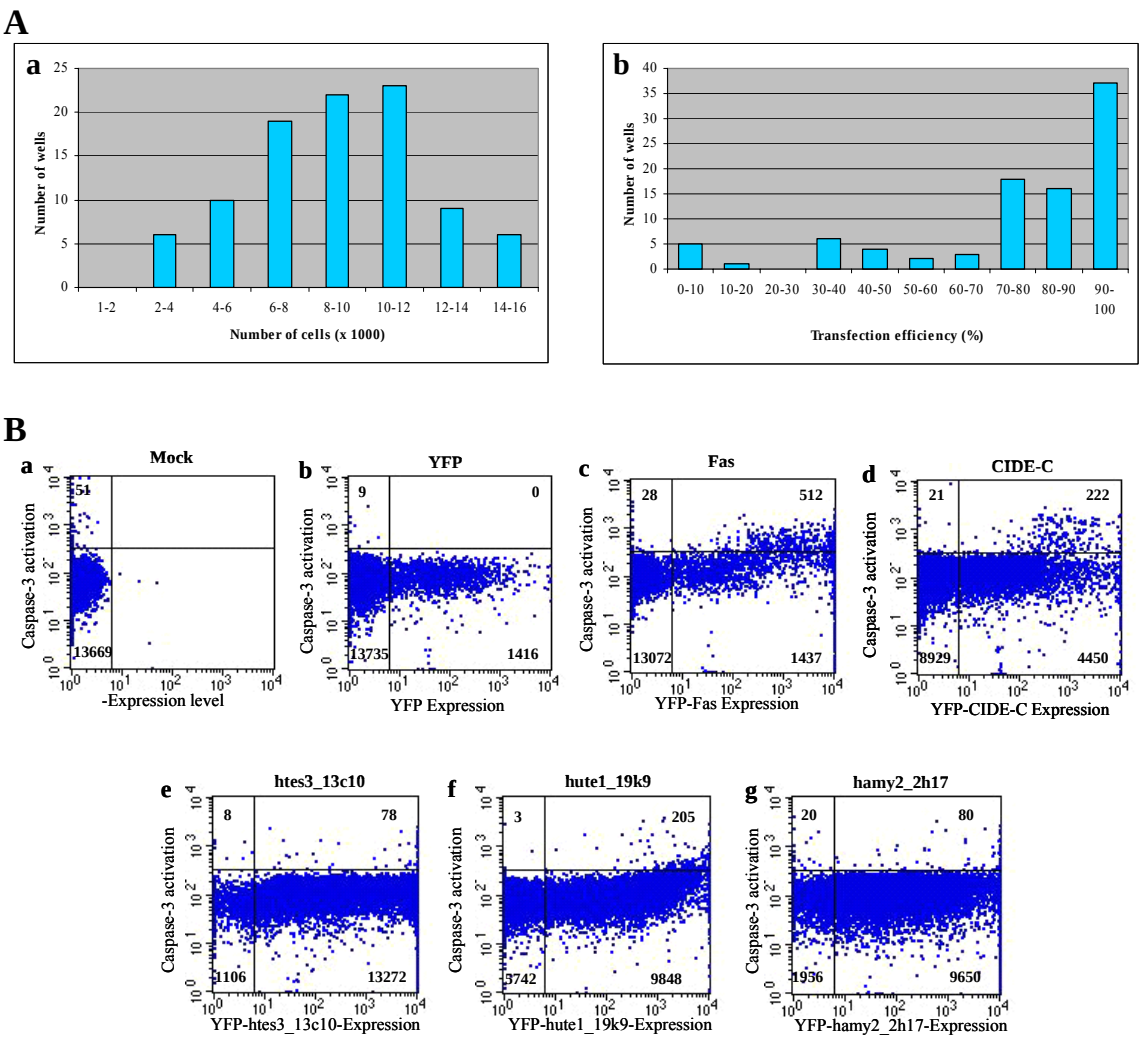

Figure 3.11. Assay effects with HEK 293T cells with mini-prep DNA
HEK 293T cells transfected in four 24 well plates (= 96-wells) with miniprep DNA were stained after 72 hours with active Caspase-3 antibody and measured with FACS. Transfection and staining were done on the robot and the data was acquired using the multiwell plate reader of FACS. **(A)** The cell number/well and the transfection efficiency of the 96 clones and **(B)** the scatter plots of controls and 3 randomly selected proteins are shown.

Table.3.6.

Protein	Total number of cells	Transfection (%)	Untransfected apoptotic cells (%) (A)	Transfected apoptotic cells (%) (B)	Difference (%) (B – A)	p-value of Fisher test
Mock transfected	13,725	0.00	0.37	--	- 0.37	0.5
YFP	15,160	9.35	0.06	0.00	-0.06	0.6
YFP-Fas	**15,949**	**10.6**	**0.19**	**26.3**	**26.11**	**0.00**
YFP-CIDE-C	**13,622**	**34.2**	**0.23**	**4.75**	**4.52**	**4.22e-50**
YFP-htes3_13c10	14,464	93.4	0.71	0.58	-0.13	2.92e-07
YFP-hute1_19h9	15,798	61.6	0.04	1.85	1.81	2.96e-259
YFP-hamy2_2h17	11,706	85.2	1.01	0.82	-0.19	3.39e-14

The percentage of untransfected apoptotic cells is very low (0.06 to 1%) which shows that this cell line is not too sensitive to stress conditions like transfection. Transfection with

Fas receptor induced apoptosis in 26.3% of transfected cells, while transfection with CIDE-C resulted in only 4.75% apoptotic cells. The effects are also visually clear from the scatter plots (Figure 3.11.Bc,d). Cells expressing YFP, htes3_13c10 and hamy2_2h17 did not undergo apoptosis, but cells expressing high levels of hute1_19h9 showed activation of caspase-3 resulting in 1.85% of apoptotic cells. The high cell number combined with good transfection efficiency resulted in p-values of <0.5 suggesting that the effects observed in the assay are statistically significant.

Compared to NIH3T3 cells, HEK293T cells showed higher transfection efficiency, lower percentage of untransfected apoptotic cells, as well as clear and statistically significant effects in the assay. Low transfection efficiency of 3T3 cells in conjunction with high amount of spontaneous cell death (as indicated by the number of untransfected apoptotic cells) would mask the specific signal generated by the overexpressed protein, leading to misinterpretation of the final effect. Based on these results, HEK293T cells were chosen for the assay instead of NIH3T3 cells.

Taken together, the conditions that were optimized for the screening are as follows:

- Method: A flow cytometry based assay would be used, in which apoptosis inducers can be detected by staining the cells with an antibody recognizing the cleaved form of caspase-3. This method offers the advantage that the transfected cells can be distinguished from untransfected cells making it possible to detect changes of activated caspase-3 levels in individual cells.
- Cell line: HEK293T cells would be used for the assay because of the high transfection efficiency that could be achieved with this cell line. Transfection efficiency of the cell line was found to be very important for obtaining statistically significant effects.
- Controls for the assay: N- and C-terminally tagged Fas receptor and CIDE-C would be used as positive controls, while YFP and CDK2 would be used as neutral controls for the assay.
- Automation: Both transfection and staining of the cells with the antibody were automated. The automation was aimed at minimizing cell loss during the process of staining and to increase the throughput of the screen. Aspiration speed of 30 µl/second and centrifugation at 1350 rpm were taken as the optimum conditions for staining on the robot.
- Plate format for screening: In order to obtain more cells for statistical analysis, the cells would be seeded and transfected in 24-well plates (32,000 cells/well). After 72

hours, both floating and adherent cells from four 24-well plates would be transferred into a polypropylene 96-deep well plate for staining on the robot.

- Data acquisition: Stained cells would then be transferred into 96-U bottom plates which are compatible with the plate reader of the FACS, and the data would be acquired using an automated fluorescence activated cell sorter.

3.2 Screening

The conditions mentioned above were used to screen for novel apoptosis inducing proteins. All the proteins used for the screen were tagged C- or N-terminally with YFP and both the tag orientations for each protein were screened in the assay. As a proof of principle of the assay the screen was initially done with a set of 100 open reading frames (ORFs) selected from a list of proteins which were differentially expressed in cancer. Later, based on the availability of full length cDNAs the screen was extended to other previously uncharacterized proteins. So far 266 ORFs (200 proteins) have been screened in the assay (table 6.1 in Supplements), which amounts to 532 expression clones (C- and N-terminally tagged ORFs). Each gene of interest was screened in 4 independent replicate experiments finally resulting in data acquisition for 2,128 wells (4 x 532 wells).

3.2.1 Statistical analysis

The raw data obtained from the assay was analyzed using specialized software based on the statistical programming language R which is openly available through the Bioconductor package *prada* (collaboration with Florian Hahne). The raw data was initially pre-processed to remove the contaminants like cell clumps and debris, and the scatter plots for all the 96 wells were then generated automatically. A measure for the effect of a protein on activation of caspase-3 was then obtained through the log-transformed odds-ratio (refer section 2.2.2.8) and a measure of significance was calculated by testing against the null-hypothesis of an odds-ratio of one, by means of the Fisher's Exact Test. Results from replicate measurements for each protein were combined using a generalized Chi^2 statistic for stratified contingency tables through the Mantel-Haenszel test.

3.2.2 Selection of potential candidates from the Caspase-3 assay

The procedure by which candidates were selected is shown in Figure 3.12, taking one 96-well screening plate as an example. To facilitate candidate selection and to obtain an overview of protein effects in a 96-well plate, the odds ratios were visualized as colour coded 96-well plate plots (Figure 3.12A). The proteins which showed an activating effect in the assay were indicated with red colour, with the intensity of colour being directly proportional to strength of the effect in the assay. For example, in the plate shown in figure 3.12.A, some of the proteins in the plate induced caspase-3 activation for both the tag orientations (wells C2 and G2; wells C8 and G8). However, some proteins induced apoptosis only when YFP is fused at the N-terminus of the protein (wells G1 and G4). This shows that orientation of the tag has an effect on the assay outcome of some ORFs probably due to mislocalization of the protein caused by masking of the localization signal by the tag.

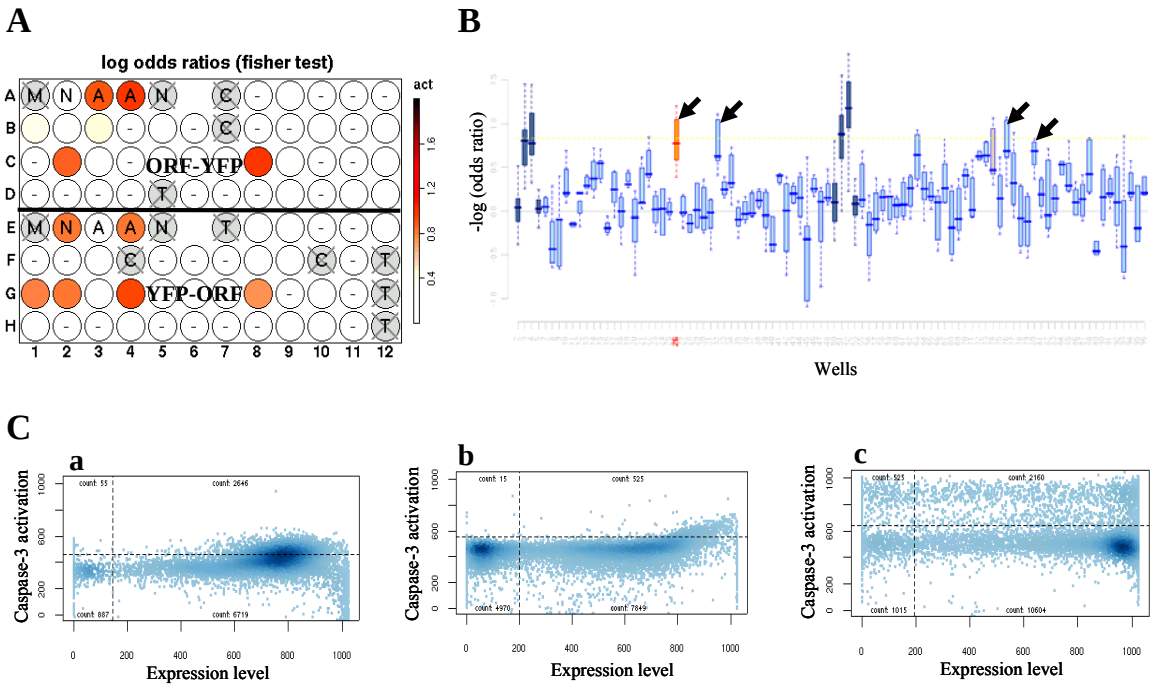

Figure 3.12. Selection of potential candidates of the apoptosis assay
(A) Visual representation of the odds ratio as colour coded 96-well plate plot. The C-terminally tagged proteins are present in the upper half of the plate, while the N-terminally tagged proteins are present in the corresponding lower half of the plate. Expression clones which showed an activating effect in the assay are indicated with red colour. **(B)** Effect of the proteins from replicate experiments is shown as an interactive boxplot. Each vertical bar represents one expression clone. The clones which show an effect size (or –log odds ratio) of more than 0.65 (shown with arrows) were selected for further analysis. **(C)** The three patterns of scatter plots seen in the assay are shown. The first and the second patterns are recognized as activators by the statistical analysis method, while the third one is not.

The results from 4 replicate experiments for this plate were combined and visualized as a box plot (Figure 3.12B). The box plot provides an overview of the effect of a protein with

respect to replicate measurements of other proteins on the same plate. Each bar in this box plot represents one expression clone. Though the effect of some proteins in the assay was observed to vary with orientation of the tag, initially all the expression clones with –log odds ratio of more than 0.65 were selected (expression clones shown with arrows in Figure 3.12B). The subcellular localization of these selected proteins was then examined in LIFEdb [4] [5] and only those fusion proteins that showed correct localization were considered as candidates for further validation (Table 3.6).

Upon examining the scatter plots of all the expression clones in the assay, three different patterns of scatter plots for activators were observed (Figure 3.12.C). In the first kind of scatter plot, a very strong apoptosis induction was observed in the transfected cells, while most of the untransfected cells were negative for active caspase-3 (Figure 3.12.Ca). In the second type of scatter plot, only the cells with very high protein expression were found to undergo apoptosis (Figure 3.12.Cb). Proteins that exhibited these two patterns were identified as apoptosis inducers by the automated analysis method, because of the high odds ratio. However, proteins that exbited the 2nd type of scatter plots (Figure 3.12.Cb) were not considered for further validation because, very high overexpression of a protein induces undesirable nonphysiological effects, which in many cases is induction of apoptosis. Therefore, 9 proteins that exhibited the first type of scatter plots were selected for validation (Table 3.6, 1-9). In the third kind of scatter plot, along with the transfected cells even the untransfected cells were found to undergo apoptosis (Figure 3.12.Bc). In this case, the odds ratio was small and these clones were not recognized by the automated analysis method as activators. However, proteins that show such a pattern might represent death inducing ligands, secreted or other proteins which induce apoptosis also in the neighbouring untransfected cells. So, three proteins that exhibited such a pattern of scatter plot were also considered for further evaluation (Table 3.6, 10-12). Thus, a total of 12 proteins were selected as candidates for a second screen, where the apoptosis inducing effect of these proteins was tested in a nuclear fragmentation assay (table 3.6).

3.2.3 Confirmation of candidates with nuclear fragmentation assay

HEK293T cells were transfected with maxi-prep DNA of the 12 candidates, and allowed to express the proteins for 3 days. After collecting the floating and adherent cells, the cells were stained with DAPI and fixed on slides using Cytospin3. Nuclei of the cells were observed under confocal laser scanning microscope, and the proteins were scored according to the extent of nuclear fragmentation seen (table 3.6). In table 3.6, proteins which caused no

evident nuclear changes were indicated by `NO´; those with only condensed but no fragmented nuclei with `+´; proteins with both condensed and fragmented nuclei are indicated by `++´; and nuclei with clear fragmentation are scored `+++´. One example for each class of nuclear change is shown in Figure 3.13. Only the proteins which are scored ´++` for both tag orientations, and those with ´+++` for either of the orientations, were considered as final candidates in the apoptosis assay. List of the proteins that were considered for this screen and the results of the nuclear fragmentation assay are shown in table 3.6.

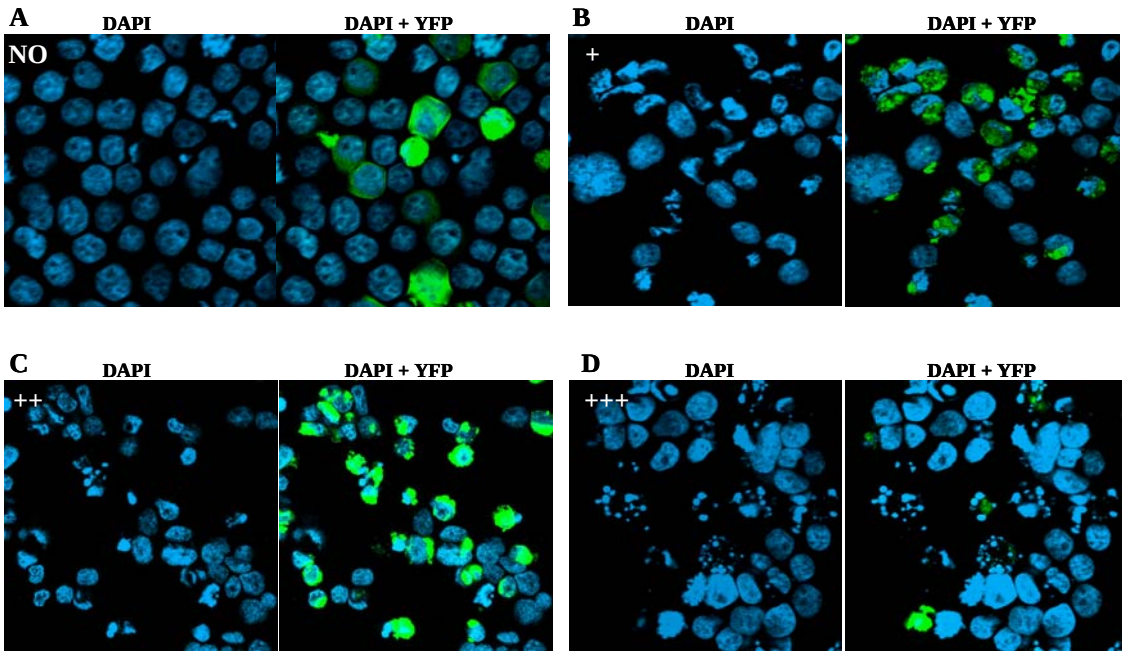

Figure 3.13. Selection of candidates based on nuclear morphology
HEK293 cells were transfected in 24-well plates with maxi preparations of DNA. After 3 days, the floating and adherent cells were pooled, fixed and stained with DAPI. The cells were fixed on slides using Cytospin 3 and images were made on the confocal microscope. Shown are the example images where **(A)** no evident nuclear changes occurred, indicated with ´NO` **(B)** Nucleus is condensed or deformed but no fragmentation, indicated with ´+` **(C)** Both condensed and fragmented nuclei are seen, indicated with ´++` **(D)** strong fragmentation is observed, indicated with ´+++`.

Table. 3.6. Candidates for Nuclear fragmentation assay

No.	ORF	p-value	Nuclear Fragmentation	
			ORF-YFP	YFP-ORF
1	akxq28i14160	0.000152	+++	+++
2	akxq28n1210739	3.3e-06	NO	++
3	hfkd2_46m10	2.5e-05	+	++
4	IRATp970A0419	6.4e-07	+++	++
5	htes3_35n12	0.00195	+++	+++
6	hfbr2_7b16	0.00043	NO	+++
7	IRATp970E129	0.0085	++	+
8	IRAUp969G0861	2.8e-06	NO	NO
9	hlcc2_1m1	0.0023	+	++
10	hfkd2_3i13	2.39e-52	++	++
11	htes3_23a19	0.038	+	+
12	akxq28j1311548	0.14	NO	+

All the 12 candidates were confirmed in the nuclear fragmentation assay. However, based on the strength of nuclear fragmentation (i.e, apoptosis induction), 5 proteins were selected for more detailed analysis (proteins marked red in table 3.6). The scatter plots of these 5 proteins from the Caspase-3 assay, and the corresponding DAPI images are shown in Figure 3.14.

xq28i14160

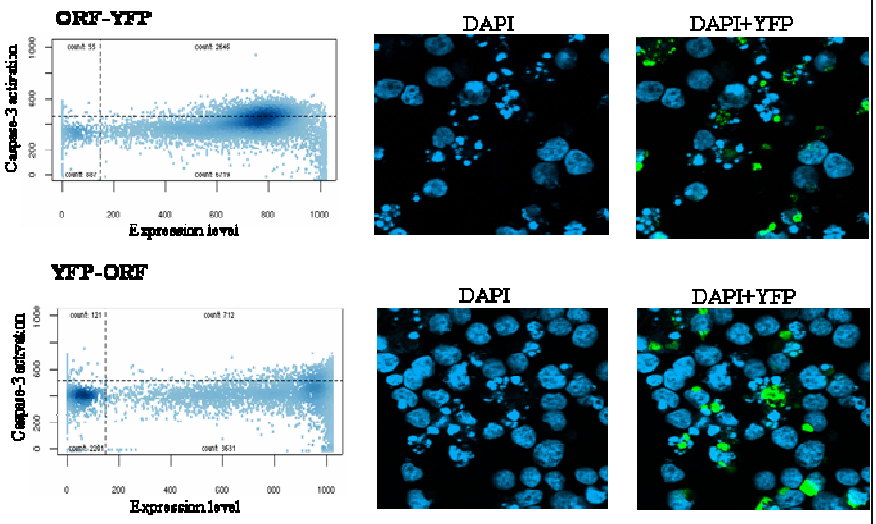

IRATp970A0419

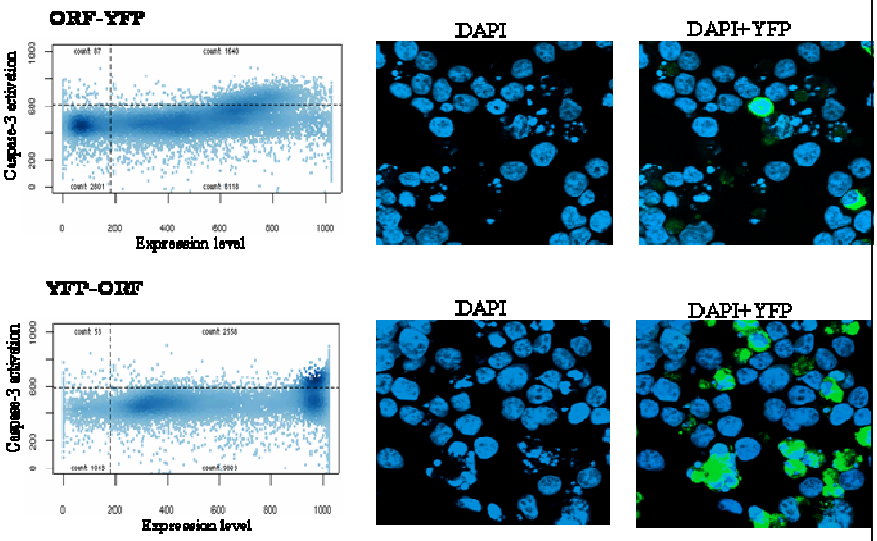

htes3_35n12

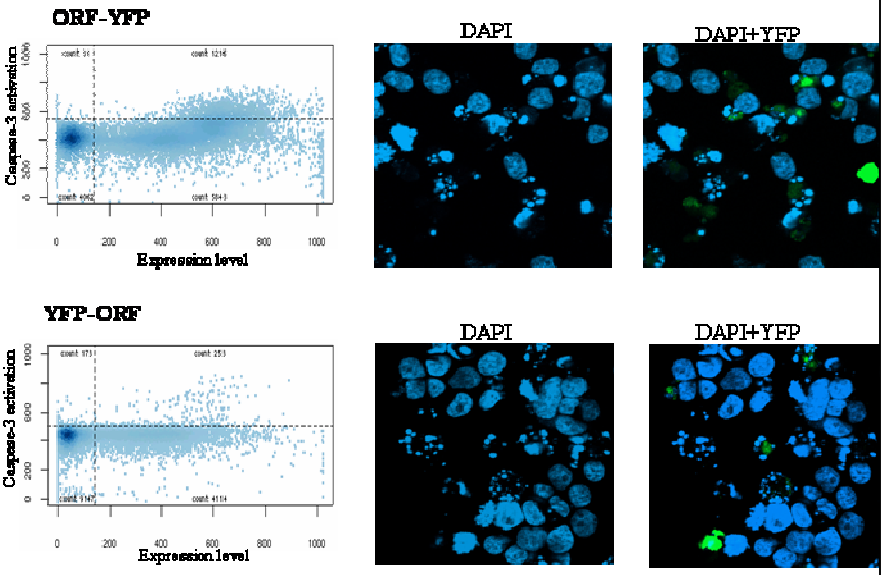

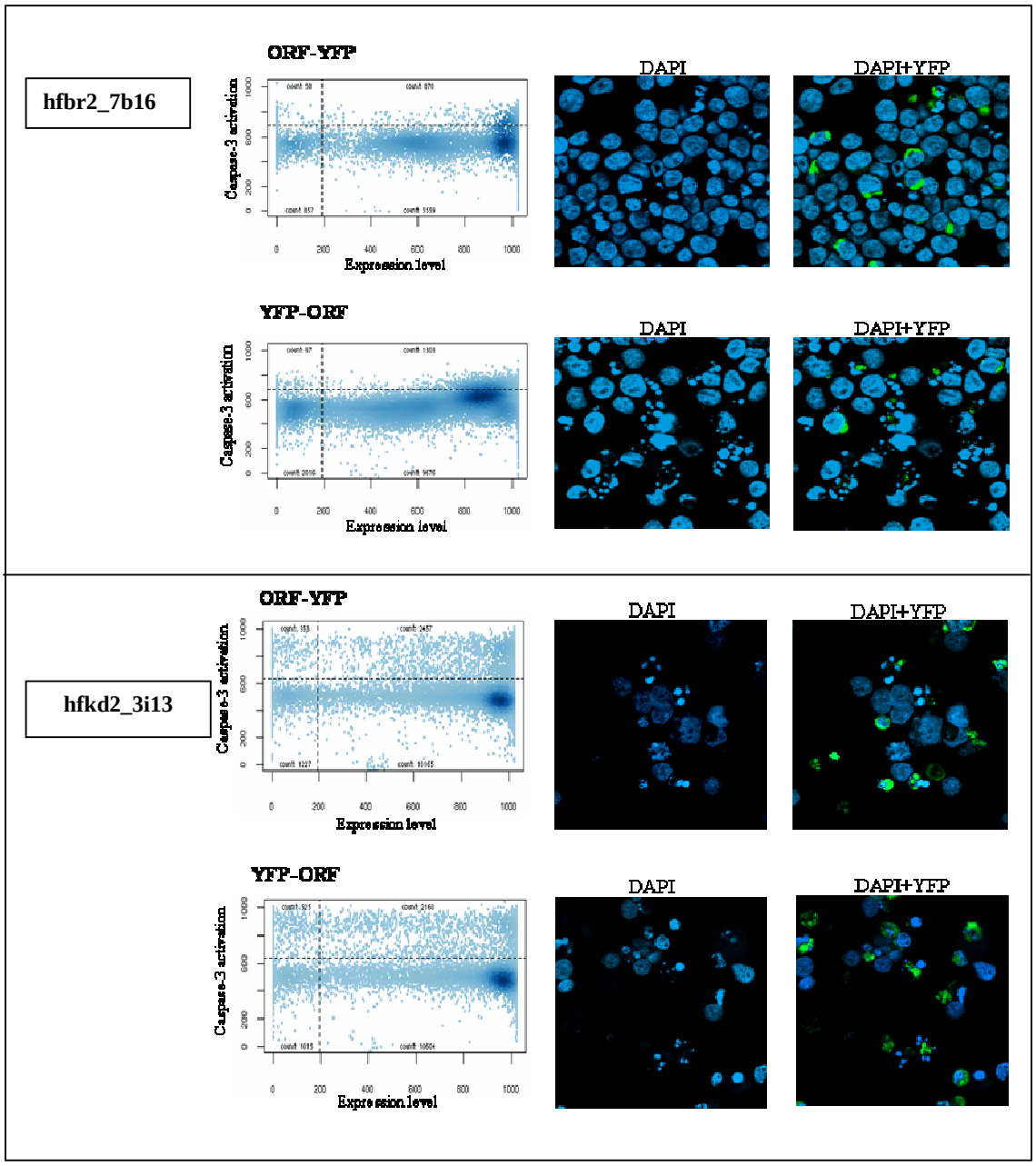

Figure 3.14. Confirmation of the candidates in a nuclear fragmentation assay
Shown are the scatter plots and images of DAPI stained nuclei of 5 proteins which showed a strong induction of apoptosis.

Examination of scatter plots and the images of DAPI stained nuclei show that the strength of the signal in the caspase-3 assay strongly correlates with the nuclear fragmentation results of the corresponding expression clone i.e., the clones which showed a strong caspase-3 activation also showed a very clear nuclear fragmentation. This further emphasizes the specificity of the caspase-3 assay. A summary of the five candidates of the apoptosis assay is shown in table 3.7. One of the candidates that were considered for detailed functional analysis is highlighted.

Table 3.7. Summary of the 5 candidate proteins of the apoptosis assay

Clone ID	Protein name	Genbank accession number	Localization		Apoptosis p-value	Annonation (Source, InterPro)
			YFP-ORF	ORF-YFP		
Xq28i14160	FUN14 domain containing 2	BC000255	Mitochondria	Mitochondria	0.000152	FUN14 domain containing 2 (Hepatitis C virus core-binding protein 6) (Cervical cancer oncogene 3) IPR007014 FUN14
IRATp970A0419	Interferon alpha inducible protein 27	BC015492	Unknown	Endoplasmic reticulum and Golgi apparatus	6.4e-07	Interferon alpha inducible protein 27 IPR002091 Aromatic amino acid permease; IPR009311 Interferon-induced 6-16
htes3_35n12	Solute carrier family 25, member 31	AL136857	Cytoplasm and Mitochondria	Mitochondria	0.00195	Solute carrier family 25 (mitochondrial carrier; adenine nucleotide translocator), member 31 IPR001993 Mitochondrial substrate carrier; IPR002113 Adenine nucleotide translocator 1; IPR002167 Graves disease carrier protein
hfbr2_7b16	Brain protein 44	AL110297	Mitochondria	Mitochondria	0.00043	Brain protein 44 IPR005336 Protein of unknown function
hfkd2_3i13	**Vacuole membrane protein 1**	**AL136711**	**Plasmamembrane**	**Plasmamembrane**	**2.39e-52**	**Likely homologue of Vacuole Membrane Protein 1 (VMP1); No InterPro hits**

3.3 The Vacuole Membrane Protein (VMP1)

The expression level of *VMP1* was found to be differentially regulated in various disease conditions like cancer, renal failure and acute pancreatitis. Though Vmp1 is associated with such diverse disease mechanisms, the function of this protein is not elucidated yet. So we selected Vmp1 for detailed functional analysis. The cDNA of *VMP1* used in the assay was obtained from human kidney library. So, we proceeded to examine the effects of Vmp1 in a kidney cell system by both overexpression as well as knock down.

3.3.1 Overexpression of Vmp1 in kidney cells

HEK293T, a ´normal` kidney cell line was chosen for the over expression experiments because of the high transfection efficiency that could be achieved with this cell line. Since overexpression of Vmp1 induced apoptosis in HEK293T cells, we started with investigating the possible reason for this.

3.3.1.1 Vmp1 induces apoptosis in neighbouring non-transfected cells

HEK293T cells were transfected with *VMP1* tagged C-terminally with YFP and the cells were observed over 3 days for the activation of caspase-3 (Figure 3.15.A). One day after transfection, only 2.66% of untransfected cells and 2.56% of transfected cells were positive for activated caspase-3. However by 48 hours, 24.3% of untransfected and 15.3% of transfected cells showed active caspase-3, indicating that overexpression of Vmp1 induces apoptosis in transfected as well as the untransfected cells. The same was observed by 72 hours of overexpression, again with a higher number of untransfected cells (22.1%) undergoing apoptosis compared to transfected cells (19.4%).

The Vmp1 transfected cells were then monitored over 3 days to verify if the observed changes in the caspase-3 activation with time correlates with the induction of other apoptotic features like plasma membrane blebbing and nuclear fragmentation. Plasma membrane changes were observed in live cells by confocal microscopy, while the nuclear fragmentation was monitored by staining fixed cells with DAPI. One day after transfection, the morphology of both the untransfected and transfected cells remained normal and the cells did not lose their adherence (Figure 3.15.Ba). However, the nucleus of the transfected cells was condensed, where as the untransfected cells did not show any nuclear changes (Figure 3.15.Ca). By 48 and 72 hours of protein expression, the cells died progressively showing features

characteristic of apoptosis i.e. loss of cell adherence, rounding and membrane blebbing (Figure 3.15.Bb and c). Untransfected cells adjacent to Vmp1 overexpressing cells also died with morphological evidence of apoptosis (cell shown with an arrow in Figure 3.15.Bc). The nucleus of the cells exhibited fragmentation starting from 48 hours after transfection (Figure 3.15.Cb and c), confirming the result of the caspase-3 assay. This shows that the cells can tolerate Vmp1 overexpression to a certain extent, but prolonged overexpression is toxic to the tranfected as well as the untransfected bystander cells, which subsequently undergo apoptosis.

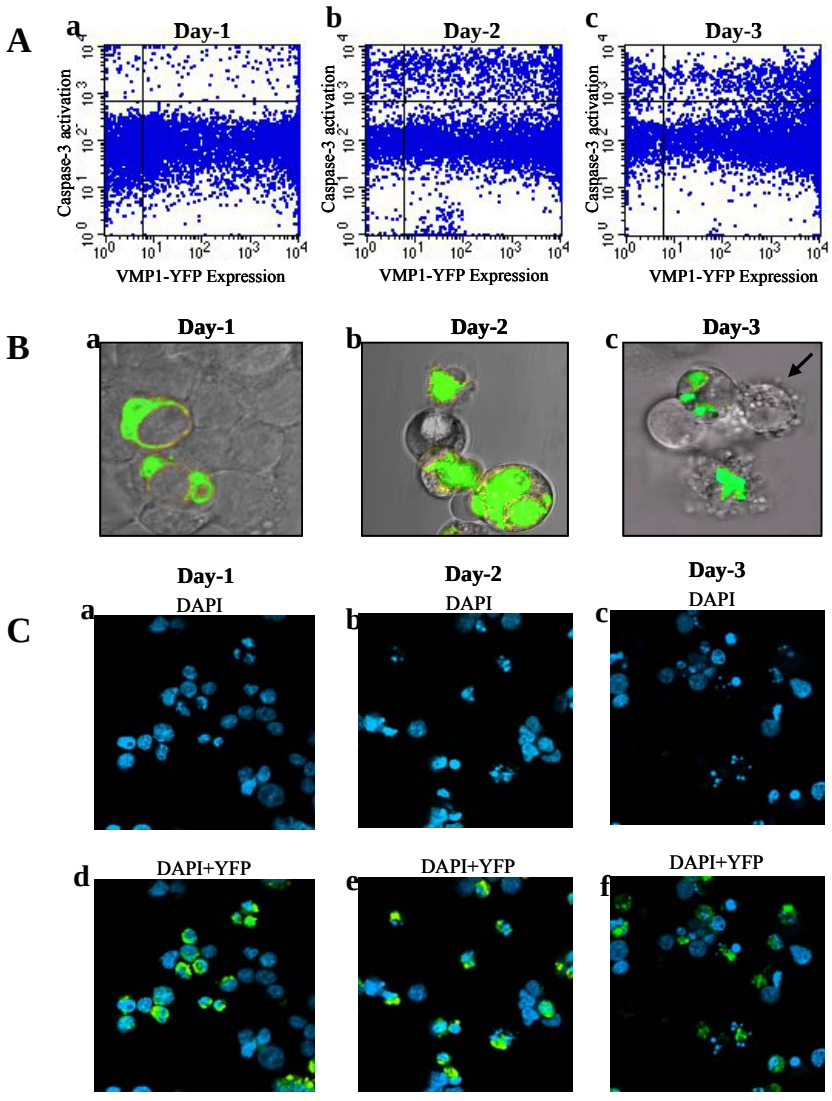

Figure 3.15. Overexpression of Vmp1 induces apoptosis in the bystander cells
(A) HEK293T cells were transfected with the construct VMP1-YFP and the cells were stained with active caspase-3 antibody for 3 days. Scatter plots show that the cells were not apoptotic on the 1st day after transfection, but on 2nd and 3rd days, more number of apoptotic cells were detected. Note that even the untransfected cells were positive for active caspase-3. **(B)** Cells were transfected with the same construct and morphology of live cells was monitored over 3 days. Shown are the confocal images of cells made 1, 2 and 3 days after transfection. On the first day, the cells did not show apoptotic morphology, but the cells died progressively after 48 hours of protein expression. Untransfected cells adjacent to Vmp1 overexpressing cells also showed apoptotic morphology (cell indicated with an arrow). **(C)** Images of DAPI stained nuclei show that on 1st day only condensed nuclei were seen. The number of fragmented nuclei increased on 2nd and 3rd days.

3.3.1.2 Subcellular localization of overexpressed Vmp1

Determining the subcellular localization of a protein in most cases provides a hint towards the function of that protein. To understand the function of Vmp1 and to determine the reasons for apoptosis induction, the subcellular localization of YFP tagged Vmp1 was studied in HEK293T cells. Dusetti et al. showed that rat Vmp1 is localized in the endoplasmic reticulum and Golgi apparatus and that overexpression of Vmp1 leads to the formation of intra-cellular vacuoles [159]. To verify this for human Vmp1, HEK293T cells were transfected with plasmids encoding Vmp1 fused to YFP at its C- or N- terminus and the subcellular localization was observed by confocal microscopy. As described for the rat homologue, human Vmp1 was also found in the endoplasmic reticulum and the Golgi apparatus (Figure. 3.16.A) and it led to the formation of vacuoles in cells (Figure. 3.16.B). However, in cells with low overexpression, Vmp1 was found at the plasma membrane where it is distributed in a punctuate pattern (Figure.3.16.C). The protein was not distributed equally all over the cell, but it seemed to cluster specifically at some areas of the cell membrane, which were represented by intense fluorescence. Vacuole formation was not detected in cells where Vmp1 localized to the membrane.

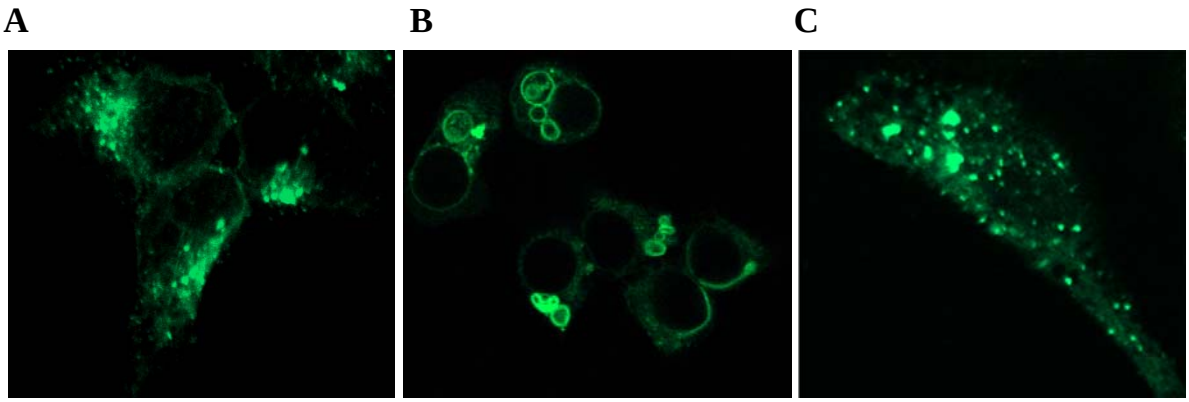

Figure 3.16. Subcellular localization of Vmp1
(A) HEK293T cells were transfected with *VMP1* tagged C-terminally with YFP, allowed to express the protein for 24 hours and images were made using the confocal laser scanning microscope. Vmp1 was found in some cells in the endoplasmic reticulum and the golgi apparatus **(B)** Overexpression of Vmp1 induced formation of intra cellular vacuoles. **(C)** In cells with very slight overexpression, Vmp1 localized to the plasmamembrane in a punctate pattern. The protein seemed to cluster at certain areas on the membrane as indicated by the bright fluorescence signal.

Vmp1 has been reported to be overexpressed during acute pancreatitis, a condition in which pancreatic acinar cells show intracellular vacuole formation followed by cell death [159]. Though the mechanism of vacuole formation is not known, it was proposed that Vmp1

might play an important role in this process. So, we investigated from which structures of Vmp1 overexpressing cells the vacuoles originated.

3.3.1.3 Vacuoles are formed from Endoplasmic Reticulum

Live cell imaging was done to monitor the formation of vacuoles. For this, HEK293T cells grown in chamber slides were transfected with VMP1-YFP and a series of time lapse images were taken every 30 minutes, using the confocal laser scanning microscope (Figure 3.17). One cell in which vacuole formation had just started (shown with an arrow in Figure 3.17a) was observed until the vacuole has completely formed ($2^{1/2}$ hours). By 30 minutes a protrusion was seen starting from the brightly stained region of the cell, which over the next 2 hours further extended into a network and finally resulted in the formation of a vacuole. The extensions resembled endoplasmic reticulum or Golgi network, which hints that the vacuoles are formed from one or both of these structures (Figure 3.17e).

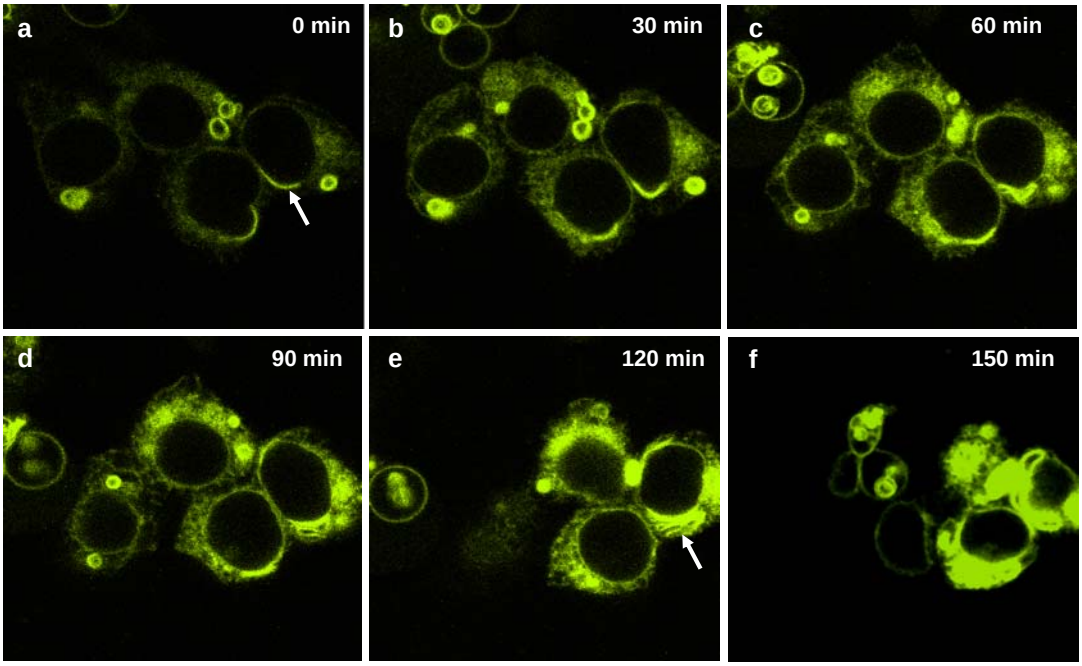

Figure 3.17. Live cell imaging to detect the origin of vacuoles
HEK293T cells were transfected in chamber slides with VMP1-YFP and 24 hours later, live cell imaging was done using the Confocal laser scanning microscope. Time lapse images were taken every 30 minutes and the cell indicated with arrow in (a) was observed for the formation of vacuoles. The protrusion seen at 0 minutes extended into a network resembling Endoplasmic reticulum or Golgi apparatus (indicated with an arrow in (e) which finally formed the vacuole.

To identify the exact origin of the vacuoles, HEK293T cells transfected with VMP1-YFP were stained with antibodies against golgin-97 and calnexin, marker proteins for Golgi

and endoplasmic reticulum respectively, and the cells were observed under a confocal microscope. Though Vmp1 was found to colocalize also with golgin-97 (Figure 3.18a, b and c), the vacuoles in Vmp1 overexpressing cells colocalized only with calnexin, but not with golgin-97 (Figure 3.18d, e and f). This shows that the vacuoles are formed by the endoplasmic reticulum.

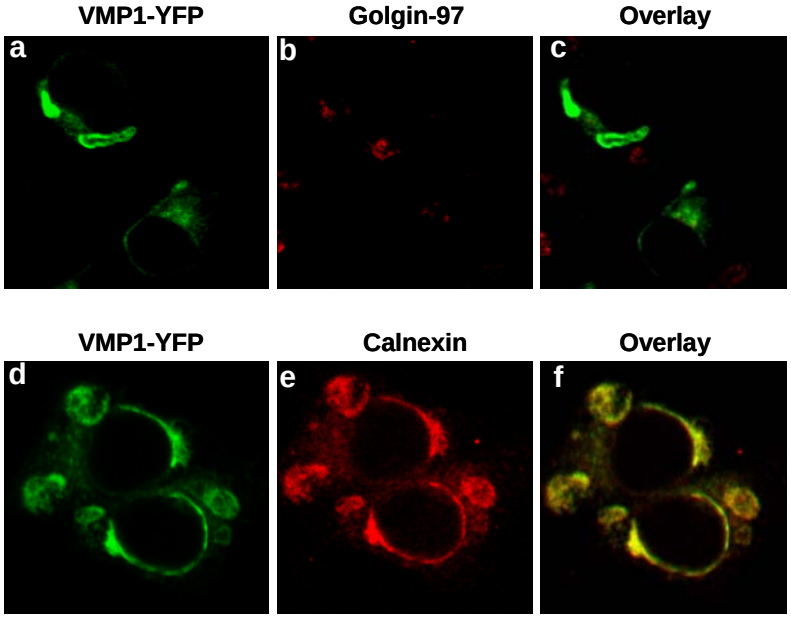

Figure 3.18. Vacuoles are formed from Endoplasmic reticulum
(A) HEK293T cells were transiently transfected with Gateway expression plasmids encoding the YFP fused VMP1. After 24 hours they were fixed, permeabilized and stained with primary antibodies against golgin-97 or calnexin followed by a secondary antibody labelled with the fluorochrome Alexa-647. The localization of Vmp1-YFP, calnexin and golgin-97 was detected with a confocal laser scanning microscope. Though Vmp1 colocalized with golgin-97 (a-c), vacuoles originated exclusively from the ER (d-f).

In summary, the overexpression studies show that Vmp1 induces apoptosis in transfected as well as in the neighbouring untransfected cells. Overexpressed YFP tagged Vmp1 localized to the Endoplasmic reticulum, Golgi apparatus and the plasma membrane and it promoted formation of vacuoles in cells. The vacuoles were formed from the endoplasmic reticulum. This suggests that the cells might have undergone apoptosis due to accumulation of the protein in the endoplasmic reticulum.

3.3.2 Functional analysis of endogenous Vmp1

Overexpression studies showed that plasma membrane is probably the final localization of Vmp1 (Figure 3.16). However, overexpressed Vmp1 is mostly retained in the ER, which hinders the functional analysis of the protein by overexpression strategies. So,

examination of the endogenous Vmp1 would be ideal for further functional analysis. To achieve this, rabbit polyclonal antibody specific for Vmp1 was generated and was tested for its specificity.

3.3.2.1 Specificity of Vmp1 antibody

The specificity of the antibody was tested in HEK293T cells by western blotting and immunofluorescence approaches (Figure 3.19). Whole cell lysates of HEK293T cells either mock transfected (lane 1), YFP (lane 2) or VMP1-YFP transfected (lane 3) were resolved by SDS-PAGE and the membrane probed with anti-Vmp1 antibody (Figure 3.19.A). A band at 46kDa representing the endogenous Vmp1 was detected in all the three samples, while only the cells transfected with VMP1-YFP showed another band at 72kDa corresponding to the size of YFP tagged Vmp1. As a control for specificity of the antibody, lysates from HEK293T cells transfected with *VMP1* siRNA were tested using the same antibody (Figure 3.19.B). A band at 46kDa was detected in control siRNA transfected cells (lane 1), whereas a reduction in protein level was detected in cells transfected with 10 and 15nM *VMP1* siRNA (lanes 2 and 3 respectively).

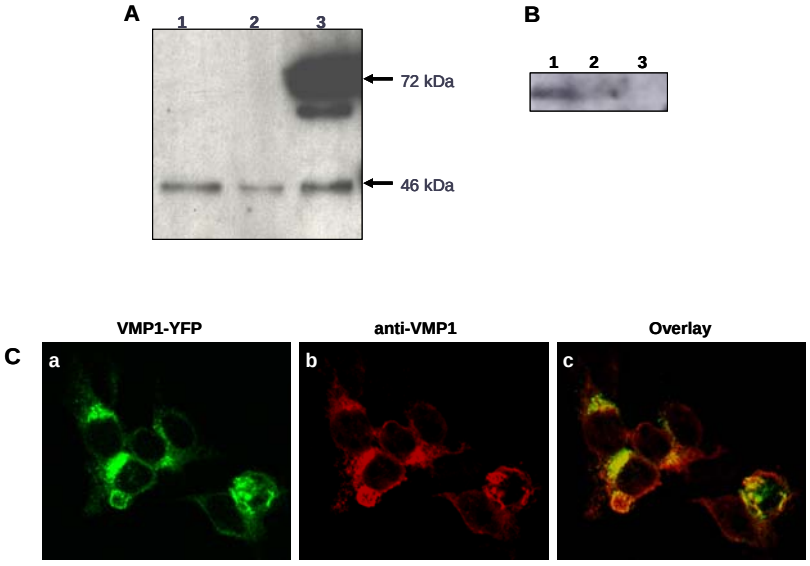

Figure 3.19. Expression of endogenous Vmp1
(A) Lysates of HEK293T cells, either mock transfected (lane 1), YFP (lane 2) or VMP1-YFP transfected (lane 3) were resolved by SDS-PAGE and the membrane probed with anti-VMP1 antibody. The band at 72kDa in lane 3 represents the combined size of Vmp1 and GFP, while the 46kDa band in lanes 1, 2 and 3 is the endogenous Vmp1. **(B)** A reduction in the protein level was observed in siRNA transfected samples, which confirms that the antibody specifically recognizes Vmp1 **(C)** (a) Cells cultured on cover slips were transfected with VMP1-YFP (b).fixed, permeabilized and stained with anti-Vmp1 antibody followed by a secondary antibody labeled with Alexa 647 (c) Confocal microscopy images showed that Vmp1 antibody specifically recognizes YFP tagged Vmp1.

Suitability and specificity of the antibody for immunofluorescence was tested using VMP1-YFP transfected cells (Figure3.19.C). Cells cultured on cover slips were transfected with VMP1-YFP, fixed, permeabilized and stained with anti-Vmp1 antibody followed by a secondary antibody labeled with Alexa 647. Confocal microscopy images showed that Vmp1 antibody specifically recognized YFP tagged Vmp1, confirming that the antibody can be used for applications based on immunofluorescence.

3.3.2.2 Subcellular localization of endogenous Vmp1

Vmp1 is predicted by SOSUI [160]to be a seven transmembrane domain protein with major parts of the protein located towards the extracellular space (Figure 3.20.A). Since no seven transmembrane domain protein known to date is located in the Endoplasmic reticulum, and as large predicted extracellular domains of Vmp1 indicate a function that might be associated with extracellular processes, we speculated the localization of Vmp1 in the ER to be due to the high expression level. Proteins destined for the plasma membrane mostly pass through the ER and Golgi network, and it is well possible that an overexpressed protein with seven transmembrane helices is not folded correctly leading to its retention in the Endoplasmic reticulum. Moreover, under conditions of low overexpression, Vmp1 was found on the plasma membrane (Figure 3.16.C). Considering this possibility, we stained cells without prior permeabilization, using a specific antibody directed against a predicted extracellular domain.

Confocal microscopy revealed that the endogenous protein is indeed present at the plasma membrane and that the expression pattern is similar to that of the lowly overexpressed YFP fused protein (Figure 3.20.Ba). Endogenous Vmp1 is distributed all over the membrane in a uniform fashion in cells which are not in contact with neighboring cells. However, in subconfluent colonies of cultured cells Vmp1 is also seen as brightly stained puncta at sites of cell-cell contact (Figure3.20.Bb). These puncta consist of two structures, each contributed by one cell, suggesting a role in the formation of initial cell-cell contacts (Figure 3.20.Bc).

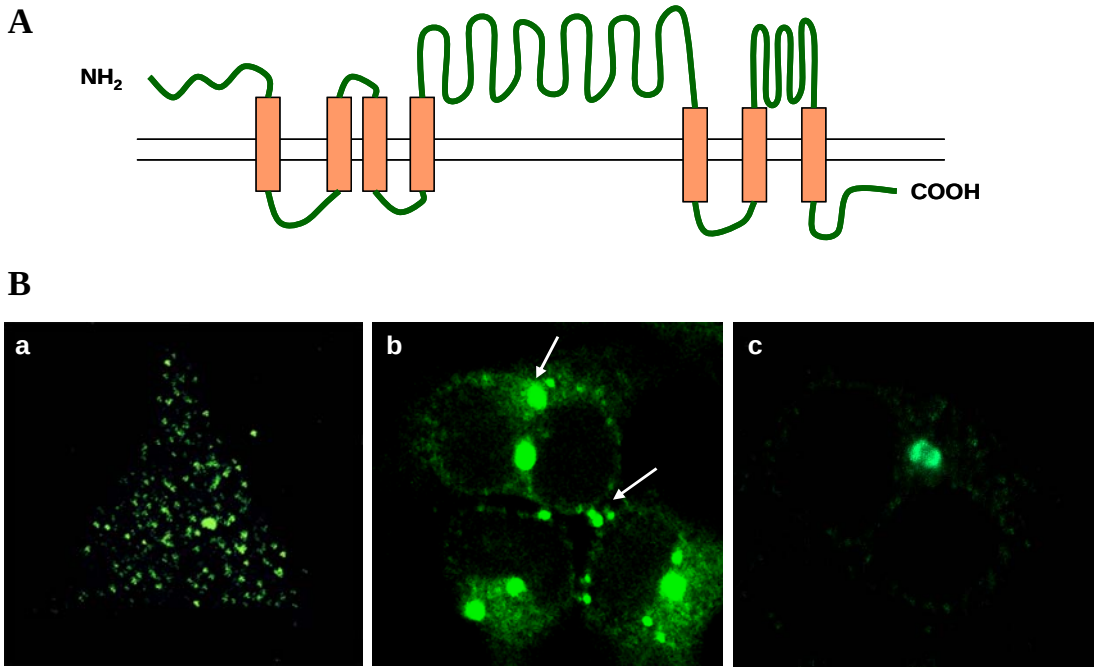

Figure 3.20. Vmp1 is a plasma membrane protein and is localized to cell-cell contact sites
(A) Scheme of the predicted Vmp1 protein structure, modified after the visualized prediction of SOUSI. Vmp1 is predicted to be a seven transmembrane domain protein, with very short cytoplasmic sequences and large extracellular domains. **(B)** Subcellular localization of endogenous Vmp1 in HEK293T cells. Cells cultured on cover slides for 24 hours were fixed and with out permeabilization, stained with Vmp1-antibody directed against a predicted extracellular domain. The secondary antibody was labeled with Alexa-488 and detection of Vmp1 was done by confocal laser scanning microscopy. (a) Vmp1 is located on the plasma membrane in a punctuate pattern. (b) Vmp1 was also detected at sites of cell-cell contact (indicated with arrows) (c) The spots are composed of two Vmp1 cores, each of them provided by one cell.

3.3.2.3 Vmp1 partially colocalizes with the tight junction protein ZO-1

To investigate if Vmp1 localizes to cell junctions, we used specific antibodies against proteins described as markers for different cell junctions and examined their possible co-localization with Vmp1 in HEK293T cells (Figure 3.21). Desmoglein-2 (Dsg-2), N-Cadherin, Zonula occludens-1 (ZO-1) and Connexin-43 were used as marker proteins for desmosomes, adherens junctions (AJ), tight junctions (TJ) and gap junctions, respectively. We could not detect co-localization of Vmp1 with Dsg-2 or N-cadherin (Figure 3.21.A and B), eliminating the possibility of Vmp1 being localized to desmosomes or adherens junctions. However, Vmp1 colocalized partially with ZO-1, a plaque protein of tight junctions (Figure 3.21.C). The colocalization was restricted to some of the brightly stained structures formed by Vmp1, but not all the puncta of Vmp1 colocalized with ZO-1. Vmp1 did not colocalize with ZO-1 where the tight junctions had already formed, rather colocalizion was restricted to spots where ZO-1 had not yet completely incorporated into the tight junctions. These observations

demonstrate that Vmp1 itself is not a structural component of tight junctions, but it might interact with ZO-1 in the early stages of junction formation.

To check if Vmp1 colocalizes with gap junction markers, cells were stained with an antibody against connexin-43, a transmembrane protein of the gap junctions. No colocalization was detected between the two proteins which suggest that Vmp1 is not a structural component of gap junctions. However, in some cells a similar staining pattern was observed, where Connexin-43 staining was seen along the edges of Vmp1 plaques (Figure 3.21.D). The similar staining patterns might be because of the formation of gap junctions immediately after the initial cell-cell contact had been established by Vmp1.

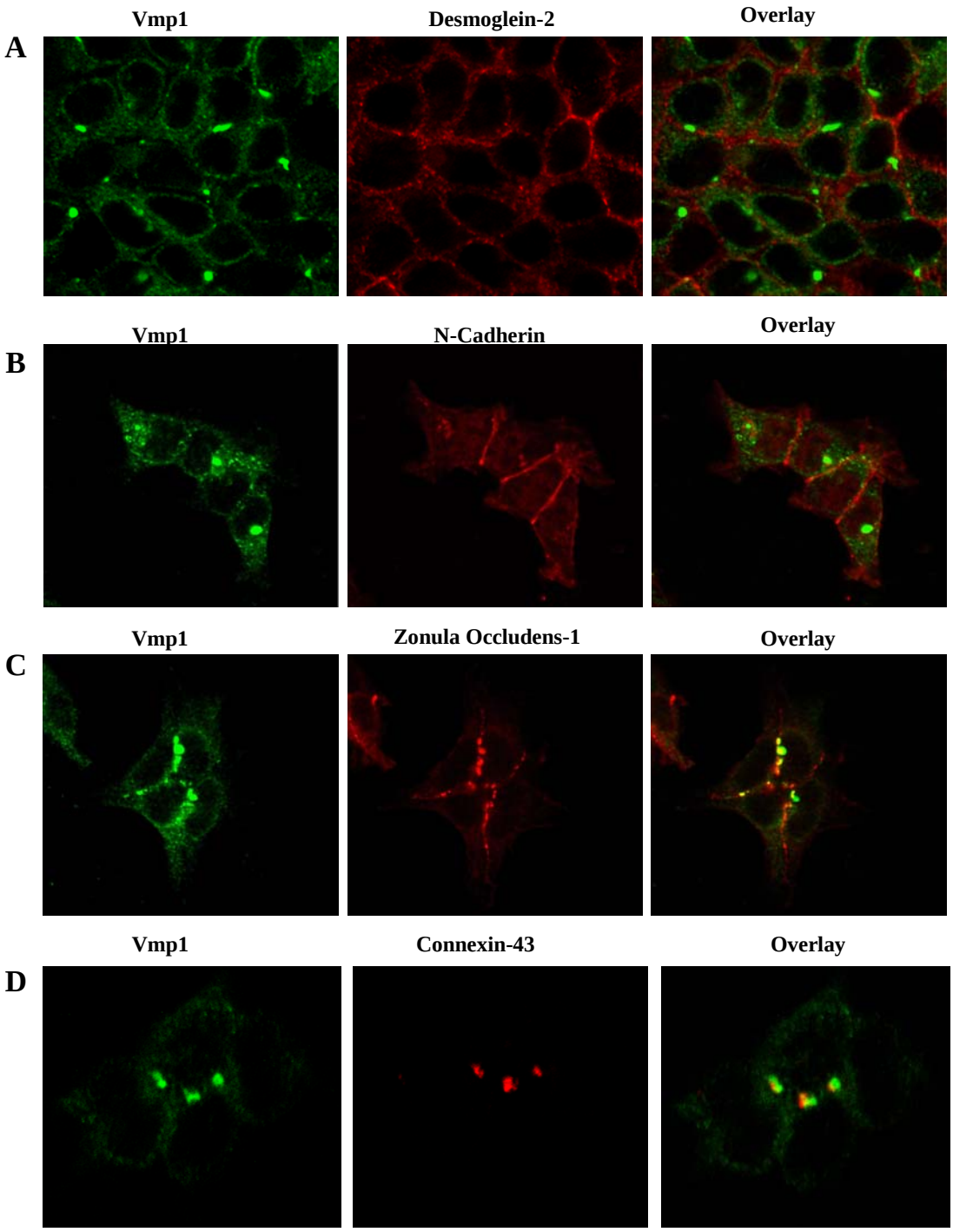

Figure 3.21. Colocalization of Vmp1 with junction markers
HEK293T cells cultured on cover slides for 24 hours were fixed, and with out prior permeabilization stained with anti-Vmp1 antibody followed by Alexa 488 labelled secondary antibody. These cells were then permeabilized and stained with antibodies against cell junction markers followed by secondary antibody coupled with Alexa 647. Images were made using the confocal laser scanning microscope. **(A)** No colocalization was detected with the desmosomal marker protein Desmoglein-2. **(B)** Vmp1 did not colocalize with adherens junction protein N-Cadherin **(C)** Vmp1 colocalized partially with tight junction marker protein Zonula Occludens-1. **(D)** Though the staining pattern of gap junction protein Connexin-43 and Vmp1 looks similar, the two proteins did not colocalize.

3.3.2.4 Vmp1 interacts with ZO-1

Colocalization studies with various cell junction markers showed that Vmp1 colocalizes partially with ZO-1. In order to check if ZO-1 also interacts with Vmp1, coimmunoprecipitations were performed using endogenous ZO-1 as the bait protein (Figure. 3.22). Since the interaction of ZO-1 with Vmp1 was expected at the initial stages of cell junction formation, HEK293T cells were seeded at a low density and cultured to a confluency that allows the formation of initial cell-cell contacts. Cell lysates made from these cells were then used to immunoprecipitate ZO-1 and there by its interacting partners using the ProFound™ Mammalian co-immunoprecipitation kit (Pierce). The proteins were resolved by SDS-PAGE and the membrane was probed with Vmp1 and ZO-1 antibodies. The cell lysate, flow through (cell lysate after incubating with the beads coupled to ZO-1 antibody) and wash before the elution were used as controls.

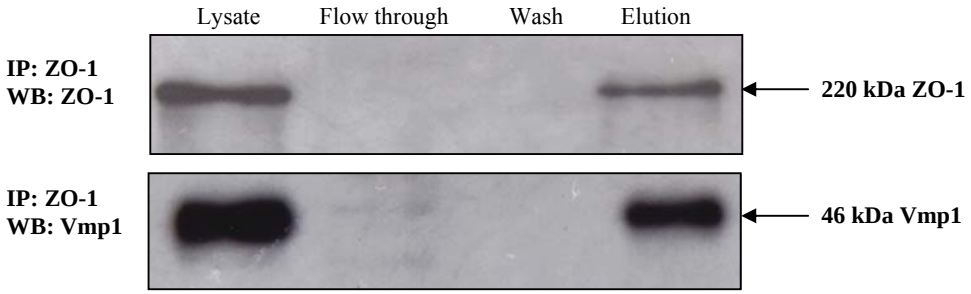

Figure 3.22 Vmp1 interacts with ZO-1
HEK293T cells were cultured to a confluency that allows the formation of cell-cell contacts and the cell lysates were used to immunoprecipitate ZO-1 together with its interacting partners. ZO-1 could be detected in the lysate and the eluate but not in the flow through and the wash. Vmp1 co-immunoprecipitated along with ZO-1 and was detected as a 47 kDa band in the elution. The size of the band is same as that of the Vmp1 detected in the lysate.

A band at 220kDa corresponding to the endogenous ZO-1 was detected in the cell lysate and the elution, while no band was seen in the flow through and the wash (Figure 3.22). Incubating the same membrane with Vmp1 antibody revealed a band at 46kDa corresponding to Vmp1 in the lysate and the elution. This shows that Vmp1 specifically elutes together with ZO-1, thus confirming the interaction between ZO-1 and Vmp1.

3.3.2.5 Reduced *VMP1* expression results in loss of cell adherence

Interaction of Vmp1 with ZO-1 confirmed the idea that Vmp1 is a cell-cell contact protein and suggests its involvement in the formation of junctions between cells. If this is true, down regulation of Vmp1 should inhibit the formation of junctions. To test this, HEK293T

cells expressing endogenous Vmp1 were cultured in 6-well plates and transfected with siRNAs against *VMP1*. The cells were seeded at low density to ensure that no junction formation could occur prior to the transfection. Morphology of the transfected cells was observed over a period of 3 days. By 3 days, cells transfected with *VMP1* siRNA had rounded up and showed loss of adherence, while transfection with control siRNA did not induce significant changes in cell morphology (Figure 3.23.A).

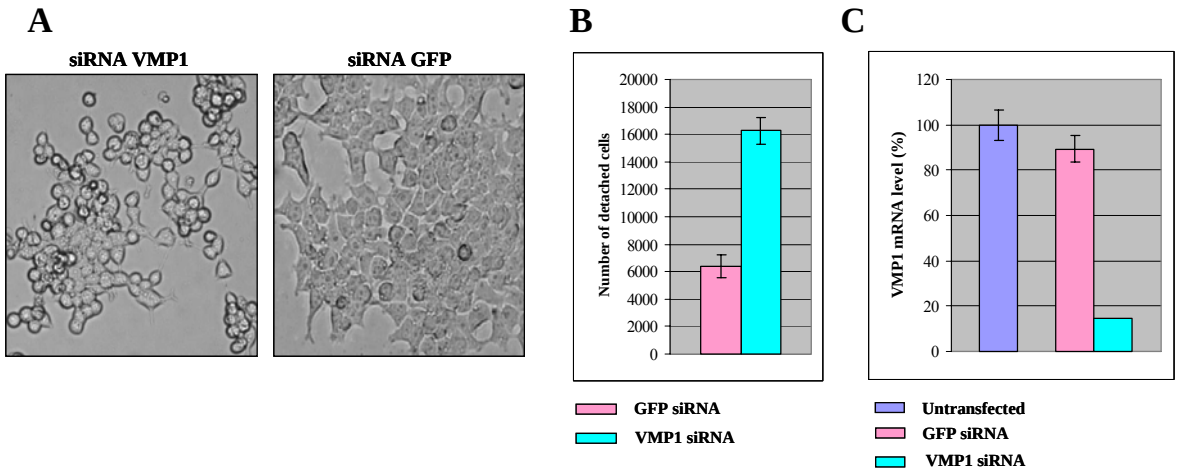

Figure 3.23. Reduction of *VMP1* expression level causes loss of cell adherence
HEK293T cells cultured in 6-well plates were transfected with control siRNA against GFP, which is not expressed in these cells, and siRNAs against *VMP1*. **(A)** Three days after transfection, morphology of the cells was observed under a light microscope. Cells transfected with *VMP1* siRNA showed loss of cell adherence. **(B)** To quantify cell detachment, the detached cells were collected separately, then centrifuged and fixed for measurement on the FACS. Knockdown of Vmp1 resulted in 2.5 fold more non-adherent cells compared to control. **(C)** Down regulation of *VMP1* due to transfection with siRNA was confirmed by quantitative taqman RT-PCR. Transfection with *VMP1* siRNA resulted in the reduction of *VMP1* mRNA by more than 80%.

To quantify the loss of cell adherence, detached cells from the wells transfected with siRNAs against GFP and *VMP1* were collected from the culture medium and counted on FACS. After gating the main population for excluding the debris and cell clumps, only the intact cells were used for analysis. The number of detached cells was >2.5 fold higher in wells transfected with *VMP1* siRNA as compared to the control (Figure 3.23.B). This suggests that the down regulation of *VMP1* and the consequential missing protein at the plasma membrane result in loss of adherence. The down regulation of *VMP1* mRNA was confirmed by quantitative Taqman PCR (Figure 3.23.C). The mRNA level of *VMP1* in siRNA transfected cells was calculated relative to that of untransfected cells which is considered as 100%. Though transfection with GFP siRNA resulted in 10% decrease of *VMP1* mRNA, cells transfected with *VMP1* siRNA showed a decrease in the level of *VMP1* mRNA by more than 80%.

3.3.2.6 Decreased *VMP1* expression in kidney cancer cells induces invasion

An increasing body of evidence indicates that reduction in cell adhesion and cell-cell communication correlates with tumor invasion and metastasis. To test if knock down of *VMP1* affects the invasion capacity of cancer cells, an *in vitro* invasion assay was done using Caki-2, a non-invasive kidney cancer cell line. Cells transfected with *VMP1* or GFP siRNAs were seeded into BioCoat™ Invasion plates (BD Bioscience) and the number of invaded cells was counted on FACS. Down regulation of *VMP1* resulted in a significant increase in the number of invading cells by 3.9 fold, compared to the GFP control (Figure 3.24.A).

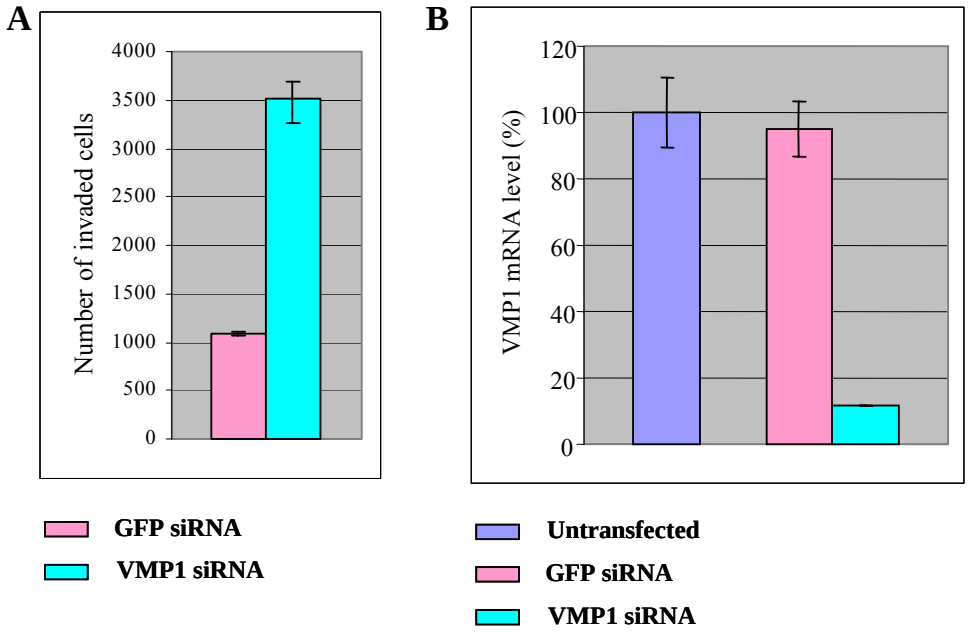

Figure 3.24. Effect of *VMP1* down regulation on tumour cell invasion
(A) Caki-2 cells cultured in 6-well plates were transfected with siRNAs against *VMP1* or GFP. After 24 hours, the cells were serum starved in 1% FCS containing medium for 24 hours. Invasion assay was done using BioCoat™ Invasion plate (BD Bioscience). After 72 hours, the invading cells were detached from the membrane by trypsinization and counted on FACS. Loss of *VMP1* resulted in 3.9 fold increase in the number of invaded cells compared to the control. **(B)** Down regulation of *VMP1* mRNA due to transfection with siRNA was confirmed by Taqman RT-PCR. Caki-2 cells were transfected with *VMP1* and GFP siRNAs and the total RNA was extracted after 48 hours. Equal amount of RNA was used to quantify expression level of *VMP1*. Transfection with *VMP1* siRNA resulted in the reduction of *VMP1* mRNA by more than 85%.

Reduction of the mRNA level due to transfection with *VMP1* siRNA was confirmed by quantitative TaqMan PCR (Figure 3.24.B). Transfection with *VMP1* siRNA resulted in a significant decrease in the mRNA level of *VMP1* (reduction of more than 85%) compared to the untransfected and the GFP siRNA transfected cells. This shows that the loss of *VMP1* increases the invasiveness of kidney tumor cells.

3.3.2.7 *VMP1* is down regulated in kidney cancer metastasis

VMP1 had been found to be up regulated in kidney tumors compared to normal tissues in two independent studies [143] [161], however, no data was available regarding the differences between primary tumors and metastasis. Therefore the expression level of *VMP1* in kidney cancer patient samples was examined for differences between primary tumors and metastasis (collaboration with Holger Sültmann).

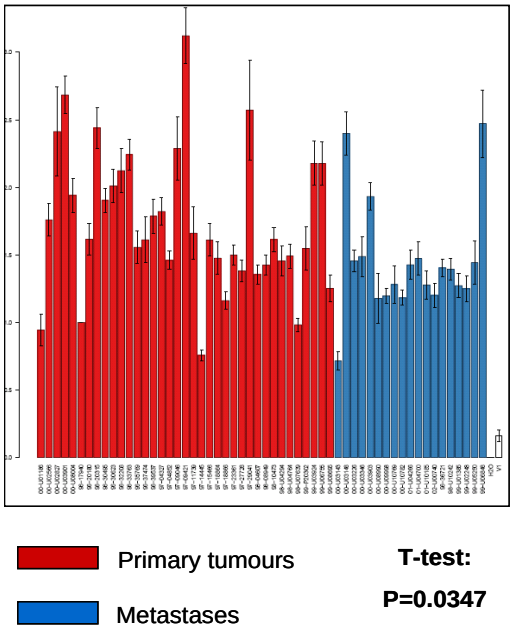

Figure 3.25. Expression analysis of VMP1 in kidney cancer patient samples
Total RNA was extracted from fifty six clear cell renal carcinoma primary tumour (n=37) and metastases (n=16) samples, and the mRNA expression level of VMP1 was analyzed by quantitative RT-PCR. VMP1 mRNA level was found to be significantly less in metastases compared to the primary tumours.

Fifty six clear cell renal cell carcinoma primary tumour (n=37) and metastases (n=16) samples were collected at the University of Göttingen between 1996 and 2002 (by Lazlo Füzesi). The mRNA level of *VMP1* in these patient samples was quantified by quantitative Taqman Real Time-PCR (Figure 3.25). *VMP1* mRNA was found to be significantly reduced in metastasis compared to primary tumors (p=0.0347). This data suggests that Vmp1 plays an important role when tumor cells leave the primary tumor and move to distant sites where they establish metastases.

In conclusion, the overexpression studies revealed that Vmp1 induces apoptosis in HEK293T cells and that the subcellular localization of Vmp1 is dependent on the protein expression level. Endogenous Vmp1 is a plasma membrane protein, but an increase in the expression level results in the accumulation of protein in the ER resulting in the formation of vacuoles ultimately leading to cell death. Vmp1 localizes to cell-cell contact sites, and it also colocalizes partially and interacts with the tight junction protein ZO-1. Loss of *VMP1* induces cell detachment and increases the invasiveness of tumour cells. Finally, the level of *VMP1* mRNA was less in kidney metastases compared to primary tumours.

4 Discussion

4.1 Establishment of high throughput apoptosis assay and screening

The current emphasis of apoptosis in disease has led many researchers to look for the mechanisms mediating its effect. The identification of novel genetic regulators of programmed cell death would provide exciting insights into the pathogenesis of certain diseases, ultimately leading to the identification of novel therapeutic targets for curing specific diseases or limiting their progression. In an effort towards this, we have established a high throughput cell based apoptosis assay and screened for dominant apoptosis inducing proteins.

4.1.1 Need for the identification of dominant apoptosis inducing genes

Along with uncontrolled proliferation, the survival of tumour cells is also in part due to their inability to activate apoptosis [162]. The current approaches for cancer therapy include the induction of apoptosis by different external stimuli such as irradiation, death factors like Fas ligand, TNF α etc., and other chemical compounds [163]. Stimulation of cells with any of these activates well defined apoptotic pathways leading to changes in the expression levels of apoptosis modulating proteins. A large number of proteins that induce or inhibit apoptosis induced by these exogenous factors have been identified. However, proteins that are able to initiate apoptosis in a dominant fashion, e.g. by transient overexpression are rare and are mostly not identified yet. Identification of dominant apoptosis inducing proteins would be helpful in the development of novel therapeutic strategies to combat cancer. Such genes could be used to induce apoptosis of cancer cells, for example in gene therapy applications involving vector dependent overexpression of the protein and/or promoting the overexpression of the protein *in vivo* by stimulating the endogenous promoter. Modulating the expression of key components of the apoptotic machinery to tip the balance between pro- and anti-apoptotic signals in tumour cells is a rational approach in cancer therapy.

Protein-protein interactions are mostly responsible for the induction of apoptosis [26] [164]. Moreover, it is known that many apoptosis inducing proteins such as death domain containing proteins, p53, pro apoptotic Bcl-2 family proteins etc achieve their effect at elevated concentrations [165] [166] [167] [168]. So, one of the approaches to identify proteins

inducing apoptosis is to overexpress them in a cell system and generate these interactions artificially which would lead to the induction of apoptosis.

4.1.2 Selection of the apoptosis assay amenable for high throughput screening

The selection and establishment of a suitable assay was one of the most important parameters in the installation of the apoptosis screen. All the high throughput apoptosis screens reported by the time this project was initiated had been applied to test chemical compounds for their activity as inhibitors or activators of apoptosis [169] [170], but no high throughput screens to identify apoptosis activating/inhibiting proteins after transiently transfecting the cells with cDNAs were described. Since the drug screening assays do not depend on transient transfection of cDNAs, the results are typically detected from the whole population of cells using uniform well readout methods such as a plate reader. However, transient transfections introduce high cell-cell variations even within the same well due to differences in the protein expression levels within a population of cells. Moreover, some proteins exert their effect only once a certain expression level has reached. In such cases, only a method of detection that allows single cell resolution, can detect changes in signal obtained from a few cells within a well. Therefore, major efforts in the first part of the work were directed towards the selection of a suitable and sensitive method, and in the automation and optimization of the assay conditions.

Technical considerations for assay selection

We aimed at selecting an assay which is highly specific for apoptosis, sensitive enough to detect even minute changes in the parameter being assessed, and at the same time robust enough to be automated for high throughput screening. Although any assay, in theory, can be applied in high throughput screening, conversion to an automated format imposes certain constraints that affect the design of the assay in practice. Plate reader based assays, though do not allow resolution up to a single cell, offer the advantage that the data acquisition times are very short (approximately 2-3 minutes/96-well plate). Many high throughput applications use this method of detection mainly because of this reason.

Methods based on flow cytometry (FACS) are most commonly used in apoptosis research because several parameters of individual cells can be measured simultaneously and it facilitates the measurement of adherent as well as floating (apoptotic) cells. Moreover, when cells are transfected with YFP tagged ORFs, the transfected cells can be distinguished from the untransfected cells by this method, thus allowing the analysis of protein effect in relation

to its expression level. Because of these advantages, I tried two different high throughput apoptosis assays – one based on plate reader and another based on FACS. More recently, automated microscopes are being used for high throughput applications to monitor changes at the level of individual cells within an assay well [3] [171]. However, microscopy based methods were not considered for high throughput detection of apoptosis because apoptotic cells lose their adherence and detach from the surface of the well easily. This might result in underestimation of the total number of apoptotic cells thus leading to misinterpretation of the assay outcome, and perhaps, missing the strongest apoptosis inducers.

A diverse range of apoptosis assays are currently available, out of which TUNEL, annexin V binding assay, detection of cells with fractional DNA content (sub-G1 peak), and the activity of proteases are most widely used (refer section 1.4). However, some of these methods are not very specific for apoptosis, while some are not compatible with the cell system used here for the assay.

1. Though extensively used, TUNEL assay detects both apoptotic and necrotic cells, and therefore can not be considered as a specific assay for apoptosis [172]. Moreover, this method is technically demanding and adapting it to a high throughput format is difficult.
2. FACS based Annexin V assay is suitable for use only with cell types that grow in suspension, because procedures applied to detach adherent cells from the surface leads to exposure of phosphatidylserine even in non-apoptotic cells [173]. But most of the suspension cell lines have a low transfection efficiency making them unsuitable for experiments based on transient transfections.
3. Late apoptotic cells reveal themselves as a sub-G1 peak in a DNA histogram. However, cellular debris (perhaps due to necrosis) also accumulates in this sub-G1 region, making this assay ambiguous.
4. Activation of caspases is likely the most specific indicator of the apoptotic process. Apoptotic pathways originating from different cellular organelles converge on the activation of effector caspases, most importantly caspase-3. Several methods are currently available to detect the activation of caspase-3.

So, I tried to establish a high throughput apoptosis assay in which either the activity of caspase-3 can be determined as a function of FRET (plate reader assay), or the presence of activated caspase-3 can be detected by a specific antibody (FACS based assay).

4.1.3 Establishment of FRET based assay

It has been demonstrated in several studies that it is feasible to use GFP based FRET method for detecting the activation of caspase-3 during apoptosis [140] [174]. A FRET based high throughput assay to identify novel apoptosis inhibiting drug compounds has been described by Tawa, P et al [169]. In this assay, HeLa cells stably expressing a FRET construct (fusion protein with the fluorophores W1B and Topaz linked together with a caspase-3 substrate site) were treated with different drugs, and changes in the FRET signal was monitored using a plate reader. I tried to adapt this assay to screen for apoptosis activators in NIH3T3 cells. Therefore, a FRET probe was constructed with CFP and YFP, linked together with a special linker containing the caspase-3 cleavage site. The design and length of the linker region plays an important role in determining the strength of the FRET signal. One of the frequent problems encountered in such FRET constructs is that the caspase-3 substrate site is not always accessible for cleavage. So an optimized 16 amino acid linker region was used, which had been previously demonstrated by Luo KQ et al. to produce a strong FRET effect and also to be efficiently cleaved by caspase-3 due to the special design of the sequence flanking the DEVD substrate site [151].

Though treatment with staurosporine (1μM for 4 hours) was demonstrated by Tawa,P et al. to result in complete cleavage of the FRET probe, only a small amount of cleavage product was detected in our experiment (Figure 3.4B). This could be because of very high expression level of the FRET protein due to transient transfections, which might be beyond the cleavage capacity of the endogenous caspase-3. However, since the occurrence of FRET could be demonstrated by microscopy in cells transiently transfected with the FRET construct (Figure 3.5), I proceeded with the generation of stable cell line which would express less amount of protein compared to transiently transfected cells.

Seven clones of the FRET protein (CFP-DEVD-YFP) and 2 clones of the control probe (CFP-YFP) were isolated and were found to constitutively express the fusion proteins. One clone stably expressing the FRET protein was used to detect the fluorescence using a plate reader. The fluorescence signal was observed only with a high cell number (18,000 cells/well). But such a high cell number/well in a 96-well plate forms a very confluent monolayer, which is not suitable for transfections. Most of the plate reader based assays use cell lysates from which the fluorescence is detected. But the instrument needs to be very sensitive to detect signal from intact cells. Based on this experience, another assay was established where the signal from individual cells can be measured by a flow cytometer.

4.1.4 Establishment of assay to detect activated caspase-3 by flow cytometry

Detection of active caspase-3 provides a direct and specific way of identifying apoptosis. Antibodies detecting the cleaved or activated forms of caspase-3 have been developed and successfully applied in some studies to detect apoptosis [175] [141]. In spite of the specificity of detecting apoptosis, this method has not been used yet for any high throughput applications. Though flow cytometry is a common detection method in apoptosis research, to date, no flow cytometry based screens have been reported. Combining these two, a flow cytometry based high throughput assay was developed to screen for novel apoptosis activating proteins. Apart from the specificity of detecting apoptosis, this assay offers the advantage that the activation of caspase-3 and the expression level of the YFP tagged protein can be measured and correlated at the level of single cell. Moreover, the amount of information that can be extracted from the individual scatter plots gives a better picture about the protein compared to the plate reader based detection methods. For example, parameters such as the expression level of the protein that is required to induce apoptosis; proteins (such as death ligands, receptors, secreted proteins) that are able to induce apoptosis also in the untransfected cells of the same well can be easily identified from the scatter plots.

Choice of cell line for the assay

The assay was initially tested with a subset of control proteins in NIH3T3 cell line. Though apoptosis activators could be identified in this cell line, the effects were statistically insignificant. Along with the poor quality of the mini-prep DNA (compared to maxi prep-DNA), this is also in part due to the nature of this cell line resulting in low transfection efficiency. Moreover, this cell line seems to be more sensitive to stress conditions including transfection, which resulted in a significant population of untransfected cells undergoing apoptosis. This finally masked the specific signal obtained from the transfected population. Apoptosis is not always synchronous i.e. the cells within a population may begin apoptosis at different times, and the length of various stages of apoptosis varies from cell to cell. Therefore, to increase the possibility of detecting significant number of positive cells from a population of cells undergoing apoptosis in an asynchronous way, it is necessary to have a high number of transfected cells. So, the human epithelial cell line HEK293T, known for its high transfectability was used for screening. With this cell line, a transfection efficiency of more than 90% could be achieved even with miniprep DNA. Moreover, this cell line is not too sensitive to stress, which resulted in a very specific detection of the effect of overexpressed protein on apoptosis.

Assay Automation

An ideal high throughput assay is one that can be performed in a single well with no other manipulation other than addition of the sample to be tested. Though it is very easy to automate such methods, the specificity and/or sensitivity of the assay will be compromised. Therefore, to develop a high throughput assay, it is necessary to maintain a balance between specificity/sensitivity of the method and the level of automation. Two high throughput screens to identify apoptosis activators (after transient transfections) have been described recently. In one of the screens, the activities of β-Galactosidase and reduction in the secretion of alkaline phosphatase from cells transfected with cDNAs were used as markers to detect apoptosis in a plate reader based assay [176]. Overexpressed proteins of the secretory pathway or proteins that are targeted to the plasmamembrane accumulate in the ER, preventing the normal protein transport mechanism of the cell. Therefore, utilizing the secretion level of a protein as a marker for apoptosis induction is not appropriate in such cases. Though it is easy to automate such a screen, the assay is not specific for apoptosis. Another screen for identifying apoptosis activators used the reverse transfection cell array technology, and the proapoptotic genes were identified by fluorescence microscopy based on the nuclear morphology (after staining with DAPI), and the formation of apoptotic bodies in transfected cells [177]. Analyzing the morphological changes of transfected cells as well as quantifying the amount of apoptosis by manual observation is very laborious, which makes this method not ideal for high throughput screening. Moreover, valid conclusions can not be drawn by analyzing less than 500 transfected cells/spot.

The caspase-3 apoptosis assay described here reached a reasonable compromise between specificity and level of automation. Detection of activated caspase-3 by flow cytometry is a very specific and sensitive assay for detecting apoptosis. The process of transfection is completely automated but the staining procedure involves some centrifugation steps which require manual intervention. Moreover, data from >10,000 cells/well could be analyzed, which resulted in statistically significant results.

4.1.5 Screening for apoptosis inducing genes and candidate selection

A total of 200 full length proteins have been screened in the assay. One frequent problem associated with the use of GFP tagged ORFs is that the localization of some proteins is affected based on the orientation of the tag [2] [4]. To circumvent this, both the tag orientations for each ORF have been screened, and each experiment was repeated 4 times. Initially a set of 12 candidate proteins which showed medium to strong activation of caspase-

3 were selected, and were then screened in a nuclear fragmentation assay to confirm the specificity of the caspase-3 assay. Though all these proteins induced morphological changes of the nucleus, only 5 proteins that induced a very strong nuclear fragmentation were finally selected as candidates of the apoptosis assay. Thus, less than 2% of the screened genes induced activation of caspase-3. The high specificity of the caspase-3 assay was confirmed by the nuclear fragmentation assay- the proteins which produced a clear effect in the caspase-3 assay also showed a strong nuclear fragmentation (Figure 3.14). The protein domain classifications from Source [178] and Interpro [179] provided the functional annotation of the candidates (Table 3.7). This screen has been done in a kidney cell system, and follow up experiments are necessary to validate these candidates in other cell types. In the following, the five candidates are described together with their association with apoptosis.

4.1.6 Candidates of the apoptosis assay

FUN14 domain containing 2

The protein encoded by cDNA xq28i14160 is a mitochondrial protein and contains a Fungal ATP synthase domain [180]. The overexpressed protein is a strong activator of apoptosis. The protein had initially been identified in a yeast two hybrid screen to interact with Hepatitis C core protein [181]. Hepatitis C virus is a major causative agent of chronic hepatitis, cirrhosis, and hepatocellular carcinoma [182], and the core protein is a structural viral protein that packages the viral genomic RNA. Besides its essential role in viral replication, the core protein is involved in a variety of functions like signal transduction, cell cycle regulation, changes in gene transcription as well as apoptosis [183]. Previous studies regarding the role of this protein in apoptosis demonstrated controversial results. There are several studies indicating that the core protein suppresses apoptosis mediated by Fas, c-myc and TNF-α [184] [185] [186], while other studies showed that it promotes apoptosis by interacting with different proapoptotic pathways like TNFR I, Fas and the p53 pathways of apoptosis [187] [188] [189]. Though the differences in activity could be cell-type specific, it is clear that the core protein regulates apoptosis. But the precise mechanism by which this is done is not fully understood. The core protein was shown to suppress the activation of caspase-3 [190], while overexpression of the protein encoded by cDNA xq28i14160 leads to the activation of caspase-3. Therefore, it is possible that the core protein suppresses the apoptosis activating effect of the protein encoded by cDNA xq28i14160 by interacting with it.

Interferon alpha inducible protein 27 or ISG12(a) protein

The protein encoded by the cDNA IRATp970A0419 is an interferon alpha inducible gene and belongs to the ISG12 gene family. Interferons are a family of cytokines which exert their biological function through the activation of interferon stimulated genes (ISGs). The ISGs participate in a variety of biological functions involving antiviral, apoptotic, antiproliferative, antitumor and immunomodulatory activities [191]. The protein sequence of ISG12 has 33% overall sequence identity to the product of the 6-16 gene (also an interferon stimulated gene), but the functions of 6-16 as well as ISG12 have not been identified yet. It has been demonstrated that a high degree of similarity exists between the induction pattern of 6-16 and ISG12 in various cell lines [192] suggesting the possibility that these proteins might play related roles in the interferon system. Increased expression of 6-16 has been found during cell growth arrest and in senescent cells [193] [194] indicating that 6-16 is involved in growth inhibitory processes. Overexpression of ISG12(a) induced activation of caspase-3 and subsequently apoptosis, which is consistent with the growth inhibitory property of 6-16. However, 6-16 and ISG12 were shown to be upregulated in gastric cancers and, breast and epithelial cancers respectively [195] [196] [197] contradicting the growth inhibitory and/or apoptosis activating functions. A similar pattern has been observed for several well known oncogenes. Activation of oncogenes is observed in many cancers and it is well established that oncogenes promote cell proliferation and tumorigenesis. However, vector-dependent overexpression of oncogenes like c-myc, E1A, E2F-1 was shown to induce powerful apoptosis or growth arrest of cancer cells [198] [199] [200].

Solute carrier family 25, member 31

The protein encoded by cDNA htes3_35n12 is a strong inducer of apoptosis and is a novel member of the mitochondrial solute carrier family 25. This family of proteins is involved in the exchange of cytosolic ADP for mitochondrial ATP [201]. Three isoforms of this protein family (Adenine nucleotide translocator (ANT) 1, 2 and 3) with tissue specific expression patterns have been described in humans [202]. The protein encoded by cDNA htes3_35n12 is the fourth isoform and shares 66-68% amino acid identity with the other three isoforms [203]. Overexpression of a well known member of this family, ANT1, has been demonstrated to induce apoptosis. Apoptosis induced by overexpressed ANT1 was shown not to be due to increased exchange of ADP/ADP by the formation of non-specific pore, but is through specific interactions with proteins of the mitochondrial permeability transition pore

and through regulation of NF-κB activity [204] [205]. The fourth isoform of this protein family might induce apoptosis in a mechanism similar to that of ANT1.

Brain protein 44

The protein encoded by cDNA hfbr2_7b16 is localized to the mitochondria and it belongs to a family of proteins of unknown function. No similarities to known proteins or domains have been found. However, genes similar to this have been found in dog, mouse, zebra fish, fruit fly and worm indicating that the function of the protein might be important in the cell (GeneCards) [206]. A similar protein called brain protein 44-like (from *Rattus norvegicus*) is predicted to be localized to the inner mitochondrial membrane and that it might be involved in the apoptosis of neuronal cells (SOURCE) [178]. This is consistent with the mitochondrial localization and the apoptosis inducing effect of brain protein 44 observed here.

Vacuole membrane protein 1

The protein encoded by cDNA hfkd2_3i13 is an apoptosis inducer and has no known domains or similarities to known proteins. Its homologue, rat Vmp1 was identified by Dusetti et al. in rat pancreas which is affected by pancreatitis [159]. Overexpressed rat Vmp1 was shown to localize to the endoplasmic reticulum (ER) and Golgi apparatus and that it promotes formation of intracellular vacuoles, with Vmp1 being integrated into the membranes of the vacuoles. Cells overexpressing Vmp1 died after 48 hours showing morphological features of apoptosis. The mRNA was shown to be absent in normal pancreas, but is strongly and rapidly activated after the induction of experimental pancreatitis. Therefore, *Vmp1* was described as a stress induced gene that might be activated by pancreas as an emergency program against pancreatitis. Furthermore, rat *Vmp1* mRNA was also found overexpressed during kidney ischemia. The expression of rat *Vmp1* mRNA was also detected in several normal tissues like intestine, kidney, liver, lung, brain etc. suggesting that Vmp1 is essential for the normal growth and survival of cells. Moreover, *VMP1* is evolutionarily conserved and its homologues are found also in lower organisms like *Drosophila melanogaster*, *Caenorhabditis elegans* and *Arabidopsis thaliana*, which further emphasizes that the function of Vmp1 protein might be very important.

4.2 Detailed analysis of Vacuole Membrane Protein 1 (Vmp1)

The human *VMP1* cDNA was isolated in our department from human fetal kidney, and the GFP tagged cDNA was used in various assays to determine the function of this protein. The overexpressed human Vmp1 was reported to localize in the endoplasmic reticulum (ER) and Golgi complex [5], and to have a repressing effect on secretory membrane transport in HeLa cells [171]. Slight overexpression in NIH3T3 cells resulted in repression of proliferation, and in human Caki-1 kidney cancer cells the overexpressed protein reduced anchorage independent growth [3]. Here overexpression of Vmp1 induced apoptosis in HEK293T cells. These results suggest a role of Vmp1 in tumour relevant cellular processes, which is further supported by expression profiling data [161] [143]. On this basis, we aimed to define the cellular processes Vmp1 is involved in, and how this protein is associated with tumorigenesis. Rat *Vmp1* was shown to be overexpressed during pancreatitis and kidney ischemia, conditions in which cells die by apoptosis as well as necrosis. Since overexpression of Vmp1 was found to induce apoptosis, I first tried to determine why cells overexpressing Vmp1 undergo apoptosis.

4.2.1 Vmp1 induces apoptosis through the ER stress pathway

Transient overexpression of GFP tagged Vmp1 induced apoptosis in HEK293T cells. Several criteria like the activation of caspase-3, morphology of the dying cells, and the fragmentation of nucleus (Figure 3.15) suggest that the Vmp1 induced cell death occurs by apoptosis rather than by necrosis. *Vmp1* mRNA is expressed in many rat tissues [159]. Apparently, physiological levels of this protein are most probably essential for the cell. However, in HEK293T cells, elevated levels of this protein are not tolerated, with the consequence of cell death. One day after protein expression, vacuoles were seen in the cells, but the cells were not apoptotic as indicated by the absence of activated caspase-3 and the apoptotic morphology. Staining with marker proteins for ER and Golgi apparatus showed that the vacuoles were formed from the endoplasmic reticulum, suggesting that overexpression of Vmp1 induces morphological changes of the ER. However, by 2 days the vacuoles/ER collapsed, which was accompanied by induction of apoptosis. Along with the transfected cells, even the non-transfected bystander cells were found to undergo apoptosis. Though the exact mechanism of vacuole formation is not known, collapse of the ER might be due to protein overload leading to accumulation of unfolded proteins in the ER. This prevents the transport of essential membrane receptors and cell adhesion proteins (like Vmp1) to the

plasma membrane, resulting in failed cell junction formation and cell-cell signaling. Missing cell-cell contacts (between Vmp1 overexpressing cells and the neighbouring non-transfected cells) initiate a stress response in cultured cells which ultimately leads to apoptosis. This might explain the death of non-transfected cells co-cultured with Vmp1 overexpressing cells. This is also consistent with the results of Starkuviene et al, reporting that overexpression of Vmp1 inhibits the secretory pathway in HeLa cells. Thus, it is probable that apoptosis induced by overexpression of Vmp1 is through the ER-stress pathway.

It is now well established that Endoplasmic Reticulum acts as a stress sensor and can initiate specific apoptosis pathways as a result of protein accumulation and/or depletion of calcium stores [62]. *Vmp1* was found to be overexpressed during pancreatitis and kidney ischemia, and it has been reported that increase in the cytosolic calcium (or decrease in the ER calcium stores) has been observed in these two conditions [207] [208]. This might be a result of accumulation of Vmp1 in the ER, resulting in collapse of the ER, thus releasing the calcium into the cytosol. Similar effect has been observed in Alzheimer's disease in which mutations in the presenilin genes was responsible for the accumulation of unfolded proteins in the ER causing apoptosis of the neuronal cells [125].

4.2.2 Vmp1 is a plasmamembrane protein

Localization studies with overexpressed GFP-tagged Vmp1 revealed two different localizations- Endoplasmic Reticulum and the Plasma membrane (Figure 3.16). Vmp1 was predicted by SOSUI [160] to be an integral membrane protein containing 7 transmembrane domains, an extracellular N-terminal and a cytoplasmic C-terminal end, two large and one small extracellular domains, and only short intracellular domains (Figure 3.20A). However, analysis of the protein sequence did not reveal specific ER retention signal. Moreover, to date no ER-located seven transmembrane domains containing protein has been described. Therefore, it was hypothesised that Vmp1 is a plasma membrane protein and the localization of Vmp1 in the ER might be only due to accumulation of the protein as a result of high expression level. To confirm this, HEK293T cells were stained without prior permeabilisation, with a Vmp1 antibody directed against a predicted extracellular domain. Confocal microscopy indeed revealed that endogenous Vmp1 is present at the plasma membrane, where it is distributed in a punctuate pattern all over the cell (Figure 3.20B). In subconfluent colonies of cultured HEK293T cells Vmp1 was also detected in sites of initial cell-cell contacts, suggesting that Vmp1 might be involved in the formation of junctions between cells.

4.2.3 Vmp1 is an essential cell-cell contact protein

The first step towards understanding the function of a protein is to find the interacting partners of the protein of interest. But no predicted protein interaction domains or similarities to known proteins were identified in the protein sequence of Vmp1. Since Vmp1 also localizes to areas of cell-cell contact, another possibility was to perform colocalization studies with cell junction marker proteins. Based on these experiments, I could exclude that Vmp1 is a structural component of any of the cell junctions. However, Vmp1 was found to colocalize with ZO-1, a tight junction protein, but the colocalization was limited to spot-like areas between cells where ZO-1 had not yet incorporated into the tight junctions (Figure 3.21C). This suggested that the interaction of Vmp1 and ZO-1 is transient and might occur before the formation of tight junctions. Coimmunoprecipitation experiments proved that Vmp1 indeed interacts with ZO-1 (Figure 3.22).

In epithelial cells, the initial cell-cell contact is established by Cadherins, which form homodimers in the intercellular space in a calcium-dependent manner [209]. Cell junction formation and polarization of epithelial cells then initiates by the formation of primordial adherens junctions at the sites of cell-cell contact [210]. The primordial junctions are spot-like structures and consist of both adherens and tight junction proteins [211] [212] [213]. When the cells start to polarize, tight junctions are formed, and the proteins specifically enriched at adherens junctions and tight junctions start to segregate. Though ZO-1 is traditionally considered as a marker for tight junctions, it was found also at the primordial junctions together with E-cadherin [211]. Since the colocalization of Vmp1 and ZO-1 was seen outside the tight junctions, I postulated that Vmp1 colocalized with ZO-1 in primordial junctions and thus might play a role in maturation of cell junctions and/or polarization of epithelial cells.

This idea was further strengthened by the finding that the staining patterns of Vmp1 and the gap junction protein Connexin-43 were similar in some cells though exact colocalization was not found. This indicates that the initial cell-cell contacts established by Vmp1 might trigger the formation of gap junctions between these cells. A similar phenomenon was observed in case of regenerating hepatocytes where E-cadherin mediated cell-cell contacts sites acted as foci for gap junction formation [214]. I thus hypothesize that, similar to E-cadherin, the initial cell-cell contacts established by Vmp1 between adjacent cells might occur by homo-or heteromerization of the large extracellular domains of Vmp1.

4.2.4 Loss of Vmp1 induces cell detachment and invasion

Down regulation of *VMP1* mRNA in HEK293T cells resulted in a reduction of cell adhesion (Figure 3.23). This is possibly due to the failed formation of cell junctions and caused by the absence of Vmp1 which is essential in the initial stages of cell junction formation. Tumour progression is frequently accompanied by decreased cell-cell and cell-matrix adhesion [215]. Reduced levels of cell-cell adhesion proteins often correlate with tumour invasion and metastasis [216] [217] [218]. To check if this holds true for Vmp1, the invasion potential of CaKi-2 cells (non-invasive kidney cancer cell line) in which *VMP1* mRNA is down regulated by transfections with siRNA was determined. Loss of Vmp1 resulted in an increase in the invasion potential of the cells, which might be due to decreased formation of cell junctions. These results are consistent with previous studies in our department showing that *VMP1* expression is lower in invasive Caki-1 cells compared to the non-invasive Caki-2 kidney cancer cells [3]. This further suggests that the expression level of Vmp1 determines the invasion capacity of cancer cells.

Disruption of cell junctions is commonly associated with metastasis of epithelial cancer cells. For example, elimination of Adherens Junction formation due to loss of E-cadherin expression has been described to correlate with the acquisition of metastatic capacity in tumour cells [216]. Kim et al. recently reported tight junctions to be significantly reduced in renal clear-cell carcinoma when compared to normal tissue [219]. In pancreatic cancer cells, the expression of the tight junction protein claudin-4 is associated with reduced invasive and metastatic potential [218]. It was shown that the tight junction plaque proteins ZO-1 and MUPP-1 were significantly lower expressed in patients with metastatic breast cancer compared to patients remaining disease-free after primary tumour excision[217]. This encouraged me to check for the expression level of *VMP1* mRNA in tumour samples. Expression profiling studies showed that *VMP1* is up regulated in kidney tumours compared to normal kidney [220] [161]. Since loss of Vmp1 in cancer cells might initiate invasion of cancer cells leading to metastases, the mRNA level of *VMP1* in primary tumours was compared with that of metastases (in collaboration with Dr. Holger Sültmann). As expected, *VMP1* mRNA was less in metastases compared to the primary tumours. This suggests that downregulation of Vmp1 is associated with the transition from primary to secondary tumours at least in kidney cancer, and that the protein is a critical determinant of cell invasiveness.

4.2.5 Role of Vmp1 in disease

Vmp1 mRNA was previously shown to be overexpressed during kidney ischemia and acute pancreatitis in rat tissues [159]. In the present work, I have shown that human Vmp1 is associated with metastasis of cancer cells. Based on the findings that Vmp1 is a cell-cell contact protein involved in the initiation of cell junction formation, and that overexpression of Vmp1 induces apoptosis in cultured cells, I propose the following models for its role in tumour invasion, kidney ischemia and pancreatitis.

4.2.5.1 Proposed role of Vmp1 in tumour invasion

The first step in the generation of intercellular adhesion is the formation of primordial junctions involving proteins of AJ and TJ. Formation of cell-cell contacts and the subsequent maturation of the components into distinct AJ and TJ take place properly only in the presence of Vmp1 (Figure 4.1.A). Consequently, downregulation of Vmp1 leads to failure in the formation of both junctions and results in non-polarised, migrating cells. In tumour cells, these events could initiate invasiveness through cytoskeletal changes, perturbed signaling pathways and transcriptional dysregulation.

On the molecular level, a comparable mechanism has been described for the primordial and AJ protein E-cadherin, which also functions as an invasion suppressor [221]. The cytoplasmic domain of E-cadherin recruits β-catenin to adherens junctions and connects the adherens junctions with the actin cytoskeleton [222] (Figure 4.1.B). Free β-catenin is normally phosphorylated by glycogen synthetase kinase 3β (GSK-3β) in the absence of E-cadherin [223], and is subsequently degraded. If this mechanism is blocked, β-catenin first accumulates in the cytoplasm and is then translocated into the nucleus [224]. There it binds to member of TCF/LEF-1 family transcription factors which activate the expression of important growth regulatory genes like cyclin-D1 and c-myc [225]. In addition, loss of functional AJ would further result in changes of cytoskeletal organization, which in turn might lead to a higher invasive potential of the tumour cells.

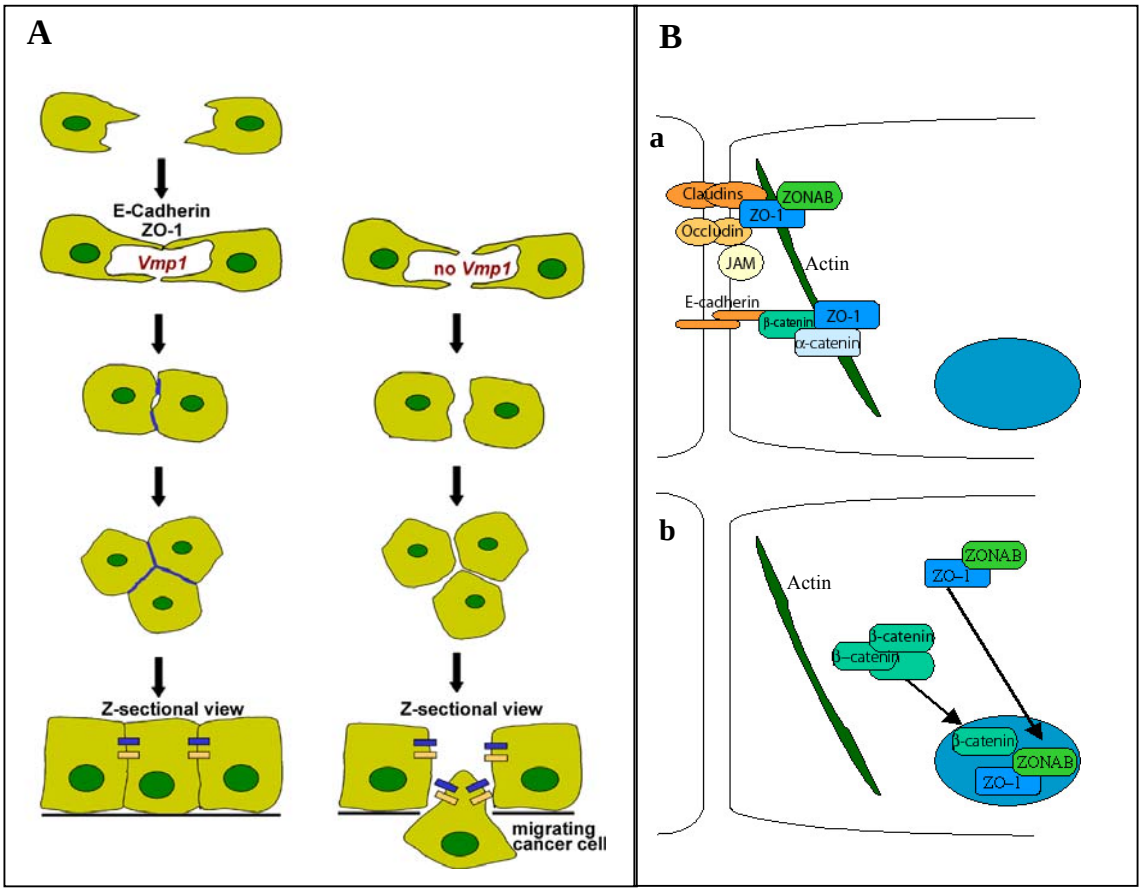

Figure 4.1. Model for the involvement of Vmp1 in tumor invasion (modified model of Ebnet et al [213].
(A) Initial contacts between epithelial cells appear as primordial, spot-like junctions, containing proteins of adherens junctions and tight junctions. Vmp1 initiates the formation of such structures, which later mature into TJs and AJs (blue and yellow bars respectively, in the Z-sectional view). Loss of Vmp1 inhibits TJ and AJ establishment, supporting cell migration and metastasis. **(B)** Presence of intact TJs and AJs recruits the cell adhesion molecules to the junctions. Failed formation of the junctions results in the translocation of some of these proteins to the nucleus where they activate genes resulting cell growth and proliferation. These events might initiate tumour growth and invasion.

The loss of functional tight junctions has also been reported to have similar effects on cell proliferation and invasion. Tight junctions act as a barrier permitting the selective passage of ions and solutes through the paracellular pathway [226]. On one hand they work as a fence separating plasma membrane into apical and basolateral areas, while on the other, they act as multifunctional complexes recruiting signaling proteins that regulate cell polarity, gene expression, and proliferation [227] [228]. In tight junctions, the peripheral membrane protein ZO-1 binds to integral membrane proteins thereby serving as an adaptor e.g. for actin and the transcription factor ZONAB (Figure 4.1.B). However, in subconfluent cells with no junction formation, and during the remodeling of cell contacts [229], ZO-1 localises to the nucleus where it interacts again with the transcription factor ZONAB. ZO-1 and ZONAB have been shown to control ErbB2 expression in MDCK cells [230]. If ZO-1 and ZONAB are not

sequestered to tight junctions as a consequence of missing tight junctions, they might act permanently as transcriptional modulators, promoting proliferation and invasiveness. Failed formation of adherens and tight junctions due to downregulation of Vmp1 could induce similar effects on cell adherence and invasion.

4.2.5.2 Proposed role of Vmp1 in Kidney Ischemia

Ischemic renal failure is characterized by loss of ability of the kidneys to excrete wastes, to concentrate urine and maintain fluid balance. This is a result of dysfunction of kidney tubules, and is associated with the shedding of viable and nonviable epithelial cells into the lumen, thus causing tubular obstruction [128, 231] (Figure 4.2.A). The major cellular and molecular changes occurring during kidney ischemia include loss of epithelial cell polarity [232], misfolding and/or aggregation of membrane and secreted proteins [233], mislocalization and degradation of proteins forming intercellular junctions [234], perturbation of integrin mediated adhesion [235] [236], and induction of apoptotic or non apoptotic cell death [237]. Kidneys damaged by ischemia have the ability to recover their structure and function completely. However, the recovery is dependent on the magnitude and duration of the ischemic insult. Sub-lethal ischemic insult results in complete recovery of the renal tubules, while prolonged ischemia leads to cell death by apoptosis and necrosis [238].

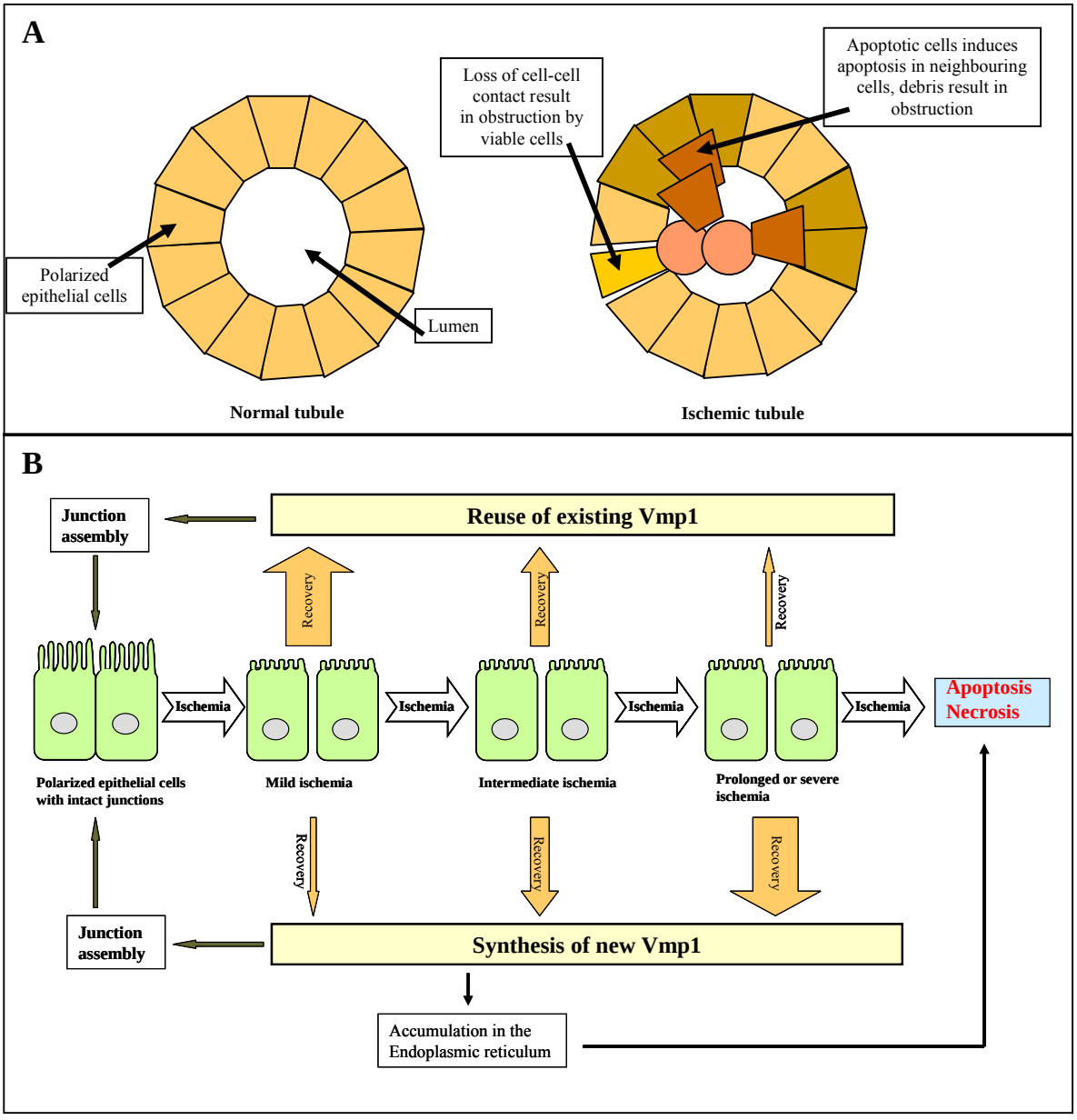

Figure 4.2 Model for the involvement of Vmp1 in Kidney ischemia (Modified models from (A) Schrier et al [128] and (B) Bush etal [238].
(A) Obstruction of the tubule during ischemia is caused by the shedding of viable cells (as a result of lost cell junctions) and nonviable cells (apoptotic and necrotic cells) into the lumen. **(B)** Cells subjected to mild ischemia mostly reuse the existing Vmp1 to assemble new junctions. With increase in the severity of ischemia, cells synthesize new Vmp1 which might accumulate in the ER causing apoptosis.

Vmp1 was shown to be overexpressed in kidney subjected to ischemic injury [159], but the role of Vmp1 in kidney ischemia is not known yet. Based on the experimental evidence that Vmp1 is a cell adhesion protein involved in the formation of initial cell-cell contacts, I hypothesise that Vmp1 might be involved in the recovery phase leading to the regeneration of epithelial cell junctions. Loss of intercellular cell junctions is a major event in

ischemic renal failure. During ischemia, cell adhesion molecules like E-Cadherin are either redistributed at the plasma membrane, internalized or degraded leading to the disruption of cell junctions [234] [239]. However, in the recovery phase following mild ischemia, the cell junctional complexes are reassembled mostly by reusing the already existing (internalized or redistributed) proteins and, to a lesser extent, by synthesis of new key adhesion molecules like E-cadherin [238] (Figure 4.2.B). During intermediate and severe ischemia, the proteins in the cell are degraded very rapidly. In an attempt to repair this, the cells synthesize large amounts of essential membrane and secreted proteins (growth factors, cytokines, adhesion molecules etc) which must pass through the secretory pathway. But under conditions of ischemia, the capacity of the endoplasmic reticulum to fold these proteins is compromised [233]. This leads to accumulation of newly synthesized proteins in the ER which in turn results in ER stress and cell death.

Since Vmp1 is involved in the initial stages of cell junction formation, it is well possible that cells synthesize Vmp1 during the recovery phase of ischemic injury to facilitate the formation of new junctions (Figure 4.2.B). This explains the observation of Dusetti et al. that *Vmp1* is overexpressed in kidney subjected to ischemia. In such cases when the ischemic insult still continues, the newly synthesized Vmp1, a protein with 6-7 transmembrane domains, might also accumulate in the ER and thus contribute to the ER stress and apoptosis through the activation of caspase-3. The dead (both apoptotic and necrotic cells) and the viable cells (due to loss of cell junctions) are shed into the lumen resulting in tubular obstruction and other symptoms of ischemic kidney failure.

4.2.5.3 Proposed role of VMP1 in Pancreatitis

Pancreatitis is characterized by the premature intracellular activation of digestive enzymes accompanied by appearance of cytosolic vacuoles within the pancreatic acinar cells. The exact mechanism responsible for enzyme activation remains unknown, but it is clear that these changes are triggered by an abnormal increase in the cytosolic calcium which is itself dependent on the release of calcium from the ER [240]. It has been reported that acinar cells die through both necrosis and apoptosis [241], and the severity of pancreatitis directly correlates with necrosis and inversely with apoptosis. However, acinar cells packed with activated enzymes prefer to die by apoptosis (rather than necrosis) to prevent release of harmful enzymes into the surrounding tissue causing inflammation. Therefore, strategies to either decrease both types of cell death or ´switch` cell death from necrosis to apoptosis will decrease the severity of the disease and improve the outcome.

Vmp1 was shown to be overexpressed during acute pancreatitis and that cells overexpressing Vmp1 die through apoptosis [159]. The present study showed that apoptosis induced by Vmp1 involves the activation of caspase-3 and that the cells die as a result of vacuolization and collapse of the ER. Accumulation of Vmp1 in the ER might lead to the depletion of calcium stores of the ER, suggesting the possibility that Vmp1 is responsible for the pathogenesis of pancreatitis. However, overexpression of Vmp1 induces apoptosis, which could as well be a part of the defence mechanism of acinar cells allowing recovery after the acute attack. The role of cell adhesion proteins in pancreatitis and the reasons for overexpression of Vmp1 during pancreatitis however remain unclear.

In summary, I have established a high throughput apoptosis assay and screened for previously non-characterized human proteins, that induce apoptosis upon overexpression. This screen led to the identification of five cancer/disease relevant proteins. Functional analysis of Vmp1, one of the candidates of the assay, revealed that Vmp1 is a cell adhesion protein involved in the formation of initial cell-cell-contacts. Further, downregulation of *VMP1* is associated with the transition from primary to secondary tumors at least in kidney cancer and the Vmp1 expression level is a critical determinant of cell invasiveness. Based on the functional data available till now, I have predicted and/or refined models for the involvement of Vmp1 in tumour metastasis, kidney ischemia and pancreatitis. The exact mechanism by which Vmp1 reduction induces a metastatic phenotype and overexpression affects kidney ischemia and pancreatitis remains to be elucidated.

5 Abbreviations

°C	degrees centigrade
µg	micro grams
µl	micro litre
µM	micro molar
µm	micro meter
a.a.	amino acids
Amp	ampicillin
APC	allophycocyanin
APS	ammonium per sulfate
ATP	adenosine triphosphate
BCA	bicinchonic acid
bp	base pairs
BrdU	bromo-deoxy uridine
BSA	bovine serum albumin
cDNA	complementary deoxyribonucleic acid
CFP	cyan fluorescent protein
Co-IP	co-immunoprecipitation
DAPI	4', 6-Diamidino-2-phenylindole
ddH_2O	double distilled water
dNTP	deoxynucleotide triphosphate
DMEM	dulbecco´s modified Eagle's medium
DMSO	dimethyl sulphoxide
DNA	deoxyribonucleic acid
E.coli	*Escherichia coli*
EDC	1-Ethyl-3-(3-dimethylaminopropyl)-carbodiimide
EDTA	ethylene diamine tetra acetic acid
ELISA	enzyme linked immunosorbant assay
FACS	fluorescence actovated cell sorter
FBS	fetal bovine serum
Fw	forward
gm	grams
GFP	green fluorescent protein
GTP	guanosine triphosphate
HRP	horse radish peroxide
IP	immunoprecipitation
Kan	kanamycin
kb	kilo bases
kDa	kilodalton
kV	kilovolts
LB	Luria Bertani
M	molar
mg	milligrams
min	minute(s)
ml	milliliter
mM	millimolar
ng	nanograms
nm	nanometer
O.D	optical density

ORF	open reading frame
PAGE	polyacrylamide gel electrophoresis
PBS	phosphate buffered saline
PCR	polymerase chain reaction
PFA	paraformaldehyde
pM	pico molar
PMSF	phenylmethylsulfonyl fluoride
PS	penicillin / streptomycin
PVDF	polyvinylidene fluoride
RFU	relative fluorescence units
RNA	ribonucleic acid
rpm	revolutions per minute
Rv	reverse
SDS	sodium dodecyl sulfate
SDS-PAGE	SDS-polyacrylamide gel electrophoresis
siRNA	small interfering ribo nucleic acid
TAE	tris/Acetate/EDTA-buffer
TEMED	N, N, N´, N´-Tetramethylethylenediamide
v	volt
YFP	yellow fluorescent protein

6 Supplements

Table 6.1. Proteins screened in the caspase-3 assay

CloneID	AccNO	RZPDID	Symbol	GeneName
akxq28A228	BC006540	IMAGp958A228	BRCC3	BRCA1/BRCA2-containing complex, subunit 3
akxq28ak055600	AK055600	NULL	NULL	NULL
akxq28c1710741	BC022064	IMAGp998C1710741	FATE1	fetal and adult testis expressed 1
akxq28c171466	BC022305	IMAGp958C171466	CLIC2	chloride intracellular channel 2
akxq28D0812213	BM541828	IMAGp998D0812213	LOC203547	hypothetical protein LOC203547
akxq28d201286	BC032121	IMAGp958D201286	FAM58A	family with sequence similarity 58, member A
akxq28D211790	BC015744	IMAGp958D211790	XX-FW81657	DNA segment on chromosome X (unique) 9879 expressed sequence
akxq28e054515	AI218223	IMAGp998E054515	CTAG1B	cancer/testis antigen 1B
akxq28e16117	BC002606	IMAGp998E16117	PDZD4	PDZ domain containing 4
akxq28f031904	AA425725	IMAGp998F031904	STK23	serine/threonine kinase 23
akxq28f10122	BC002416	IMAGp958F10122	BGN	biglycan
akxq28G021845	BC025298	IMAGp958G021845	IL9R	interleukin 9 receptor
akxq28g159617	BC008203	IMAGp998G159617	CXorf12	chromosome X open reading frame 12
akxq28g17175	R59087	IMAGp998G17175	NULL	NULL
akxq28g228444	BC001561	IMAGp998G228444	DNASE1L1	deoxyribonuclease I-like 1
akxq28i0610741	BC040301	IMAGp998I0610741	PASD1	PAS domain containing 1
akxq28i1411448	BI824481	IMAGp998I1411448	AVPR2	arginine vasopressin receptor 2 (nephrogenic diabetes insipidus)
akxq28i14160	BC000255	IMAGp958I14160	FUNDC2	FUN14 domain containing 2
akxq28i19182	BC000738	IMAGp958I19182	EMD	emerin (Emery-Dreifuss muscular dystrophy)
akxq28i205	BC000308	IMAGp958I205	ARD1A	ARD1 homolog A, N-acetyltransferase (S. cerevisiae)
akxq28i231435	BC012114	IMAGp958I231435	IKBKG	inhibitor of kappa light polypeptide gene enhancer in B-cells, kinase gamma
akxq28j056793	AW517432	IMAGp998J056793	NULL	NULL
akxq28j1311548	BC032351	IMAGp998J1311548	SSR4	signal sequence receptor, delta (translocon-associated protein delta)
akxq28j234	BC002392	IMAGp958J234	MPP1	membrane protein, palmitoylated 1, 55kDa
akxq28k05855	BC006170	IMAGp958K05855	IDS	iduronate 2-sulfatase (Hunter syndrome)
akxq28l16384	BC025269	IMAGp958L16384	TMLHE	trimethyllysine hydroxylase, epsilon
akxq28L23832	BC011612	IMAGp958L23832	MECP2	methyl CpG binding protein 2 (Rett syndrome)
akxq28m09186	BC007631	IMAGp958M09186	PNMA6A	paraneoplastic antigen like 6A
akxq28n1210739	BC025382	IMAGp998N1210739	TKTL1	transketolase-like 1
akxq28n167159	BC003358	IMAGp998N167159	RPL10	ribosomal protein L10
akxq28o048419	BC000933	IMAGp998O048419	IDH3G	isocitrate dehydrogenase 3 (NAD+) gamma
akxq28o05362	H40393	IMAGp998O05362	CXorf52	chromosome X open reading frame 52
akxq28o054208	AI038709	IMAGp998O054208	SPRY3	sprouty homolog 3 (Drosophila)
akxq28o22185	BC000724	IMAGp958O22185	ATP6AP1	ATPase, H+ transporting, lysosomal accessory protein 1
akxq28u66048	BG430930	IMAGp958J081364	NULL	NULL

hamy2_11n4	AL136544	DKFZp761N0411	SMC6L1	SMC6 structural maintenance of chromosomes 6-like 1 (yeast)
hamy2_16n19	NULL	DKFZp761N1916	NULL	NULL
hamy2_1f24	AL136562	DKFZp761F241	CCDC3	coiled-coil domain containing 3
hamy2_1h17	AL137502	DKFZp761H171	RRAGD	Ras-related GTP binding D
hamy2_24k15	AL136581	DKFZp761K1524	C14orf135	chromosome 14 open reading frame 135
hamy2_2h17	AL157429	DKFZp761H172	BANP	BTG3 associated nuclear protein
hamy2_7j19	AL583909	DKFZp761J197	KIAA1539	KIAA1539
hfbr1_10j21	AL834397	DKFZp547J2110	TRNT1	tRNA nucleotidyl transferase, CCA-adding, 1
hfbr1_15b14	AL834131	DKFZp547B1415	FLJ36888	hypothetical protein FLJ36888
hfbr1_15f6	AL834132	DKFZp547F0615	C10orf83	chromosome 10 open reading frame 83
hfbr1_3f21	AL512743	DKFZp547F213	SYT13	synaptotagmin XIII
hfbr1_4l13	AL162061	DKFZp547L134	NUP62	nucleoporin 62kDa
hfbr1_5c24	AL834449	DKFZp547C245	RTN4R	reticulon 4 receptor
hfbr1_6j22	AL834457	DKFZp547J226	SYNPR	synaptoporin
hfbr1_6l10	AL512715	DKFZp547L106	ARHGEF2	rho/rac guanine nucleotide exchange factor (GEF) 2
hfbr2_16p15	AL110128	DKFZp564P1516	PPT2	palmitoyl-protein thioesterase 2
hfbr2_2h1	AL136633	DKFZp564H012	MRPL18	mitochondrial ribosomal protein L18
hfbr2_2h10	AL136634	DKFZp564H102	SUHW4	suppressor of hairy wing homolog 4 (Drosophila)
hfbr2_3b16	AL050268	DKFZp564B163	RAB1A	RAB1A, member RAS oncogene family
hfbr2_3c10	AL050269	DKFZp564C103	NAT9	N-acetyltransferase 9
hfbr2_3m17	AL136644	DKFZp564M173	PHPT1	phosphohistidine phosphatase 1
hfbr2_62f10	AL713790	DKFZp564F1062	SLC30A8	solute carrier family 30 (zinc transporter), member 8
hfbr2_6i20	AL136665	DKFZp564I206	MRPL15	mitochondrial ribosomal protein L15
hfbr2_72b11	AL136669	DKFZp564B1172	ICF45	interphase cyctoplasmic foci protein 45
hfbr2_72b18	AL136670	DKFZp564B1872	POLI	polymerase (DNA directed) iota
hfbr2_72n12	AL136676	DKFZp564N1272	GABARAPL1	GABA(A) receptor-associated protein like 1
hfbr2_78c24	AL136680	DKFZp564C2478	GBP3	guanylate binding protein 3
hfbr2_78k24	AL136690	DKFZp564K2478	USP18	ubiquitin specific peptidase 18
hfbr2_7a24	AL713701	DKFZp564A247	C21orf7	chromosome 21 open reading frame 7
hfbr2_7b16	AL110297	DKFZp564B167	BRP44	brain protein 44
hfbr2_7c4	AL133600	DKFZp564C047	STAM2	signal transducing adaptor molecule (SH3 domain and ITAM motif) 2
hfbr2_7j4	AL136694	DKFZp564J047	C1orf49	chromosome 1 open reading frame 49
hfbr2_7k24	AL110233	DKFZp564K247	HIGD1A	HIG1 domain family, member 1A
hfkd2_24a15	AL136704	DKFZp566A1524	FAM49A	family with sequence similarity 49, member A
hfkd2_24e23	AL136708	DKFZp566E2324	C6orf59	chromosome 6 open reading frame 59
hfkd2_24n20	AL136709	DKFZp566N2024	ABI3	ABI gene family, member 3
hfkd2_3i13	AL136711	DKFZp566I133	VMP1	transmembrane protein 49
hfkd2_46k19	AL136721	DKFZp566K1946	PCBD2	pterin-4 alpha-carbinolamine dehydratase/dimerization cofactor of hepatocyte nuclear factor 1 alpha (TCF1) 2
hfkd2_46m10	AL136723	DKFZp566M1046	C11orf56	chromosome 11 open reading frame 56

hfkd2_4j16	AL117566	DKFZp566J164	UBE1C	ubiquitin-activating enzyme E1C (UBA3 homolog, yeast)
hlcc1_18i9	AL832636	DKFZp451I0918	TXLNA	taxilin alpha
hlcc1_1m20	NULL	DKFZp451M201	NULL	NULL
hlcc1_3e22	AL831980	DKFZp451E223	NRAP	nebulin-related anchoring protein
hlcc2_1m1	NULL	DKFZp313M011	NULL	NULL
hlcc3_116l20	BX538218	DKFZp686L20116	RP11-308B5	similar to hypothetical protein MGC17347
hlcc3_148h13	NULL	DKFZp686H13148	NULL	NULL
hlcc3_159g12r1s1	NULL	NULL	NULL	NULL
hlcc3_171f5	BX647330	DKFZp686F05171	IFI27	interferon, alpha-inducible protein 27
hlcc3_223m12	NULL	DKFZp686M12223	NULL	NULL
hlcc3_261i1r1s1	NULL	NULL	NULL	NULL
hlcc3_51c2	NULL	DKFZp686C0251	NULL	NULL
hlcc3_52b8	BX537406	DKFZp686B0852	TRIAD3	TRIAD3 protein
hlcc3_52f6	BX537408	DKFZp686F0652	RAB5B	RAB5B, member RAS oncogene family
hlcc3_52k13	BX537967	DKFZp686K1352	TCF12	transcription factor 12 (HTF4, helix-loop-helix transcription factors 4)
hlcc3_59e24	BX537969	DKFZp686E2459	RBM10	RNA binding motif protein 10
hlcc3_59o14	BX537412	DKFZp686O1459	DYNC1I2	dynein, cytoplasmic 1, intermediate chain 2
hlcc3_59p19	BX537413	DKFZp686P1959	STRA6	stimulated by retinoic acid gene 6 homolog (mouse)
hlcc3_74g21	NULL	DKFZp686G2174	NULL	NULL
hlcc3_82o22	BX537382	DKFZp686O2282	SLC38A3	solute carrier family 38, member 3
hlcc3_86a15	BX537971	DKFZp686A1586	LOC493856	similar to RIKEN cDNA 1500009M05 gene
hlcc3_86f23	BX537972	DKFZp686F2386	LYSMD3	LysM, putative peptidoglycan-binding, domain containing 3
hlcc3_98b23	NULL	DKFZp686B2398	NULL	NULL
hlcc4_5d1r1s1	NULL	NULL	NULL	NULL
hmel2_11h17	AL359618	DKFZp762H1711	CHCHD8	coiled-coil-helix-coiled-coil-helix domain containing 8
hmel2_12e11	AL162047	DKFZp762E1112	NCOA4	nuclear receptor coactivator 4
hmel2_12j1	AL713689	DKFZp762J0112	KIAA1524	KIAA1524
hncc1_42m18	BX648228	NULL	MIA2	melanoma inhibitory activity 2
htes3_10n10	AL136733	DKFZp434N1010	UBAP1	ubiquitin associated protein 1
htes3_10n4	AL136734	DKFZp434N0410	RAB18	RAB18, member RAS oncogene family
htes3_13c10	AL136747	DKFZp434C1013	CSTF2T	cleavage stimulation factor, 3' pre-RNA, subunit 2, 64kDa, tau variant
htes3_14g5	AL136750	DKFZp434G0514	LYAR	hypothetical protein FLJ20425
htes3_15c5	AL133046	DKFZp434C0515	SSX2IP	synovial sarcoma, X breakpoint 2 interacting protein
htes3_15h1	AL136760	DKFZp434H0115	TTC25	tetratricopeptide repeat domain 25
htes3_15i5	AL136761	DKFZp434I0515	RSHL-1	Radial spokehead-like 1
htes3_17b4	AL133067	DKFZp434B0417	PDZRN4	PDZ domain containing RING finger 4
htes3_17i21	AL136777	DKFZp434I2117	FAM57B	family with sequence similarity 57, member B
htes3_17j6	AL136778	DKFZp434J0617	RKHD3	ring finger and KH domain containing 3
htes3_17n18	AL136781	DKFZp434N1817	C3orf20	chromosome 3 open reading frame 20
htes3_19a13	AL136786	DKFZp434A1319	C16orf48	chromosome 16 open reading frame 48

htes3_1c15	AL080168	DKFZp434C151	ATG4B	ATG4 autophagy related 4 homolog B (S. cerevisiae)
htes3_1k11	AL136796	DKFZp434K111	KLHL25	kelch-like 25 (Drosophila)
htes3_1k15	AL080177	DKFZp434K151	UBL3	ubiquitin-like 3
htes3_1l15	AL117487	DKFZp434L151	TADA3L	transcriptional adaptor 3 (NGG1 homolog, yeast)-like
htes3_20k2	AL136801	DKFZp434K0220	TRPV1	transient receptor potential cation channel, subfamily V, member 1
htes3_22n13	AL713710	DKFZp434N1322	MKL1	megakaryoblastic leukemia (translocation) 1
htes3_23a19	AL136813	DKFZp434A1923	CPSF3L	cleavage and polyadenylation specific factor 3-like
htes3_26g22	AL136819	DKFZp434G2226	KIF18A	kinesin family member 18A
htes3_29f24	AL136832	DKFZp434F2429	ARHGEF3	Rho guanine nucleotide exchange factor (GEF) 3
htes3_2d11	AL080197	DKFZp434D112	LOC51233	hypothetical protein LOC51233
htes3_2d15	AL136835	DKFZp434D152	TOLLIP	toll interacting protein
htes3_2i17	AL834386	DKFZp434I172	C3orf20	chromosome 3 open reading frame 20
htes3_30a5	AL136842	DKFZp434A0530	CDC42EP3	CDC42 effector protein (Rho GTPase binding) 3
htes3_35a11	AL122068	DKFZp434A1135	RAD17	RAD17 homolog (S. pombe)
htes3_35g6	AL136853	DKFZp434G0635	BTBD1	BTB (POZ) domain containing 1
htes3_35n12	AL136857	DKFZp434N1235	SLC25A31	solute carrier family 25 (mitochondrial carrier; adenine nucleotide translocator), member 31
htes3_35n9	AL713761	DKFZp434N0935	CES2	carboxylesterase 2 (intestine, liver)
htes3_35p17	AL136859	DKFZp434P1735	ARMC4	armadillo repeat containing 4
htes3_3a7	AL080126	DKFZp434A073	KIAA0683	KIAA0683 gene product
htes3_4d6	AL110225	DKFZp434D064	DBN1	drebrin 1
htes3_4f5	AL136863	DKFZp434F054	WDR24	WD repeat domain 24
htes3_4h6	AL136864	DKFZp434H064	KLC2	kinesin light chain 2
htes3_4i11	AL080154	DKFZp434I114	C20orf28	chromosome 20 open reading frame 28
htes3_50n23	AL713673	DKFZp434N2350	C12orf25	chromosome 12 open reading frame 25
htes3_5c13	AL136874	DKFZp434C135	RNF32	ring finger protein 32
htes3_7j3	AL136891	DKFZp434J037	NUAK2	NUAK family, SNF1-like kinase, 2
htes3_7j8	AL136892	DKFZp434J087	FLJ20323	hypothetical protein FLJ20323
htes3_8g5	AL136899	DKFZp434G058	FBXO21	F-box protein 21
hute1_17k7	AL136910	DKFZp586K0717	FIP1L1	FIP1 like 1 (S. cerevisiae)
hute1_18i19	AL136911	DKFZp586I1918	LIMA1	LIM domain and actin binding 1
hute1_18i4	AL136912	DKFZp586I0418	ATG10	ATG10 autophagy related 10 homolog (S. cerevisiae)
hute1_19k9	AL050283	DKFZp586K0919	SENP3	SUMO1/sentrin/SMT3 specific peptidase 3
hute1_21p24	AL110267	DKFZp586P2421	OGN	osteoglycin (osteoinductive factor, mimecan)
hute1_23e13	AL136936	DKFZp586E1323	HSPB8	heat shock 22kDa protein 8
hute1_23h7	AL080212	DKFZp586H0723	RAP1B	RAP1B, member of RAS oncogene family
hute1_24b4	AL136940	DKFZp586B0424	HSPC049	HSPC049 protein
hute1_24j6	AL136944	DKFZp586J0624	SLC40A1	solute carrier family 40 (iron-regulated transporter), member 1
IMAGp958C20216	BC004352	IMAGp958C20216	KIF22	kinesin family member 22
IMAGp958D0156	BC015149	IMAGp958D0156	MAP4	microtubule-associated protein 4
IMAGp958D231833	BC042168	IMAGp958D231833	CTSZ	cathepsin Z

IMAGp958E161161	BC011656	IMAGp958E161161	CDC27	cell division cycle 27
IMAGp958G021430	BC018739	IMAGp958G021430	BUB1B	BUB1 budding uninhibited by benzimidazoles 1 homolog beta (yeast)
IMAGp958I1955	BC008718	IMAGp958I1955	BIRC5	baculoviral IAP repeat-containing 5 (survivin)
IMAGp958O04299	BC018634	IMAGp958O04299	MAP1LC3B	microtubule-associated protein 1 light chain 3 beta
IMAGp958O182624	BC062691	IMAGp958O182624	HSPC159	HSPC159 protein
IMAGp998A1112724	BC036801	IMAGp998A1112724	LOC387856	similar to expressed sequence AI836003
IMAGp998D0110102	BC017713	IMAGp998D0110102	CDC23	CDC23 (cell division cycle 23, yeast, homolog)
IMAGp998d2012760	BM554036	IMAGp998D2012760	NUP62	nucleoporin 62kDa
IMAGp998E1010430	BC013757	IMAGp998E1010430	LRRC58	leucine rich repeat containing 58
IMAGp998H159957	BC021901	IMAGp998H159957	RAB21	RAB21, member RAS oncogene family
IMAGp998J0312216	BC035925	IMAGp998J0312216	C1orf31	chromosome 1 open reading frame 31
IMAGp998K0111687	BC057767	IMAGp998K0111687	C20orf132	chromosome 20 open reading frame 132
IRALp962A2027	BC010090	IRALp962A2027	ACTR1B	ARP1 actin-related protein 1 homolog B, centractin beta (yeast)
IRALp962G143	BC007318	IRALp962G143	MAPRE2	microtubule-associated protein, RP/EB family, member 2
IRATp970A0419	BC015492	IRATp970A0419	IFI27	interferon, alpha-inducible protein 27
IRATp970A0916	BC018190	IRATp970A0916	MT1X	metallothionein 1X
IRATp970B025	BC000870	IRATp970B025	FLJ20516	timeless-interacting protein
IRATp970C094	BC006794	IRATp970C094	IFITM3	interferon induced transmembrane protein 3 (1-8U)
IRATp970D076	BC008640	IRATp970D076	ICA1	islet cell autoantigen 1, 69kDa
IRATp970E119	BC009685	IRATp970E119	CAV1	caveolin 1, caveolae protein, 22kDa
IRATp970E1212	BC015044	IRATp970E1212	MOAP1	modulator of apoptosis 1
IRATp970E129	BC009698	IRATp970E129	APOC1	apolipoprotein C-I
IRATp970F0215	BC012841	IRATp970F0215	XBP1	X-box binding protein 1
IRAUp969A115	BC001105	IRAUp969A115	DBNDD2	dysbindin (dystrobrevin binding protein 1) domain containing 2
IRAUp969B0615	BC000785	IRAUp969B0615	SCAND1	SCAN domain containing 1
IRAUp969B0732	BC006245	IRAUp969B0732	FGF18	fibroblast growth factor 18
IRAUp969B1123	BC003513	IRAUp969B1123	CXCL14	chemokine (C-X-C motif) ligand 14
IRAUp969B1159	BC009830	IRAUp969B1159	RDH14	retinol dehydrogenase 14 (all-trans/9-cis/11-cis)
IRAUp969C0366	BC011551	IRAUp969C0366	ZC3HC1	zinc finger, C3HC-type containing 1
IRAUp969C1021	BC002778	IRAUp969C1021	MYLC2PL	myosin light chain 2, precursor lymphocyte-specific
IRAUp969C1049	BC013401	IRAUp969C1049	PHB	prohibitin
IRAUp969D0269	BC014310	IRAUp969D0269	RPL10L	ribosomal protein L10-like
IRAUp969D0336	BC007936	IRAUp969D0336	GAP43	growth associated protein 43
IRAUp969E0545	BC005916	IRAUp969E0545	PTN	pleiotrophin (heparin binding growth factor 8, neurite growth-promoting factor 1)
IRAUp969F0711	BC000198	IRAUp969F0711	SF3B5	splicing factor 3b, subunit 5, 10kDa
IRAUp969G0266	BC012340	IRAUp969G0266	C12orf5	chromosome 12 open reading frame 5
IRAUp969G0523	BC004309	IRAUp969G0523	RAB4A	RAB4A, member RAS oncogene family
IRAUp969G0648	BC009471	IRAUp969G0648	AMACR	alpha-methylacyl-CoA racemase
IRAUp969G065	BC001693	IRAUp969G065	LGALS1	lectin, galactoside-binding, soluble, 1

				(galectin 1)
IRAUp969G086	BC002503	IRAUp969G086	SAT	spermidine/spermine N1-acetyltransferase
IRAUp969G0861	BC011757	IRAUp969G0861	GADD45A	growth arrest and DNA-damage-inducible, alpha
IRAUp969G0939	BC008361	IRAUp969G0939	FBXO7	F-box protein 7
IRAUp969H0369	BC019230	IRAUp969H0369	AKR1C3	aldo-keto reductase family 1, member C3 (3-alpha hydroxysteroid dehydrogenase, type II)
IRAUp969H1045	BC005919	IRAUp969H1045	PLA2G2A	phospholipase A2, group IIA (platelets, synovial fluid)
IRAUp969H1218	BC004993	IRAUp969H1218	ANXA5	annexin A5

7 Acknowledgements

I would like to thank Prof. Dr. Annemarie Poustka and PD. Dr. Stefan Wiemann for giving me the opportunity to work for my doctoral thesis at the department of Molecular Genome Analysis, DKFZ, Heidelberg. I specially thank PD. Dr. Stefan Wiemann for being the first referee of my Ph.D work, and for his support and helpful discussions throughout the project.

I thank Prof. Dr. Jeremy Smith for acting as the second referee of my Ph.D work.

I am extremely grateful to Dr. Dorit Arlt for patiently supervising me, for her valuable suggestions during the entire work, and also during preparation of this thesis.

I would like to thank Christian Schmidt for automating the assay and, Florian Hahne and Wolfgang Huber (EBI, Cambridge, UK) for statistical analysis of the apoptosis assay.

I appreciate the expert technical assistance of Sandra Blaszkiewicz, Saskia Stegmuller, Stefanie Krauth, Jens Mattern, Heike Wilhelm, Esther Backes and Nina Claudino. I thank my other colleagues Meher Majety and Özgür Sahin for their help in various experiments.

I also thank Heiko Rosenfelder, Markus Seiler and Alexander Mehrle for their help with data organization and bioinformatic analysis.

I thank Olga Friedekind and Markus Ruschhaupt for their help with the TaqMan analysis.

I would like to thank Dr. Lazlo Füzesi (Institute of Pathology, Georg August University Hospital, Göttingen) for providing the patient tumour samples, and Dr. Holger Sültmann (Molecular genome analysis, DKFZ, Heidelberg) for TaqMan analysis of the patient samples.

I specially thank my husband Florian Sauermann for his never-ending patience, and for his constant support and encouragement through out this work. I also thank my parents, brother and parents-in-law for their support and encouragement.

Finally, I thank all my friends for their helpful suggestions, and for the good time I had with them.

8 Own Publications

Wiemann, S., Arlt, D., Huber, W., Wellenreuther, R., Schleeger, S., Mehrle, A., Bechtel, S., **Sauermann, M.**, Korf, U., Pepperkok, R., Sültmann, H., Poustka, A. (2004). From ORFeome to biology: a functional genomics pipeline. **Genome Res** *14*, 2136-2144.

Arlt, D., Huber, W., Liebel, U., Schmidt, C., Majety, M., **Sauermann, M.**, Rosenfelder, H., Bechtel, S., Mehrle, A., Bannasch, D., *et al.* (2005). Functional profiling: from microarrays via cell-based assays to novel tumor relevant modulators of the cell cycle. **Cancer Res** *65*, 7733-7742.

Sauermann, M., Sahin, Ö., Sültmann, H., Hahne, F., Blaszkiewicz, S., Majety, M., Füzesi, L., Poustka, A., Wiemann, S., Arlt, D. (2006). Vacuole membrane protein (Vmp1) is a cell-cell contact protein and acts as a metastasis suppressor. **Submitted**

Sauermann, M., Hahne, F., Schmidt, C., Majety, M., Poustka, A., Arlt, D., Wiemann, S. (2006). Identification of caspase-3 activating proteins in a high throughput apoptosis assay. **In Preparation**

Hahne, F., Arlt, D., **Sauermann, M.**, Majety, M., Poustka, A., Wiemann, S., Huber, W. (2006). Analysis of high throughput flow cytometry data. **Submitted**

9 References

1. International human genome sequencing consortium, *Finishing the euchromatic sequence of the human genome.* Nature, 2004. **431**(7011): p. 931-45.

2. Wiemann, S., et al., *From ORFeome to biology: a functional genomics pipeline.* Genome Res, 2004. **14**(10B): p. 2136-44.

3. Arlt, D., et al., *Functional profiling: from microarrays via cell-based assays to novel tumor relevant modulators of the cell cycle.* Cancer Res, 2005. **65**(17): p. 7733-42.

4. Simpson, J.C., et al., *Systematic subcellular localization of novel proteins identified by large-scale cDNA sequencing.* EMBO Rep, 2000. **1**(3): p. 287-92.

5. Bannasch, D., et al., *LIFEdb: a database for functional genomics experiments integrating information from external sources, and serving as a sample tracking system.* Nucleic Acids Res, 2004. **32**(Database issue): p. D505-8.

6. Vousden, K.H. and X. Lu, *Live or let die: the cell's response to p53.* Nat Rev Cancer, 2002. **2**(8): p. 594-604.

7. Shen, X., K. Zhang, and R.J. Kaufman, *The unfolded protein response--a stress signaling pathway of the endoplasmic reticulum.* J Chem Neuroanat, 2004. **28**(1-2): p. 79-92.

8. Grossmann, J., *Molecular mechanisms of "detachment-induced apoptosis--Anoikis".* Apoptosis, 2002. **7**(3): p. 247-60.

9. Kim, J. and D.J. Klionsky, *Autophagy, cytoplasm-to-vacuole targeting pathway, and pexophagy in yeast and mammalian cells.* Annu Rev Biochem, 2000. **69**: p. 303-42.

10. Levine, B. and D.J. Klionsky, *Development by self-digestion: molecular mechanisms and biological functions of autophagy.* Dev Cell, 2004. **6**(4): p. 463-77.

11. Majno, G. and I. Joris, *Apoptosis, oncosis, and necrosis. An overview of cell death.* Am J Pathol, 1995. **146**(1): p. 3-15.

12. Campisi, J., *Cellular senescence as a tumor-suppressor mechanism.* Trends Cell Biol, 2001. **11**(11): p. S27-31.

13. Kerr, J.F., A.H. Wyllie, and A.R. Currie, *Apoptosis: a basic biological phenomenon with wide-ranging implications in tissue kinetics.* Br J Cancer, 1972. **26**(4): p. 239-57.

14. Proskuryakov, S.Y., V.L. Gabai, and A.G. Konoplyannikov, *Necrosis is an active and controlled form of programmed cell death.* Biochemistry (Mosc), 2002. **67**(4): p. 387-408.

15. Strasser, A., L. O'Connor, and V.M. Dixit, *Apoptosis signaling.* Annu Rev Biochem, 2000. **69**: p. 217-45.

16. Itoh, N., et al., *The polypeptide encoded by the cDNA for human cell surface antigen Fas can mediate apoptosis.* Cell, 1991. **66**(2): p. 233-43.

17. Suda, T., et al., *Molecular cloning and expression of the Fas ligand, a novel member of the tumor necrosis factor family.* Cell, 1993. **75**(6): p. 1169-78.

18. Nagata, S., *Apoptosis by death factor.* Cell, 1997. **88**(3): p. 355-65.

19. Muzio, M., *Signalling by proteolysis: death receptors induce apoptosis.* Int J Clin Lab Res, 1998. **28**(3): p. 141-7.

20. Banner, D.W., et al., *Crystal structure of the soluble human 55 kd TNF receptor-human TNF beta complex: implications for TNF receptor activation.* Cell, 1993. **73**(3): p. 431-45.

21. Kischkel, F.C., et al., *Cytotoxicity-dependent APO-1 (Fas/CD95)-associated proteins form a death-inducing signaling complex (DISC) with the receptor.* Embo J, 1995. **14**(22): p. 5579-88.

22. Chinnaiyan, A.M., et al., *FADD/MORT1 is a common mediator of CD95 (Fas/APO-1) and tumor necrosis factor receptor-induced apoptosis.* J Biol Chem, 1996. **271**(9): p. 4961-5.

23. Hsu, H., J. Xiong, and D.V. Goeddel, *The TNF receptor 1-associated protein TRADD signals cell death and NF-kappa B activation.* Cell, 1995. **81**(4): p. 495-504.

24. Algeciras-Schimnich, A., et al., *Molecular ordering of the initial signaling events of CD95.* Mol Cell Biol, 2002. **22**(1): p. 207-20.

25. Muzio, M., et al., *An induced proximity model for caspase-8 activation.* J Biol Chem, 1998. **273**(5): p. 2926-30.

26. Yang, X., H.Y. Chang, and D. Baltimore, *Autoproteolytic activation of pro-caspases by oligomerization.* Mol Cell, 1998. **1**(2): p. 319-25.

27. Newmeyer, D.D., D.M. Farschon, and J.C. Reed, *Cell-free apoptosis in Xenopus egg extracts: inhibition by Bcl-2 and requirement for an organelle fraction enriched in mitochondria.* Cell, 1994. **79**(2): p. 353-64.

28. Buttke, T.M. and P.A. Sandstrom, *Oxidative stress as a mediator of apoptosis.* Immunol Today, 1994. **15**(1): p. 7-10.

29. Zamzami, N., et al., *Sequential reduction of mitochondrial transmembrane potential and generation of reactive oxygen species in early programmed cell death.* J Exp Med, 1995. **182**(2): p. 367-77.

30. Marchetti, P., et al., *Mitochondrial permeability transition is a central coordinating event of apoptosis.* J Exp Med, 1996. **184**(3): p. 1155-60.

31. Marzo, I., et al., *The permeability transition pore complex: a target for apoptosis regulation by caspases and bcl-2-related proteins.* J Exp Med, 1998. **187**(8): p. 1261-71.

32. Hirsch, T., et al., *Mitochondrial permeability transition in apoptosis and necrosis.* Cell Biol Toxicol, 1998. **14**(2): p. 141-5.

33. Hsu, Y.T. and R.J. Youle, *Bax in murine thymus is a soluble monomeric protein that displays differential detergent-induced conformations.* J Biol Chem, 1998. **273**(17): p. 10777-83.

34. Antonsson, B., et al., *Bax oligomerization is required for channel-forming activity in liposomes and to trigger cytochrome c release from mitochondria.* Biochem J, 2000. **345 Pt 2**: p. 271-8.

35. Desagher, S., et al., *Bid-induced conformational change of Bax is responsible for mitochondrial cytochrome c release during apoptosis.* J Cell Biol, 1999. **144**(5): p. 891-901.

36. Nechushtan, A., et al., *Conformation of the Bax C-terminus regulates subcellular location and cell death.* Embo J, 1999. **18**(9): p. 2330-41.

37. Wolter, K.G., et al., *Movement of Bax from the cytosol to mitochondria during apoptosis.* J Cell Biol, 1997. **139**(5): p. 1281-92.

38. Antonsson, B., et al., *Bax is present as a high molecular weight oligomer/complex in the mitochondrial membrane of apoptotic cells.* J Biol Chem, 2001. **276**(15): p. 11615-23.

39. Griffiths, G.J., et al., *Cell damage-induced conformational changes of the pro-apoptotic protein Bak in vivo precede the onset of apoptosis.* J Cell Biol, 1999. **144**(5): p. 903-14.

40. Korsmeyer, S.J., et al., *Pro-apoptotic cascade activates BID, which oligomerizes BAK or BAX into pores that result in the release of cytochrome c.* Cell Death Differ, 2000. **7**(12): p. 1166-73.

41. Wei, M.C., et al., *Proapoptotic BAX and BAK: a requisite gateway to mitochondrial dysfunction and death.* Science, 2001. **292**(5517): p. 727-30.

42. Verhagen, A.M., et al., *Identification of DIABLO, a mammalian protein that promotes apoptosis by binding to and antagonizing IAP proteins.* Cell, 2000. **102**(1): p. 43-53.

43. Waterhouse, N.J., J.E. Ricci, and D.R. Green, *And all of a sudden it's over: mitochondrial outer-membrane permeabilization in apoptosis.* Biochimie, 2002. **84**(2-3): p. 113-21.

44. Deveraux, Q.L., et al., *X-linked IAP is a direct inhibitor of cell-death proteases.* Nature, 1997. **388**(6639): p. 300-4.

45. Du, C., et al., *Smac, a mitochondrial protein that promotes cytochrome c-dependent caspase activation by eliminating IAP inhibition.* Cell, 2000. **102**(1): p. 33-42.

46. Pauklin, S., et al., *ARF and ATM/ATR cooperate in p53-mediated apoptosis upon oncogenic stress.* Biochem Biophys Res Commun, 2005. **334**(2): p. 386-94.

47. Helt, C.E., et al., *Ataxia telangiectasia mutated (ATM) and ATM and Rad3-related protein exhibit selective target specificities in response to different forms of DNA damage.* J Biol Chem, 2005. **280**(2): p. 1186-92.

48. Siliciano, J.D., et al., *DNA damage induces phosphorylation of the amino terminus of p53.* Genes Dev, 1997. **11**(24): p. 3471-81.

49. Canman, C.E., et al., *Activation of the ATM kinase by ionizing radiation and phosphorylation of p53.* Science, 1998. **281**(5383): p. 1677-9.

50. Haupt, Y., et al., *Mdm2 promotes the rapid degradation of p53.* Nature, 1997. **387**(6630): p. 296-9.

51. Kubbutat, M.H., S.N. Jones, and K.H. Vousden, *Regulation of p53 stability by Mdm2.* Nature, 1997. **387**(6630): p. 299-303.

52. Honda, R., H. Tanaka, and H. Yasuda, *Oncoprotein MDM2 is a ubiquitin ligase E3 for tumor suppressor p53.* FEBS Lett, 1997. **420**(1): p. 25-7.

53. Grossman, S.R., et al., *p300/MDM2 complexes participate in MDM2-mediated p53 degradation.* Mol Cell, 1998. **2**(4): p. 405-15.

54. Bates, S. and K.H. Vousden, *Mechanisms of p53-mediated apoptosis.* Cell Mol Life Sci, 1999. **55**(1): p. 28-37.

55. Yu, J., et al., *Identification and classification of p53-regulated genes.* Proc Natl Acad Sci U S A, 1999. **96**(25): p. 14517-22.

56. Oda, E., et al., *Noxa, a BH3-only member of the Bcl-2 family and candidate mediator of p53-induced apoptosis.* Science, 2000. **288**(5468): p. 1053-8.

57. Oda, K., et al., *p53AIP1, a potential mediator of p53-dependent apoptosis, and its regulation by Ser-46-phosphorylated p53.* Cell, 2000. **102**(6): p. 849-62.

58. Yu, J., et al., *PUMA induces the rapid apoptosis of colorectal cancer cells.* Mol Cell, 2001. **7**(3): p. 673-82.

59. Moroni, M.C., et al., *Apaf-1 is a transcriptional target for E2F and p53.* Nat Cell Biol, 2001. **3**(6): p. 552-8.

60. Meylan, E. and J. Tschopp, *The RIP kinases: crucial integrators of cellular stress.* Trends Biochem Sci, 2005. **30**(3): p. 151-9.

61. Lassus, P., X. Opitz-Araya, and Y. Lazebnik, *Requirement for caspase-2 in stress-induced apoptosis before mitochondrial permeabilization.* Science, 2002. **297**(5585): p. 1352-4.

62. Kadowaki, H., H. Nishitoh, and H. Ichijo, *Survival and apoptosis signals in ER stress: the role of protein kinases.* J Chem Neuroanat, 2004. **28**(1-2): p. 93-100.

63. Travers, K.J., et al., *Functional and genomic analyses reveal an essential coordination between the unfolded protein response and ER-associated degradation.* Cell, 2000. **101**(3): p. 249-58.

64. Patil, C. and P. Walter, *Intracellular signaling from the endoplasmic reticulum to the nucleus: the unfolded protein response in yeast and mammals.* Curr Opin Cell Biol, 2001. **13**(3): p. 349-55.

65. Kaufman, R.J., *Stress signaling from the lumen of the endoplasmic reticulum: coordination of gene transcriptional and translational controls.* Genes Dev, 1999. **13**(10): p. 1211-33.

66. Wang, X.Z., et al., *Cloning of mammalian Ire1 reveals diversity in the ER stress responses.* Embo J, 1998. **17**(19): p. 5708-17.

67. Harding, H.P., Y. Zhang, and D. Ron, *Protein translation and folding are coupled by an endoplasmic-reticulum-resident kinase.* Nature, 1999. **397**(6716): p. 271-4.

68. Ye, J., et al., *ER stress induces cleavage of membrane-bound ATF6 by the same proteases that process SREBPs.* Mol Cell, 2000. **6**(6): p. 1355-64.

69. Yoshida, H., et al., *Identification of the cis-acting endoplasmic reticulum stress response element responsible for transcriptional induction of mammalian glucose-regulated proteins. Involvement of basic leucine zipper transcription factors.* J Biol Chem, 1998. **273**(50): p. 33741-9.

70. Yoneda, T., et al., *Activation of caspase-12, an endoplastic reticulum (ER) resident caspase, through tumor necrosis factor receptor-associated factor 2-dependent mechanism in response to the ER stress.* J Biol Chem, 2001. **276**(17): p. 13935-40.

71. Nakagawa, T., et al., *Caspase-12 mediates endoplasmic-reticulum-specific apoptosis and cytotoxicity by amyloid-beta.* Nature, 2000. **403**(6765): p. 98-103.

72. Fischer, H., et al., *Human caspase 12 has acquired deleterious mutations.* Biochem Biophys Res Commun, 2002. **293**(2): p. 722-6.

73. Urano, F., et al., *Coupling of stress in the ER to activation of JNK protein kinases by transmembrane protein kinase IRE1.* Science, 2000. **287**(5453): p. 664-6.

74. Nishitoh, H., et al., *ASK1 is essential for endoplasmic reticulum stress-induced neuronal cell death triggered by expanded polyglutamine repeats.* Genes Dev, 2002. **16**(11): p. 1345-55.

75. Putcha, G.V., et al., *JNK-mediated BIM phosphorylation potentiates BAX-dependent apoptosis.* Neuron, 2003. **38**(6): p. 899-914.

76. Yamamoto, K., H. Ichijo, and S.J. Korsmeyer, *BCL-2 is phosphorylated and inactivated by an ASK1/Jun N-terminal protein kinase pathway normally activated at G(2)/M.* Mol Cell Biol, 1999. **19**(12): p. 8469-78.

77. Ron, D. and J.F. Habener, *CHOP, a novel developmentally regulated nuclear protein that dimerizes with transcription factors C/EBP and LAP and functions as a dominant-negative inhibitor of gene transcription.* Genes Dev, 1992. **6**(3): p. 439-53.

78. Barone, M.V., et al., *CHOP (GADD153) and its oncogenic variant, TLS-CHOP, have opposing effects on the induction of G1/S arrest.* Genes Dev, 1994. **8**(4): p. 453-64.

79. Friedman, A.D., *GADD153/CHOP, a DNA damage-inducible protein, reduced CAAT/enhancer binding protein activities and increased apoptosis in 32D c13 myeloid cells.* Cancer Res, 1996. **56**(14): p. 3250-6.

80. Berridge, M.J., P. Lipp, and M.D. Bootman, *The versatility and universality of calcium signalling.* Nat Rev Mol Cell Biol, 2000. **1**(1): p. 11-21.

81. Mattson, M.P., et al., *Calcium signaling in the ER: its role in neuronal plasticity and neurodegenerative disorders.* Trends Neurosci, 2000. **23**(5): p. 222-9.

82. Wang, K.K., *Calpain and caspase: can you tell the difference?* Trends Neurosci, 2000. **23**(1): p. 20-6.

83. Nakagawa, T. and J. Yuan, *Cross-talk between two cysteine protease families. Activation of caspase-12 by calpain in apoptosis.* J Cell Biol, 2000. **150**(4): p. 887-94.

84. Nutt, L.K., et al., *Bax-mediated Ca2+ mobilization promotes cytochrome c release during apoptosis.* J Biol Chem, 2002. **277**(23): p. 20301-8.

85. Morishima, N., et al., *Translocation of Bim to the endoplasmic reticulum (ER) mediates ER stress signaling for activation of caspase-12 during ER stress-induced apoptosis.* J Biol Chem, 2004. **279**(48): p. 50375-81.

86. Rao, R.V., et al., *Coupling endoplasmic reticulum stress to the cell death program. Mechanism of caspase activation.* J Biol Chem, 2001. **276**(36): p. 33869-74.

87. Morishima, N., et al., *An endoplasmic reticulum stress-specific caspase cascade in apoptosis. Cytochrome c-independent activation of caspase-9 by caspase-12.* J Biol Chem, 2002. **277**(37): p. 34287-94.

88. Hitomi, J., et al., *Apoptosis induced by endoplasmic reticulum stress depends on activation of caspase-3 via caspase-12.* Neurosci Lett, 2004. **357**(2): p. 127-30.

89. Mancini, M., et al., *Caspase-2 is localized at the Golgi complex and cleaves golgin-160 during apoptosis.* J Cell Biol, 2000. **149**(3): p. 603-12.

90. Bennett, M., et al., *Cell surface trafficking of Fas: a rapid mechanism of p53-mediated apoptosis.* Science, 1998. **282**(5387): p. 290-3.

91. Goss, P.E., et al., *Inhibitors of carbohydrate processing: A new class of anticancer agents.* Clin Cancer Res, 1995. **1**(9): p. 935-44.

92. Bursch, W., *The autophagosomal-lysosomal compartment in programmed cell death.* Cell Death Differ, 2001. **8**(6): p. 569-81.

93. Turk, B., et al., *Apoptotic pathways: involvement of lysosomal proteases.* Biol Chem, 2002. **383**(7-8): p. 1035-44.

94. Schotte, P., et al., *Cathepsin B-mediated activation of the proinflammatory caspase-11.* Biochem Biophys Res Commun, 1998. **251**(1): p. 379-87.

95. Vancompernolle, K., et al., *Atractyloside-induced release of cathepsin B, a protease with caspase-processing activity.* FEBS Lett, 1998. **438**(3): p. 150-8.

96. Katunuma, N., et al., *Insights into the roles of cathepsins in antigen processing and presentation revealed by specific inhibitors.* Biol Chem, 2003. **384**(6): p. 883-90.

97. Cirman, T., et al., *Selective disruption of lysosomes in HeLa cells triggers apoptosis mediated by cleavage of Bid by multiple papain-like lysosomal cathepsins.* J Biol Chem, 2004. **279**(5): p. 3578-87.

98. Bidere, N., et al., *Cathepsin D triggers Bax activation, resulting in selective apoptosis-inducing factor (AIF) relocation in T lymphocytes entering the early commitment phase to apoptosis.* J Biol Chem, 2003. **278**(33): p. 31401-11.

99. Coultas, L. and A. Strasser, *The role of the Bcl-2 protein family in cancer.* Semin Cancer Biol, 2003. **13**(2): p. 115-23.

100. Reddig, P.J. and R.L. Juliano, *Clinging to life: cell to matrix adhesion and cell survival.* Cancer Metastasis Rev, 2005. **24**(3): p. 425-39.

101. Jamora, C. and E. Fuchs, *Intercellular adhesion, signalling and the cytoskeleton.* Nat Cell Biol, 2002. **4**(4): p. E101-8.

102. Ley, R., et al., *Extracellular signal-regulated kinases 1/2 are serum-stimulated "Bim(EL) kinases" that bind to the BH3-only protein Bim(EL) causing its phosphorylation and turnover.* J Biol Chem, 2004. **279**(10): p. 8837-47.

103. Grutter, M.G., *Caspases: key players in programmed cell death.* Curr Opin Struct Biol, 2000. **10**(6): p. 649-55.

104. Stennicke, H.R., et al., *Caspase-9 can be activated without proteolytic processing.* J Biol Chem, 1999. **274**(13): p. 8359-62.

105. Boatright, K.M., et al., *A unified model for apical caspase activation.* Mol Cell, 2003. **11**(2): p. 529-41.

106. Earnshaw, W.C., L.M. Martins, and S.H. Kaufmann, *Mammalian caspases: structure, activation, substrates, and functions during apoptosis.* Annu Rev Biochem, 1999. **68**: p. 383-424.

107. Sebbagh, M., et al., *Caspase-3-mediated cleavage of ROCK I induces MLC phosphorylation and apoptotic membrane blebbing.* Nat Cell Biol, 2001. **3**(4): p. 346-52.

108. Nagata, S., *Apoptotic DNA fragmentation.* Exp Cell Res, 2000. **256**(1): p. 12-8.

109. Evan, G.I. and K.H. Vousden, *Proliferation, cell cycle and apoptosis in cancer.* Nature, 2001. **411**(6835): p. 342-8.

110. Reed, J.C., *Apoptosis-regulating proteins as targets for drug discovery.* Trends Mol Med, 2001. **7**(7): p. 314-9.

111. Simpson, L. and R. Parsons, *PTEN: life as a tumor suppressor.* Exp Cell Res, 2001. **264**(1): p. 29-41.

112. Mathiasen, I.S. and M. Jaattela, *Triggering caspase-independent cell death to combat cancer.* Trends Mol Med, 2002. **8**(5): p. 212-20.

113. Downward, J., *Targeting RAS signalling pathways in cancer therapy.* Nat Rev Cancer, 2003. **3**(1): p. 11-22.

114. Soengas, M.S., et al., *Inactivation of the apoptosis effector Apaf-1 in malignant melanoma.* Nature, 2001. **409**(6817): p. 207-11.

115. Jaattela, M., *Multiple cell death pathways as regulators of tumour initiation and progression.* Oncogene, 2004. **23**(16): p. 2746-56.

116. Kuhtreiber, W.M., et al., *Central role of defective apoptosis in autoimmunity.* J Mol Endocrinol, 2003. **31**(3): p. 373-99.

117. Rieux-Laucat, F., F. Le Deist, and A. Fischer, *Autoimmune lymphoproliferative syndromes: genetic defects of apoptosis pathways.* Cell Death Differ, 2003. **10**(1): p. 124-33.

118. Drappa, J., et al., *Fas gene mutations in the Canale-Smith syndrome, an inherited lymphoproliferative disorder associated with autoimmunity.* N Engl J Med, 1996. **335**(22): p. 1643-9.

119. Takahashi, T., et al., *Generalized lymphoproliferative disease in mice, caused by a point mutation in the Fas ligand.* Cell, 1994. **76**(6): p. 969-76.

120. Hayashi, T. and D. Faustman, *NOD mice are defective in proteasome production and activation of NF-kappaB.* Mol Cell Biol, 1999. **19**(12): p. 8646-59.

121. Lenardo, M., et al., *Mature T lymphocyte apoptosis--immune regulation in a dynamic and unpredictable antigenic environment.* Annu Rev Immunol, 1999. **17**: p. 221-53.

122. Alimonti, J.B., T.B. Ball, and K.R. Fowke, *Mechanisms of CD4+ T lymphocyte cell death in human immunodeficiency virus infection and AIDS.* J Gen Virol, 2003. **84**(Pt 7): p. 1649-61.

123. Takuma, K., et al., *Mitochondrial dysfunction, endoplasmic reticulum stress, and apoptosis in Alzheimer's disease.* J Pharmacol Sci, 2005. **97**(3): p. 312-6.

124. Selkoe, D.J., *Cell biology of protein misfolding: the examples of Alzheimer's and Parkinson's diseases.* Nat Cell Biol, 2004. **6**(11): p. 1054-61.

125. Katayama, T., et al., *Induction of neuronal death by ER stress in Alzheimer's disease.* J Chem Neuroanat, 2004. **28**(1-2): p. 67-78.

126. Ferri, K.F. and G. Kroemer, *Organelle-specific initiation of cell death pathways.* Nat Cell Biol, 2001. **3**(11): p. E255-63.

127. Woo, D., *Apoptosis and loss of renal tissue in polycystic kidney diseases.* N Engl J Med, 1995. **333**(1): p. 18-25.

128. Schrier, R.W., et al., *Acute renal failure: definitions, diagnosis, pathogenesis, and therapy.* J Clin Invest, 2004. **114**(1): p. 5-14.

129. Wilcock, C. and J.A. Hickman, *Characterisation of a Na+/K+/Cl- cotransporter in alkylating agent-sensitive L1210 murine leukemia cells.* Biochim Biophys Acta, 1988. **946**(2): p. 359-67.

130. Ormerod, M.G., et al., *Discrimination of apoptotic thymocytes by forward light scatter.* Cytometry, 1995. **21**(3): p. 300-4.

131. Martin, S.J., et al., *Early redistribution of plasma membrane phosphatidylserine is a general feature of apoptosis regardless of the initiating stimulus: inhibition by overexpression of Bcl-2 and Abl.* J Exp Med, 1995. **182**(5): p. 1545-56.

132. Ormerod, M.G., et al., *Increased membrane permeability of apoptotic thymocytes: a flow cytometric study.* Cytometry, 1993. **14**(6): p. 595-602.

133. Zamai, L., et al., *Supravital exposure to propidium iodide identifies apoptosis on adherent cells.* Cytometry, 2001. **44**(1): p. 57-64.

134. Cossarizza, A., D. Ceccarelli, and A. Masini, *Functional heterogeneity of an isolated mitochondrial population revealed by cytofluorometric analysis at the single organelle level.* Exp Cell Res, 1996. **222**(1): p. 84-94.

135. Oberhammer, F., et al., *Apoptotic death in epithelial cells: cleavage of DNA to 300 and/or 50 kb fragments prior to or in the absence of internucleosomal fragmentation.* Embo J, 1993. **12**(9): p. 3679-84.

136. Allen, R.T., W.J. Hunter, 3rd, and D.K. Agrawal, *Morphological and biochemical characterization and analysis of apoptosis.* J Pharmacol Toxicol Methods, 1997. **37**(4): p. 215-28.

137. Darzynkiewicz, Z., et al., *Features of apoptotic cells measured by flow cytometry.* Cytometry, 1992. **13**(8): p. 795-808.

138. Olive, P.L., G. Frazer, and J.P. Banath, *Radiation-induced apoptosis measured in TK6 human B lymphoblast cells using the comet assay.* Radiat Res, 1993. **136**(1): p. 130-6.

139. Yasuhara, S., et al., *Comparison of comet assay, electron microscopy, and flow cytometry for detection of apoptosis.* J Histochem Cytochem, 2003. **51**(7): p. 873-85.

140. Xu, X., et al., *Detection of programmed cell death using fluorescence energy transfer.* Nucleic Acids Res, 1998. **26**(8): p. 2034-5.

141. Belloc, F., et al., *Flow cytometry detection of caspase 3 activation in preapoptotic leukemic cells.* Cytometry, 2000. **40**(2): p. 151-60.

142. Wiemann, S., et al., *Toward a catalog of human genes and proteins: sequencing and analysis of 500 novel complete protein coding human cDNAs.* Genome Res, 2001. **11**(3): p. 422-35.

143. Boer, J.M., et al., *Identification and classification of differentially expressed genes in renal cell carcinoma by expression profiling on a global human 31,500-element cDNA array.* Genome Res, 2001. **11**(11): p. 1861-70.

144. Sultmann, H., et al., *Gene expression in kidney cancer is associated with cytogenetic abnormalities, metastasis formation, and patient survival.* Clin Cancer Res, 2005. **11**(2 Pt 1): p. 646-55.

145. Bernard, P. and M. Couturier, *Cell killing by the F plasmid CcdB protein involves poisoning of DNA-topoisomerase II complexes.* J Mol Biol, 1992. **226**(3): p. 735-45.

146. Neumann, E. and K. Rosenheck, *Permeability changes induced by electric impulses in vesicular membranes.* J Membr Biol, 1972. **10**(3): p. 279-90.

147. Kolkhorst, V., J. Sturzebecher, and B. Wiederanders, *Inhibition of tumour cell invasion by protease inhibitors: correlation with the protease profile.* J Cancer Res Clin Oncol, 1998. **124**(11): p. 598-606.

148. Smith, P.K., et al., *Measurement of protein using bicinchoninic acid.* Anal Biochem, 1985. **150**(1): p. 76-85.

149. Sun, X.M., et al., *Distinct caspase cascades are initiated in receptor-mediated and chemical-induced apoptosis.* J Biol Chem, 1999. **274**(8): p. 5053-60.

150. Caballero-Benitez, A. and J. Moran, *Caspase activation pathways induced by staurosporine and low potassium: role of caspase-2.* J Neurosci Res, 2003. **71**(3): p. 383-96.

151. Luo, K.Q., et al., *Application of the fluorescence resonance energy transfer method for studying the dynamics of caspase-3 activation during UV-induced apoptosis in living HeLa cells.* Biochem Biophys Res Commun, 2001. **283**(5): p. 1054-60.

152. Karpova, T.S., et al., *Fluorescence resonance energy transfer from cyan to yellow fluorescent protein detected by acceptor photobleaching using confocal microscopy and a single laser.* J Microsc, 2003. **209**(Pt 1): p. 56-70.

153. Haendeler, J., et al., *Cathepsin D and H2O2 stimulate degradation of thioredoxin-1: implication for endothelial cell apoptosis.* J Biol Chem, 2005. **280**(52): p. 42945-51.

154. Kissil, J.L., et al., *Structure-function analysis of an evolutionary conserved protein, DAP3, which mediates TNF-alpha- and Fas-induced cell death.* Embo J, 1999. **18**(2): p. 353-62.

155. Inohara, N., et al., *CIDE, a novel family of cell death activators with homology to the 45 kDa subunit of the DNA fragmentation factor.* Embo J, 1998. **17**(9): p. 2526-33.

156. Vahsen, N., et al., *Physical interaction of apoptosis-inducing factor with DNA and RNA.* Oncogene, 2005.

157. Kaldis, P. and E. Aleem, *Cell cycle sibling rivalry: Cdc2 vs. Cdk2.* Cell Cycle, 2005. **4**(11): p. 1491-4.

158. Wachter, R.M., et al., *Structural basis of spectral shifts in the yellow-emission variants of green fluorescent protein.* Structure, 1998. **6**(10): p. 1267-77.

159. Dusetti, N.J., et al., *Cloning and expression of the rat vacuole membrane protein 1 (VMP1), a new gene activated in pancreas with acute pancreatitis, which promotes vacuole formation.* Biochem Biophys Res Commun, 2002. **290**(2): p. 641-9.

160. Hirokawa, T., S. Boon-Chieng, and S. Mitaku, *SOSUI: classification and secondary structure prediction system for membrane proteins.* Bioinformatics, 1998. **14**(4): p. 378-9.

161. Higgins, J.P., et al., *Gene expression patterns in renal cell carcinoma assessed by complementary DNA microarray.* Am J Pathol, 2003. **162**(3): p. 925-32.

162. Hanahan, D. and R.A. Weinberg, *The hallmarks of cancer.* Cell, 2000. **100**(1): p. 57-70.

163. Kaufmann, S.H. and W.C. Earnshaw, *Induction of apoptosis by cancer chemotherapy.* Exp Cell Res, 2000. **256**(1): p. 42-9.

164. Yang, X., H.Y. Chang, and D. Baltimore, *Essential role of CED-4 oligomerization in CED-3 activation and apoptosis.* Science, 1998. **281**(5381): p. 1355-7.

165. Zhang, S., C.N. Ong, and H.M. Shen, *Involvement of proapoptotic Bcl-2 family members in parthenolide-induced mitochondrial dysfunction and apoptosis.* Cancer Lett, 2004. **211**(2): p. 175-88.

166. Kosmider, B., et al., *Evaluation of P53 and BAX gene expression and induction of apoptosis and necrosis by the cis-Pt(II) complex of 3-aminoflavone in comparison with cis-diamminedichloroplatinum(II) (cis-DDP) in human lymphocytes.* Mutat Res, 2006. **604**(1-2): p. 28-35.

167. Hu, C., et al., *Enhanced Basal Apoptosis in Cultured Term Human Cytotrophoblasts is Associated with a Higher Expression and Physical Interaction of p53 and Bak.* Placenta, 2005.

168. Zhou, Z., et al., *Interleukin-12 up-regulates Fas expression in human osteosarcoma and Ewing's sarcoma cells by enhancing its promoter activity.* Mol Cancer Res, 2005. **3**(12): p. 685-91.

169. Tawa, P., et al., *Quantitative analysis of fluorescent caspase substrate cleavage in intact cells and identification of novel inhibitors of apoptosis.* Cell Death Differ, 2001. **8**(1): p. 30-7.

170. Park, S.Y., et al., *Establishment of a high-throughput screening system for caspase-3 inhibitors.* Arch Pharm Res, 2000. **23**(3): p. 246-51.

171. Starkuviene, V., et al., *High-content screening microscopy identifies novel proteins with a putative role in secretory membrane traffic.* Genome Res, 2004. **14**(10A): p. 1948-56.

172. Frankfurt, O.S. and A. Krishan, *Identification of apoptotic cells by formamide-induced dna denaturation in condensed chromatin.* J Histochem Cytochem, 2001. **49**(3): p. 369-78.

173. van Engeland, M., et al., *A novel assay to measure loss of plasma membrane asymmetry during apoptosis of adherent cells in culture.* Cytometry, 1996. **24**(2): p. 131-9.

174. Jones, J., et al., *Development and application of a GFP-FRET intracellular caspase assay for drug screening.* J Biomol Screen, 2000. **5**(5): p. 307-18.

175. Srinivasan, A., et al., *In situ immunodetection of activated caspase-3 in apoptotic neurons in the developing nervous system.* Cell Death Differ, 1998. **5**(12): p. 1004-16.

176. Grimm, S. and V. Kachel, *Robotic high-throughput assay for isolating apoptosis-inducing genes.* Biotechniques, 2002. **32**(3): p. 670-2, 674-7.

177. Mannherz, O., et al., *Functional screening for proapoptotic genes by reverse transfection cell array technology.* Genomics, 2006. **87**(5): p. 665-72.

178. Diehn, M., et al., *SOURCE: a unified genomic resource of functional annotations, ontologies, and gene expression data.* Nucleic Acids Res, 2003. **31**(1): p. 219-23.

179. Mulder, N.J., et al., *InterPro, progress and status in 2005.* Nucleic Acids Res, 2005. **33**(Database issue): p. D201-5.

180. Rappas, M., H. Niwa, and X. Zhang, *Mechanisms of ATPases--a multi-disciplinary approach.* Curr Protein Pept Sci, 2004. **5**(2): p. 89-105.

181. Li, K., et al., *[Screening and cloning gene of hepatocyte protein interacting with hepatitis C virus core protein].* Zhonghua Shi Yan He Lin Chuang Bing Du Xue Za Zhi, 2002. **16**(4): p. 351-3.

182. Saito, I., et al., *Hepatitis C virus infection is associated with the development of hepatocellular carcinoma.* Proc Natl Acad Sci U S A, 1990. **87**(17): p. 6547-9.

183. Watashi, K. and K. Shimotohno, *The roles of hepatitis C virus proteins in modulation of cellular functions: a novel action mechanism of the HCV core protein on gene regulation by nuclear hormone receptors.* Cancer Sci, 2003. **94**(11): p. 937-43.

184. Ray, R.B., K. Meyer, and R. Ray, *Suppression of apoptotic cell death by hepatitis C virus core protein.* Virology, 1996. **226**(2): p. 176-82.

185. Ray, R.B., et al., *Inhibition of tumor necrosis factor (TNF-alpha)-mediated apoptosis by hepatitis C virus core protein.* J Biol Chem, 1998. **273**(4): p. 2256-9.

186. Marusawa, H., et al., *Hepatitis C virus core protein inhibits Fas- and tumor necrosis factor alpha-mediated apoptosis via NF-kappaB activation.* J Virol, 1999. **73**(6): p. 4713-20.

187. Ruggieri, A., et al., *Sensitization to Fas-mediated apoptosis by hepatitis C virus core protein.* Virology, 1997. **229**(1): p. 68-76.

188. Zhu, N., et al., *Hepatitis C virus core protein binds to the cytoplasmic domain of tumor necrosis factor (TNF) receptor 1 and enhances TNF-induced apoptosis.* J Virol, 1998. **72**(5): p. 3691-7.

189. Honda, M., et al., *Hepatitis C virus core protein induces apoptosis and impairs cell-cycle regulation in stably transformed Chinese hamster ovary cells.* Hepatology, 2000. **31**(6): p. 1351-9.

190. Otsuka, M., et al., *Hepatitis C virus core protein inhibits apoptosis via enhanced Bcl-xL expression.* Virology, 2002. **296**(1): p. 84-93.

191. Stark, G.R., et al., *How cells respond to interferons.* Annu Rev Biochem, 1998. **67**: p. 227-64.

192. Gjermandsen, I.M., J. Justesen, and P.M. Martensen, *The interferon-induced gene ISG12 is regulated by various cytokines as the gene 6-16 in human cell lines.* Cytokine, 2000. **12**(3): p. 233-8.

193. Tahara, H., et al., *Increase in expression levels of interferon-inducible genes in senescent human diploid fibroblasts and in SV40-transformed human fibroblasts with extended lifespan.* Oncogene, 1995. **11**(6): p. 1125-32.

194. Tiwari, R.K., et al., *Interferon-alpha and gamma mediated gene responses in a human breast carcinoma cell line.* Breast Cancer Res Treat, 1991. **18**(1): p. 33-41.

195. Tahara, E., Jr., et al., *G1P3, an interferon inducible gene 6-16, is expressed in gastric cancers and inhibits mitochondrial-mediated apoptosis in gastric cancer cell line TMK-1 cell.* Cancer Immunol Immunother, 2005. **54**(8): p. 729-40.

196. Suomela, S., et al., *Interferon alpha-inducible protein 27 (IFI27) is upregulated in psoriatic skin and certain epithelial cancers.* J Invest Dermatol, 2004. **122**(3): p. 717-21.

197. Rasmussen, U.B., et al., *Identification of a new interferon-alpha-inducible gene (p27) on human chromosome 14q32 and its expression in breast carcinoma.* Cancer Res, 1993. **53**(17): p. 4096-101.

198. Askew, D.S., et al., *Constitutive c-myc expression in an IL-3-dependent myeloid cell line suppresses cell cycle arrest and accelerates apoptosis.* Oncogene, 1991. **6**(10): p. 1915-22.

199. Rao, L., et al., *The adenovirus E1A proteins induce apoptosis, which is inhibited by the E1B 19-kDa and Bcl-2 proteins.* Proc Natl Acad Sci U S A, 1992. **89**(16): p. 7742-6.

200. Qin, X.Q., et al., *Deregulated transcription factor E2F-1 expression leads to S-phase entry and p53-mediated apoptosis.* Proc Natl Acad Sci U S A, 1994. **91**(23): p. 10918-22.

201. Klingenberg, M., *Molecular aspects of the adenine nucleotide carrier from mitochondria.* Arch Biochem Biophys, 1989. **270**(1): p. 1-14.

202. Doerner, A., et al., *Tissue-specific transcription pattern of the adenine nucleotide translocase isoforms in humans.* FEBS Lett, 1997. **414**(2): p. 258-62.

203. Dolce, V., et al., *A fourth ADP/ATP carrier isoform in man: identification, bacterial expression, functional characterization and tissue distribution.* FEBS Lett, 2005. **579**(3): p. 633-7.

204. Bauer, M.K., et al., *Adenine nucleotide translocase-1, a component of the permeability transition pore, can dominantly induce apoptosis.* J Cell Biol, 1999. **147**(7): p. 1493-502.

205. Zamora, M., et al., *Recruitment of NF-kappaB into mitochondria is involved in adenine nucleotide translocase 1 (ANT1)-induced apoptosis.* J Biol Chem, 2004. **279**(37): p. 38415-23.

206. Rebhan, M., et al., *GeneCards: integrating information about genes, proteins and diseases.* Trends Genet, 1997. **13**(4): p. 163.

207. Conger, J.D., J.B. Robinette, and R.W. Schrier, *Smooth muscle calcium and endothelium-derived relaxing factor in the abnormal vascular responses of acute renal failure.* J Clin Invest, 1988. **82**(2): p. 532-7.

208. Sutton, R., et al., *Signal transduction, calcium and acute pancreatitis.* Pancreatology, 2003. **3**(6): p. 497-505.

209. Shapiro, L., et al., *Structural basis of cell-cell adhesion by cadherins.* Nature, 1995. **374**(6520): p. 327-37.

210. Satohisa, S., et al., *Behavior of tight-junction, adherens-junction and cell polarity proteins during HNF-4alpha-induced epithelial polarization.* Exp Cell Res, 2005. **310**(1): p. 66-78.

211. Yonemura, S., et al., *Cell-to-cell adherens junction formation and actin filament organization: similarities and differences between non-polarized fibroblasts and polarized epithelial cells.* J Cell Sci, 1995. **108 (Pt 1)**: p. 127-42.

212. Ando-Akatsuka, Y., et al., *Differential behavior of E-cadherin and occludin in their colocalization with ZO-1 during the establishment of epithelial cell polarity.* J Cell Physiol, 1999. **179**(2): p. 115-25.

213. Ebnet, K., et al., *Junctional adhesion molecules (JAMs): more molecules with dual functions?* J Cell Sci, 2004. **117**(Pt 1): p. 19-29.

214. Fujimoto, K., et al., *Dynamics of connexins, E-cadherin and alpha-catenin on cell membranes during gap junction formation.* J Cell Sci, 1997. **110 (Pt 3)**: p. 311-22.

215. Cavallaro, U. and G. Christofori, *Cell adhesion in tumor invasion and metastasis: loss of the glue is not enough.* Biochim Biophys Acta, 2001. **1552**(1): p. 39-45.

216. Perl, A.K., et al., *A causal role for E-cadherin in the transition from adenoma to carcinoma.* Nature, 1998. **392**(6672): p. 190-3.

217. Martin, T.A., et al., *Loss of tight junction plaque molecules in breast cancer tissues is associated with a poor prognosis in patients with breast cancer.* Eur J Cancer, 2004. **40**(18): p. 2717-25.

218. Michl, P., et al., *Claudin-4 expression decreases invasiveness and metastatic potential of pancreatic cancer.* Cancer Res, 2003. **63**(19): p. 6265-71.

219. Kim, G., et al., *Renal clear-cell carcinoma: an ultrastructural study on the junctional complexes.* Histol Histopathol, 2005. **20**(1): p. 35-44.

220. Boer, J.M., et al., *Identification and classification of differentially expressed genes in renal cell carcinoma by expression profiling on a global human 31,500-element cDNA array*, in *Genome Res*. 2001. p. 1861-70.

221. Vleminckx, K., et al., *Genetic manipulation of E-cadherin expression by epithelial tumor cells reveals an invasion suppressor role.* Cell, 1991. **66**(1): p. 107-19.

222. Aberle, H., H. Schwartz, and R. Kemler, *Cadherin-catenin complex: protein interactions and their implications for cadherin function.* J Cell Biochem, 1996. **61**(4): p. 514-23.

223. Aberle, H., et al., *beta-catenin is a target for the ubiquitin-proteasome pathway.* Embo J, 1997. **16**(13): p. 3797-804.

224. Orsulic, S., et al., *E-cadherin binding prevents beta-catenin nuclear localization and beta-catenin/LEF-1-mediated transactivation.* J Cell Sci, 1999. **112 (Pt 8)**: p. 1237-45.

225. Tetsu, O. and F. McCormick, *Beta-catenin regulates expression of cyclin D1 in colon carcinoma cells.* Nature, 1999. **398**(6726): p. 422-6.

226. Tsukita, S., M. Furuse, and M. Itoh, *Multifunctional strands in tight junctions.* Nat Rev Mol Cell Biol, 2001. **2**(4): p. 285-93.

227. Matter, K. and M.S. Balda, *Signalling to and from tight junctions.* Nat Rev Mol Cell Biol, 2003. **4**(3): p. 225-36.

228. Schneeberger, E.E. and R.D. Lynch, *The tight junction: a multifunctional complex.* Am J Physiol Cell Physiol, 2004. **286**(6): p. C1213-28.

229. Gottardi, C.J., et al., *The junction-associated protein, zonula occludens-1, localizes to the nucleus before the maturation and during the remodeling of cell-cell contacts.* Proc Natl Acad Sci U S A, 1996. **93**(20): p. 10779-84.

230. Balda, M.S. and K. Matter, *The tight junction protein ZO-1 and an interacting transcription factor regulate ErbB-2 expression.* Embo J, 2000. **19**(9): p. 2024-33.

231. Racusen, L.C., *Epithelial cell shedding in acute renal injury.* Clin Exp Pharmacol Physiol, 1998. **25**(3-4): p. 273-5.

232. Fish, E.M. and B.A. Molitoris, *Alterations in epithelial polarity and the pathogenesis of disease states.* N Engl J Med, 1994. **330**(22): p. 1580-8.

233. Kuznetsov, G., et al., *Perturbations in maturation of secretory proteins and their association with endoplasmic reticulum chaperones in a cell culture model for epithelial ischemia.* Proc Natl Acad Sci U S A, 1996. **93**(16): p. 8584-9.

234. Bush, K.T., T. Tsukamoto, and S.K. Nigam, *Selective degradation of E-cadherin and dissolution of E-cadherin-catenin complexes in epithelial ischemia.* Am J Physiol Renal Physiol, 2000. **278**(5): p. F847-52.

235. Zuk, A., et al., *Polarity, integrin, and extracellular matrix dynamics in the postischemic rat kidney.* Am J Physiol, 1998. **275**(3 Pt 1): p. C711-31.

236. Gailit, J., et al., *Redistribution and dysfunction of integrins in cultured renal epithelial cells exposed to oxidative stress.* Am J Physiol, 1993. **264**(1 Pt 2): p. F149-57.

237. Ueda, N. and S.V. Shah, *Tubular cell damage in acute renal failure-apoptosis, necrosis, or both.* Nephrol Dial Transplant, 2000. **15**(3): p. 318-23.

238. Bush, K.T., S.H. Keller, and S.K. Nigam, *Genesis and reversal of the ischemic phenotype in epithelial cells.* J Clin Invest, 2000. **106**(5): p. 621-6.

239. Mandel, L.J., R.B. Doctor, and R. Bacallao, *ATP depletion: a novel method to study junctional properties in epithelial tissues. II. Internalization of Na+,K(+)-ATPase and E-cadherin.* J Cell Sci, 1994. **107 (Pt 12)**: p. 3315-24.

240. Ward, J.B., et al., *Is an elevated concentration of acinar cytosolic free ionised calcium the trigger for acute pancreatitis?* Lancet, 1995. **346**(8981): p. 1016-9.

241. Gukovskaya, A.S., et al., *Mechanisms of cell death after pancreatic duct obstruction in the opossum and the rat.* Gastroenterology, 1996. **110**(3): p. 875-84.